Transport of polymer solutions in controlled low permeability porous media of various mineralogies

Imane Guetni

THÈSE

Présentée pour obtenir le grade de

DOCTEUR DE
L'UNIVERSITÉ DE LORRAINE

Spécialité: Géosciences

Présentée par:

Imane Guetni

Sujet de la thèse :

Transport of polymer solutions in controlled low permeability porous media of various mineralogies

Transport de solutions de polymère dans des milieux poreux contrôlés de différentes minéralogies

Thèse soutenue le 15 octobre 2019

devant le jury composé de :

M.	Arne	**Skauge**	Rapporteur
M.	Henri	**Bertin**	Rapporteur
Mme.	Emmanuelle	**Montargès-Pelletier**	Examinatrice
Mme.	Jocelyne	**Brendlé**	Examinatrice
M.	Nicolas	**Gaillard**	Examinateur
M.	Eric	**Delamaide**	Invité
M.	Frédéric	**Villiéras**	Directeur de thèse
Mme.	Claire	**Marlière**	Co-directrice de thèse
M.	David	**Rousseau**	Invité

Remerciements

Ce travail de thèse est le fruit des contributions d'un bon nombre de personnes dont les échanges, les idées et les critiques constructives m'ont fortement aidé à progresser tout au long de ces trois années. Je tiens alors à sincèrement les remercier.

Je remercie IFP Energies nouvelles et plus particulièrement Olga Vizika et Jean-Marc Lombard de m'avoir accueillie au sein de la direction Géosciences et du département Géofluides et roches.

Mes sincères remerciements vont à mon directeur de thèse, Frédéric Villiéras, pour ses conseils précieux, sa rigueur scientifique et sa disponibilité malgré toutes ses responsabilités. Et puis surtout, merci à toi Frédéric pour m'avoir initiée au monde des argiles.

Je remercie très chaleureusement mes promoteurs à IFPEn Claire Marlière et David Rousseau pour leur implication et leur soutien exceptionnel dans ma thèse. J'ai appris énormément à vos côtés : pendant nos réunions hebdomadaires, au labo ou dans le train... Et j'y ai pris beaucoup de plaisir. Sans vous, ce travail n'aurait pas été aussi abouti. Merci à toi David pour ton enthousiasme contagieux à l'égard de ces travaux. Merci à toi Claire pour ta rigueur et pour le temps que tu m'as accordée en particulier pendant la rédaction. Je vous suis profondément reconnaissante.

Je remercie les rapporteurs Henri Bertin et Arne Skauge, qui ont accepté de lire et d'évaluer ma thèse, ainsi que Emmanuelle Montargès-Pelletier et Jocelyne Brendlé pour leurs remarques pendant la soutenance. Je remercie particulièrement Nicolas Gaillard pour les discussions enrichissantes que nous avons eu en amont de la soutenance et Eric Delamaide pour nos différents échanges lors des congrès. Un grand merci à vous tous.

Je tiens à remercier également toutes les personnes du LIEC à Nancy, qui ont contribué de près ou de loin à ce travail. Je commence par remercier Manuel Pelletier pour sa disponibilité, la qualité de nos échanges lors des réunions, de m'avoir accueillie au LIEC et de m'avoir initiée aux multiples techniques de caractérisation des minéraux. Je remercie également Isabelle Bihannic, Fabien Thomas et Yves Waldvogel pour les travaux sur les suspensions ainsi que nos discussions enrichissantes. Je tiens enfin à remercier Angelina Razafitianamaharavo pour son temps et pour les expériences BET.

Mon aventure expérimentale n'aurait sans doute pas abouti sans l'aide précieuse du "trio de choc" : Nicolas Rousseau, Elsa Métayer et Clémence Le Gallo. Merci à toi Nicolas de m'avoir aidé à construire mon montage expérimental partant de "zéro", de m'avoir formée sur les corefloods et de m'avoir transmis ta passion et ta rigueur expérimentale. Merci à toi Elsa de m'avoir formée sur la préparation et la caractérisation des solutions de polymère ainsi que ta disponibilité et tes conseils. Merci à toi Clémence pour toute ton aide durant ces trois ans surtout lors des expériences d'injection de tensioactif. Merci à tous les trois pour votre amabilité et votre accueil.

Ce travail comporte une grande partie dédiée à la caractérisation des matériaux. Je souhaite alors remercier toutes les personnes qui y ont contribué. Je remercie particulièrement Marie-Claude Lynch et Elisabeth Rosenberg pour les expériences CT-Scan, Eric Kohler, Joel Lopes de Azevedo et Florent Moreau pour les expériences MEB : merci à tous pour votre disponibilité et votre aide. Je remercie Didier Frot pour m'avoir initiée à la diffusion de lumière ainsi que pour les discussions enrichissantes que nous avons eues. Mes remerciements vont également à Perrine Cologon et Antony Vanheghe pour leur disponibilité et les expériences HPLC.

Je tiens également à remercier Samir Bekri, Jalila Boujlel, Aline Delbos et Thibaud Chevalier pour leurs conseils et leur gentillesse.

Merci à Sylvie Louis, Meriem Jehl et Djaméla Buda pour leur disponibilité et leur aide administrative ainsi que François Lamy pour son aide sur le plan logistique.

Je remercie l'ensemble du personnel IFPEn avec qui j'ai eu le plaisir de travailler ou simplement échanger. Merci à Matthieu M., Philippe, Hervé, Adeline, Néomie, Nicolas P., Ameline, Maria, Violaine, Sylvie S., Joelle, Hermann, Sonia, Virginie et Daniel.

Mes remerciements vont maintenant aux doctorants pour les moments mémorables de convivialité. Merci à Hafssa C., Imane Y. et Zaineb Z. pour leur amitié et leur soutien. Merci à mes co-bureau Sebastian et Aurélien pour leur gentillesse. Merci à Hamza et Anabel pour leurs conseils et leur bonne humeur. Merci à Claire, Pauline, Jean, Omar, Ariane, Chakib, Christopher, Nicolas, Dandan, Sophie, Adriana, Narges, Gael et Elie pour tous les bons moments passés ensemble.

Je remercie également mes amis Yasmine, Jihad, Zineb, Fadoua, Achraf, Issam, Ilias et Anas pour leur présence et leurs encouragements.

Je remercie du fond du coeur mes parents, ma soeur et mon frère pour leur soutien sans faille, leur confiance et leur amour inconditionnel. Je remercie également les membres de ma belle famille pour leurs encouragements et leur support. Enfin, je remercie mon cher mari, Iliass, pour sa présence et son affection tout au long de cette aventure. Merci d'avoir cru en moi.

Résumé long

Compte tenu de l'incessante croissance de la demande en énergie, et malgré l'émergence des énergies renouvelables, les hydrocarbures restent au centre du marché mondial de l'énergie.

L'exploitation des hydrocarbures, particulièrement l'huile, passe par plusieurs phases. Tout d'abord, la récupération primaire durant laquelle l'huile remonte à la surface dû à la différence de pression entre le corps et la surface du réservoir. Cette méthode permet, selon les conditions du réservoir, de récupérer autour de 10 à 15% de l'huile en place. Une méthode de récupération dite secondaire est par la suite appliquée moyennant l'injection d'eau ou de gaz dans le puit d'injection afin de maintenir la pression du réservoir, balayer et récupérer l'huile résiduelle à partir des puits de production. La récupération secondaire, en l'occurrence par injection d'eau, permet de produire 15 à 20% additionnels d'huile. En troisième lieu, afin d'augmenter le taux de récupération d'un réservoir pétrolier, des méthodes de récupération dite tertiaire et communément appelée Récupération Assistée du Pétrole (EOR pour Enhanced Oil Recovery), sont utilisées. Ces techniques consistent principalement en l'injection de gaz miscibles ou non-miscibles, l'injection d'énergie thermique (vapeur) et/ou d'additifs chimique. Ces méthodes permettent la récupération de jusqu'à 70% de l'huile en place.

Parmi les différentes techniques d'EOR utilisées, l'EOR chimique semble être particulièrement prometteur avec un potentiel de récupération de 40% additionnels d'huile en place. Cette technique, qui consiste essentiellement en l'injection d'agent viscosifiant ou

de molécules tensioactives, vise à améliorer l'efficacité du balayage du réservoir comparé à l'injection d'eau et de mobiliser l'huile piégée dans le réservoir.

Durant l'injection d'eau, des effets de digitation visqueuse peuvent apparaître dû à la différence de viscosité entre l'eau et l'huile, ce qui cause la création de chemins préférentiels et par conséquent un mauvais balayage du réservoir. L'ajout de polymère augmente la viscosité du fluide injecté, ce qui élimine ces effets de digitation visqueuse et par la suite améliore l'efficacité du balayage. Par ailleurs, suite à l'injection d'eau, l'huile reste piégée dans le réservoir à cause du piégeage capillaire. Le nombre capillaire Ca étant défini comme le ratio entre les forces visqueuses et la tension interfaciale, la saturation résiduelle en huile (SOR) diminue considérablement lorsque le nombre capillaire augmente. En plus du polymère, un autre additif chimique est souvent utilisé en EOR afin de réduire la tension interfaciale (IFT) entre l'huile et les fluides injectés : le tensioactif. La réduction de l'IFT est associée à l'augmentation du nombre capillaire, permettant ainsi le dépiégeage de l'huile résiduelle.

Bien que l'EOR chimique soit maintenant considérée comme une technique prouvée dans les réservoirs de perméabilités supérieures à $100mD$, son application aux réservoirs de plus faibles perméabilités (entre 10 et $100mD$) représente un véritable enjeu.

A la lumière des résultats et conclusions tirés de la bibliographie, plusieurs défis se présentent lors de l'application de l'EOR chimique par injection de polymère et/ou de tensioactifs dans des milieux poreux de faible perméabilité ($10 - 100mD$). En effet, des problèmes comme la rétention chimique, une faible injectivité ainsi qu'une mauvaise propagation en profondeur des fluides sont souvent observés pour ces milieux poreux. Ceci est dû principalement à leur minéralogie naturellement riche en argile ainsi que leur faible perméabilité et leur structure poreuse complexe. Ces problèmes impliquent des risques élevés d'endommagement des formations, mais présentent également des défis économiques et environnementaux considérables en raison de l'utilisation de grandes quantités d'additifs chimiques. Par conséquent, la compréhension des mécanismes qui régissent ces procédés

est d'une grande importance afin d'optimiser l'utilisation de l'EOR chimique dans cette gamme de perméabilité.

La principale motivation de cette étude est alors d'hiérarchiser les paramètres influençant le transport des additifs chimiques dans les milieux poreux de faible perméabilité. Pour cela, nous étudierons les caractéristiques des milieux poreux (minéralogie, perméabilité), des fluides injectés (salinité, concentration, viscosité) et des conditions d'injection (température, débit) selon leur degré d'influence sur les mécanismes de transport des fluides.

Pour ce faire, nous avons choisi de baser notre étude sur des milieux poreux granulaires synthétiques composés de grains de quartz et de différentes argiles (kaolinite, illite et smectite). Ainsi, les expériences peuvent être simplifiées, les effets de chaque phase minérale peuvent être mieux compris et la complexité et l'hétérogénéité ainsi que les variations lithologiques et texturales des roches naturelles peuvent être évitées autant que possible. Par ailleurs, le principal défi est d'assurer la reproductibilité de ces expériences afin de pouvoir mieux comparer les résultats. En terme de méthodes expérimentales, des tests d'injection seront réalisés avec le développement de nouveaux procédés permettant de travailler avec différents milieux poreux et fluides puis de collecter des données qui pourront par la suite être analysées.

Préalablement aux tests d'injection en milieux poreux, une attention particulière a été portée à la préparation et la caractérisation des matériaux.

Pour les fluides, des solutions de polyacrylamide partiellement hydrolysé (HPAM) ont été préparées dans des saumures de différentes forces ioniques et duretés (en utilisant les sels $NaCl$ et $CaCl_2$). Pour la caractérisation, des mesures de viscosité ainsi que des tests de diffusion dynamique de la lumière (DLS) ont été menés et les résultats ont mis en évidence deux effets majeures : i) L'augmentation de la force ionique entraîne une augmentation de la densité des chaînes de polymère ainsi qu'une diminution de leur volume hydrodynamique ii) L'augmentation de la dureté entraîne une augmentation de la

densité et du volume hydrodynamique des chaînes de polymère, ce qui suggère un éventuel pontage entre les chaînes et les cations divalents (calcium dans ce cas) Enfin, des saumures ayant différentes forces ioniques ($0,01$ et $1mol/L$) et différentes duretés (0 et 20%) ont été sélectionnées pour étudier ces effets au cours des expériences d'injection en milieux poreux.

Pour les milieux poreux, des milieux granulaires de différente composition minéralogique, quartz puis quartz + argile (kaolinite, illite et smectite séparément), ont été préparés. Les milieux préparés ont montré des propriétés pétrophysiques très similaires avec une porosité de $31,3 \pm 1,8\%$, un volume poreux de $5,5 \pm 0,3mL$ et une perméabilité comprise entre 50 et $100mD$ avec différentes valeurs de surfaces spécifiques. Ces milieux ont également été observés sous Microscope Electronique à Balayage (MEB) afin d'étudier le changement de structure microscopique dû au changement de minéralogie d'une part et de la salinité de l'autre. En effet, pour les milieux contenant l'illite et la smectite, les images MEB ont mis en évidence la structure particulière de ces milieux poreux à très faible salinité et ont montré la formation d'agrégats d'argile à très forte salinité.

Après la caractérisation des matériaux, et afin d'étudier les propriétés de transport des solutions de polymère dans les milieux poreux de faible perméabilité, des expériences d'injection ont été réalisées.

Les essais d'injection ont été menés dans quatre types de milieux poreux à base de quartz et trois argiles différentes : kaolinite, illite et smectite. Les solutions de polymère injectées ont été préparées dans trois saumures différentes $S001-0$, $S1-0$ et $S1-02$ avec différentes concentrations de polymère permettant l'injection d'une viscosité relative fixe de 10. Les observables de ces expériences sont la réduction de mobilité Rm, la rétention irréversible du polymère, la réduction de perméabilité Rk ainsi que l'épaisseur et la densité de la couche adsorbée.

La première discussion a permis de mettre en évidence l'impact de la force ionique et de la dureté sur les propriétés de transport du polymère dans les milieux poreux étudiés,

montrant que globalement, l'augmentation de la force ionique entraîne une augmentation de la réduction de mobilité, de la rétention du polymère et de la réduction de perméabilité. Par ailleurs, la présence des cations divalents entraîne une forte augmentation de la rétention du polymère et de la réduction de perméabilité dans tous les milieux poreux tandis que son effet sur la réduction de mobilité paraît plus complexe.

La deuxième discussion a permis de mieux comprendre l'impact de la minéralogie sur le transport des polymères dans les milieux poreux, en montrant que la présence d'argiles induit une forte augmentation de la réduction de mobilité et de la rétention irréversible du polymère. Par ailleurs, dans les milieux poreux riches en argile, l'illite et la smectite présentent des comportements comparables dans la réduction de mobilité, la rétention du polymère ainsi que la réduction de perméabilité. Etonnamment, la kaolinite présente la valeur la plus élevée de rétention de polymère malgré sa nature (non gonflante, sans charge permanente) et sa faible surface spécifique comparée à l'illite et la smectite.

L'analyse en terme d'épaisseur et de densité de couche adsorbée a montré une bonne cohérence avec les mesures de viscosité et de DLS pour le quartz, mais n'était pas cohérente pour les milieux poreux contant de l'argile en raison des hétérogénéités chimiques des surfaces. Par ailleurs, la surface spécifique mesurée dans ces milieux poreux, en particulier pour les milieux avec illite ou smectite, semble être différente et beaucoup plus élevée que les surfaces effectivement accessibles au polymère. Ce résultat a été mis en évidence grâce aux observations MEB avec la formation d'agrégats argileux qui ont un impact significatif sur le transport des polymères : les molécules de polymère ne semblent interagir qu'avec la surface extérieure des agrégats argileux.

Les résultats de ces travaux devraient aider à orienter les opérations d'EOR chimique en terme de faisabilité de l'injection de polymère dans des réservoirs gréseux de perméabilité inférieure à 100mD, dans la mesure où ils montrent qu'une forte réduction de perméabilité ne signifie pas toujours une rétention élevée du polymère. En outre, il a été souligné que l'interprétation en terme de couche adsorbée moyenne (approche classique

du modèle de faisceau de capillaires) n'est pas toujours valable pour les formations riches en argile vu que la surface spécifique mesurée est différente et semble être beaucoup plus élevée que la surface effectivement accessible au polymère.

Parallèlement à cette étude, des expériences sur les suspensions aqueuses argile-polymère ont été menées dans le laboratoire d'attachement de la thèse (Laboratoire Interdisciplinaire des Environnements Continentaux, à Nancy). Ces suspensions ont été étudiées en terme de taille de particules, de turbidité et de mobilité électrophorétique pour différentes concentrations d'argile et de polymère ainsi que différentes forces ioniques. Cette étude a montré que le HPAM déplace la concentration critique de coagulation vers des valeurs plus élevées. De plus, l'interaction argile-polymère n'a été que légèrement influencée par la force ionique et aucune différence majeure n'a été observée en ce qui concerne le type d'argile. La mobilité électrophorétique du polymère quant à elle n'a pas été affectée en présence d'argile, suggérant ainsi l'incorporation de particules d'argile dans les agrégats de polymère.

Des expériences en basse pression ont également été réalisées au LIEC, sur des échantillons de milieux poreux post-injection de polymère. L'analyse des résultats n'a montré aucune différence significative dans l'interaction polymère-roche basée sur le type d'argile.

Afin de compléter ces travaux de thèse, des tests d'injection de tensioactifs ont été réalisés dans les différents types de milieux poreux en utilisant la saumure $S1-0$ (force ionique élevée, absence de cations divalents) et une formulation combinant deux tensioactifs : un anionique IOS (Internal Olefin Sulfonates) et un nonionique AGES (AlkoxyGlycidylEther Sulfonates) tous les deux largement utilisés dans les procédés EOR. Les résultats des corefloods ont montré une forte adsorption des tensioactifs ainsi que des tendances non négligeables de bouchage dans les milieux poreux contenant de l'argile par rapport au milieu de référence contenant le quartz seulement. Une expérience additionnelle dans le milieu poreux avec kaolinite a été menée en utilisation l'injection de polymère et tensioactif toujours avec la même saumure $S1-0$, le même polymère et la même formulation

de tensioactifs. Les résultats de cette expérience ont montré une légère diminution de la rétention de polymère ainsi qu'une légère dégradation de la qualité de propagation en profondeur en présence du tensioactif.

En perspectives, il serait intéressant de continuer les expériences sur les suspensions argile-polymère afin d'identifier et mieux cerner les mécanismes d'interaction. Des tests d'injection dans des roches réservoirs peuvent également être intéressants dans le but d'étudier l'impact de la structure poreuse ainsi que la localisation d'argile dans l'espace poral sur le transport des fluides. Enfin, des expériences en présence d'huile pourraient être intéressantes pour évaluer l'impact de l'huile sur le transport du polymère dans ces milieux poreux de faible perméabilité.

Contents

List of Figures

List of Tables

List of Notations

$< v >$	Average flow velocity	m/s
ΔP	Differential pressure	bar
$\Delta P_{polymer}$	Differential pressure during polymer injection	bar
$\Delta P_{post-injection}$	Differential pressure after polymer injection	bar
$\Delta P_{ref\ brine}$	Reference differential pressure during brine injection	bar
$\dot{\gamma}_{wall}$	Wall shear rate	s^{-1}
η	Viscosity	$Pa.s$
η_r	Relative viscosity of polymer	$-$
η_s	Solvant viscosity	$Pa.s$
η_{brine}	Brine viscosity	$Pa.s$
$\eta_{polymer}$	Polymer viscosity	$Pa.s$
η_{r0}	Relative viscosity at the Newtonian plateau	$-$
$\eta_{r_{app}}$	Apparent relative viscosity	$-$
η_{spr}	Reduced specific viscosity of polymer	cm^3/g
γ	Interfacial tension	mN/m

$\Gamma_{retention}$	Polymer irreversible retention	$\mu g/g$
λ_0	Wavelength of the light source	nm
λ_o	Mobility of oil	$D/Pa.s$
λ_w	Mobility of water	$D/Pa.s$
$[\eta]$	Intrinsic viscosity of polymer	cm^3/g
ϕ	Porosity	%
ρ	Spheres density	g/cm^3
ρ_s	Mineral density	g/cm^3
ρ_{ads}	Adsorbed layer density	g/cm^3
τ	Relaxation time	s
θ	Angle of diffusion	rad
ε_h	Adsorbed layer thickness	μm
φ	Volume fraction occupied by macromolecules of polymer	%
A	Capillary section	m^2
A_i	Contribution in scattered light intensity of the particles of popuplation i	$-$
b	Persistence length of polymer chain	Å
C	Polymer concentration	g/L
C^*	Overlap concentration	g/L
C^{**}	Entanglement concentration	g/L

C_i	Molar concentration of the ion i	mol/L
Ca	Capillary number	–
D	Diffusion coefficient of chains	cm^2/s
D_0	Hydrodynamic diffusion coefficient of chains	cm^2/s
f_0	Macromolecule friction coefficient	gm/s
g_1	Electrical field	V/m
G_2	Temporal autocorrelation function of scattered light intensity	–
I	Ionic strength	mol/L
$I(t)$	Scattered light intensity at time t	–
IPV	Inaccessible pore volume	%
k	Permeability	D
k_B	Boltzmann constant	J/K
K_H	Huggin's constant	–
k_r	Relative permeability	–
L	Length	m
M	Mobility ratio	–
M_w	Molecular weight	$Da, g/mol$
N	Number of monomers	–
n	Refractive index of the medium	–

N_A	Avogadro's number	–
PV	Pore volume	–
Q	Flow rate	m^3/s
q	Wave factor	m^{-1}
R	Radius of capillary tube	m
R^+	Hardness	%
R_g	Radius of gyration	mm
R_h	Polymer's hydrodynamic radius	mm
r_h	Pore throat's hydrodynamic radius	μm
R_k	Permeability reduction	–
R_m	Mobility reduction	–
S	Porous medium' section	m^2
S_w	Water saturation of a porous medium	%
SSA	Specific surface area	m^2/g
T	Temperature	K
V_C	Cumulated volume	cm^3
V_D	Dead volumes	cm^3
V_i	Interstitial velocity	m/day
V_s	Volume of the solid fraction	cm^3

V_t	Total volume	cm^3
V_w	Volume occupied by water	cm^3
V_{max}	Maximum flow velocity	m/s
z_i	Charge of the ion i	–

Introduction

Given the constantly growing demand for energy, hydrocarbons remain at the center of the global energy market. For oil recovery, three phases can be identified. A combination of primary and secondary recovery methods allows the recovery of only up to 40% of the original oil in place (OOIP). Consequently, tertiary recovery also known as Enhanced Oil Recovery (EOR) is carried out using gas, steam or chemicals injection allowing the recovery of up to 70% of the OOIP. As chemical EOR seems to be particularly promising regarding potential additional recovery of oil, it has been of interest in several studies.

In order to enhance the water sweeping efficiency and untrap residual trapped oil, chemical EOR consists of the injection of polymers (viscosifying agents) and surfactants. Although this technique is now considered a proven technique in reservoirs with permeabilities higher than $100mD$, its application to reservoir of lower permeabilities (between 10 and $100mD$) remains challenging.

Several difficulties can be encountered during the application of polymer flood to low permeability reservoirs. This type of reservoirs is characterized by small pore throats potentially leading to poor injectivity, mechanical degradation of polymer and uncontrolled fracturing. Besides, the naturally high clay content in these reservoirs causes significant chemicals retention. High retention can result in formation damage and is linked to environmental and economical challenges because of the use of large quantities of chemicals.

Although several studies have addressed these challenges, the overall understanding of the mechanisms governing the transport of these complex fluids in low permeability porous media remains incomplete in the literature.

The objective of this work is to provide elements for a better assessment of these mechanisms with a focus on injection water composition and porous media properties. For that, the transport properties of polymer solutions in controlled low permeability porous media has been studied regarding the impacts of salinity and mineralogy.

This thesis is structured around four chapters:

In Chapter 1 elements of the state of the art are presented. First, the characteristics of the chemical solutions used in the EOR, i.e. polymers and surfactants, are introduced. Then, the properties of chemical flooding in low permeability porous media are presented with a focus on related challenges. Finally, the research motivation and outline are detailed.

Chapter 2 is dedicated to polymer solutions. Polymer theoretical background and physico-chemical properties are first introduced, followed by the description of materials and methods used to prepare and characterize the solutions. Then characterization results are presented and discussed.

In Chapter 3, porous media used in this study are introduced. After presenting general characteristics of porous media, materials and methods used to prepare and characterize them are detailed. Characterization results are finally presented and discussed.

The last chapter, Chapter 4, concerns the transport properties of polymer in porous media. Materials and methods used for injection experiments are first described, then,

corresponding results are presented and discussed regarding the impacts of salinity and mineralogy.

Chapter 1

State of the art

Contents

1.1 Context

Hydrocarbons (oil and gas) are initially formed as a result of slow and complex transformations of marine sediments that are rich in organic matter. These sediments sink and solidify as organic matter decomposes, under the influence of pressure and temperature, into liquid and gaseous hydrocarbons. All of these elements are commonly referred to as source rock. As a result of this transformation, and because of their low density, hydrocarbons migrate from source rock to the Earth's surface through several stratified geological layers. The possible presence of an impermeable layer called seal or cap rock causes these hydrocarbons to be retained and accumulate in the underlying porous rock called reservoir rock. (Figure 1.1)

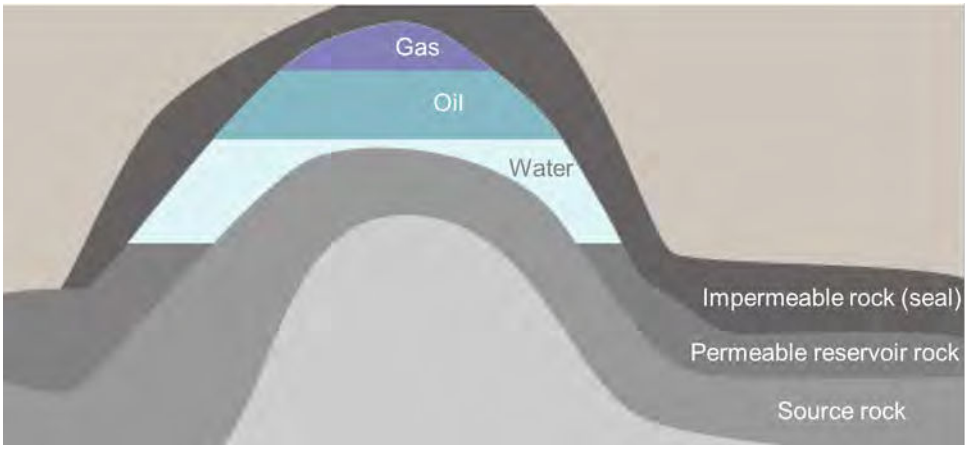

Figure 1.1 – Petroleum system. ©Connaissance des Energies

The exploitation of hydrocarbons, particularly hydrocarbons in liquid form called oil, goes through several phases. First of all, the primary recovery during which the oil rises to the surface due to the pressure difference between the reservoir and the surface. This primary method allows, depending on the reservoir conditions, to recover around 10 to 15% of the oil in place. A secondary recovery phase is then carried out by injecting water or gas in the injection well in order to maintain the pressure of the reservoir, sweep away and recover the remaining oil from the production wells. Secondary recovery, particularly using water injection, can produce an additional 15 to 20% of oil. Finally, in order to increase the recovery rate of an oil reservoir, tertiary recovery methods, also known as Enhanced Oil Recovery (EOR), are used. These techniques mainly include the injection of miscible or non-miscible gases, the injection of thermal energy (steam injection) and/or chemicals [15, 1]. The tertiary processes allow the recovery of up to 70% of the original oil in place (OOIP) as shown in Figure 1.2.

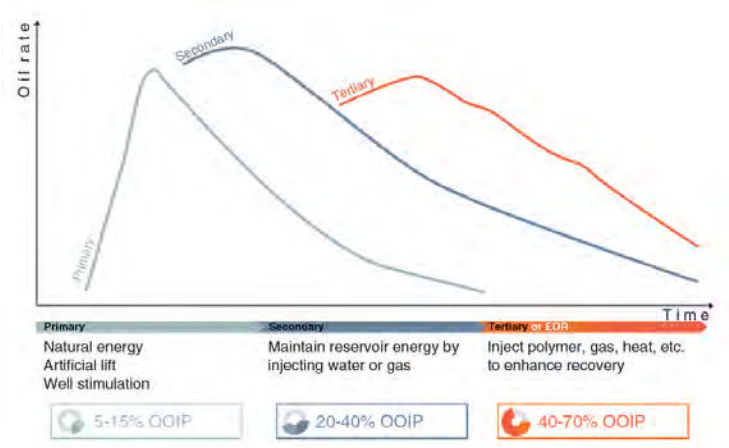

Figure 1.2 – Hydrocarbons recovery mechanisms [1]

Among the different EOR techniques, the chemical process seems to be particularly promising with a recovery potential up to 40% additional recovery of the oil in place [14]. This technique, which mainly consists of the injection of viscosifying agents and/or surfactant molecules, aims to improve the efficiency of the sweeping process compared to water injection and to untrap residual oil trapped in the reservoir.

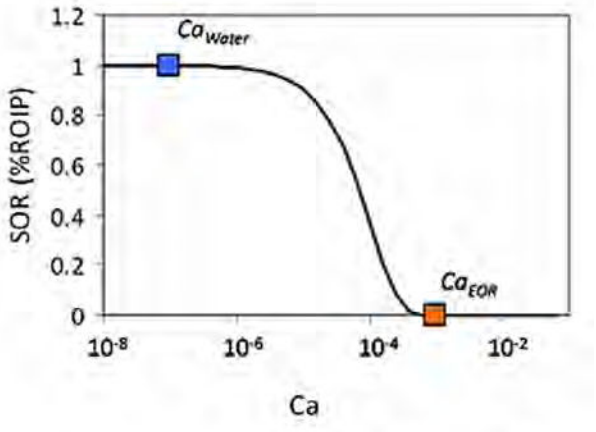

Figure 1.3 – Typical capillary desaturation curve (CDC)

During water injection, viscous fingering effects can occur due to the differences in water and oil viscosity, creating preferential paths and thus a poor sweeping of the reservoir. After waterflooding, oil remains trapped in the reservoir because of capillary trapping. In Figure 1.3, a typical capillary desaturation curve showing the residual oil saturation SOR as a function of the capillary number Ca which is defined as the ratio between viscous forces $\eta\nu$ and the interfacial tension γ , in both water and EOR cases.

The addition of polymer increases the viscosity of the injected solution, which eliminates these fingering effects and thus improves the sweeping efficiency as shown in Figure 1.4 [2].

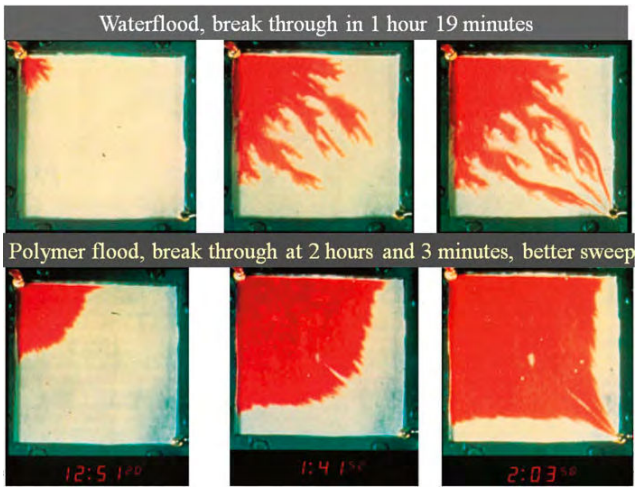

Figure 1.4 – Improvement of sweeping efficiency - case of water injection (upper part) and polymer solution injection (lower part) [2]

In addition to polymer, another chemical is often used in EOR to reduce the interfacial tension (IFT): the surfactant. This IFT reduction is associated with the increase in the capillary number, thus allowing the release of the residual oil.

Although chemical EOR is now considered a proven technique in reservoirs with permeabilities higher than 100mD, its application to reservoir of lower permeabilities (between 10 and 100mD) remains challenging.

Several issues are related to the application of chemical EOR to low permeability reservoirs. On the one hand, problems due to small pore size such as poor injectivity of the fluids that can lead to uncontrolled fracturing, or the mechanical degradation of polymer that significantly reduces its viscosity and subsequently leads to a decrease in sweeping efficiency. On the other hand, due to the mineralogical composition of low permeable reservoir naturally rich in clay, significant chemicals retention is observed. This high retention can lead to formation damage but also presents considerable economical and environmental challenges due to the use of large quantities of chemicals.

Despite the major challenges, the overall understanding of the mechanisms governing the transport of these complex fluids in low permeability porous media remains incomplete in the literature.

The objective of this study is to provide elements for a better understanding of these mechanisms and to suggest strategies to optimize the application of chemical EOR in low permeability reservoirs.

In this chapter, we will first introduce polymer and surfactant solutions. Then, we will focus on the application of chemical flooding to low permeability reservoirs where we will present the characteristics of these porous media, the challenges they represent and some suggested solutions from the literature. Finally, we will describe the objective of this study and the approach of this work.

1.2 Characteristics of chemical solutions

In this section, we will present the two main agents used in chemical EOR: polymers, which act on sweep efficiency at the macroscopic scale by increasing water viscosity and surfactants which act on displacement efficiency at the pore scale by reducing the interfacial tension between the displacing fluids and oil [16].

1.2.1 Polymer

In EOR, two main types of polymers are used: synthetic polymers such as partially hydrolyzed polyacrylamides (HPAM) and biopolymers such as xanthan gum. Less commonly, natural polymers and their derivatives such as quar gum, hydroxyl ethyl cellulose (HEC) are used.

According to *Sheng* [15] a good polymer should have carbon chain in the backbone for thermal stability, negative ionic hydrophilic group to reduce adsorption on rock surfaces, good viscosifying power and nonionic hydrophilic group for chemical stability.

For these reasons, HPAM is a good polymer and is the most widely used synthetic polymer in EOR.

1.2.1.1 EOR polymer: HPAM

HPAM is a synthetic straight-chain polymer of acrylamide monomers, some of which have been hydrolyzed. They are obtained by polymerization of acrylamide and subsequent hydrolysis to reduce adsorption and improve viscosity at low salinity. Hydrolysis converts some of the amide groups (NH_2) to carboxyl groups (COO^-) as shown in Figure 1.5. This modification introduces negative charges on the backbones of polymer chains which has a significant effect on the rheological properties of the polymer solution. In commercial products, hydrolysis degree ranges from 15 to 35%. The molecular weights M_w of commercial HPAM for EOR applications are usually in the range ($M_w = 2 - 20MDa$) [2].

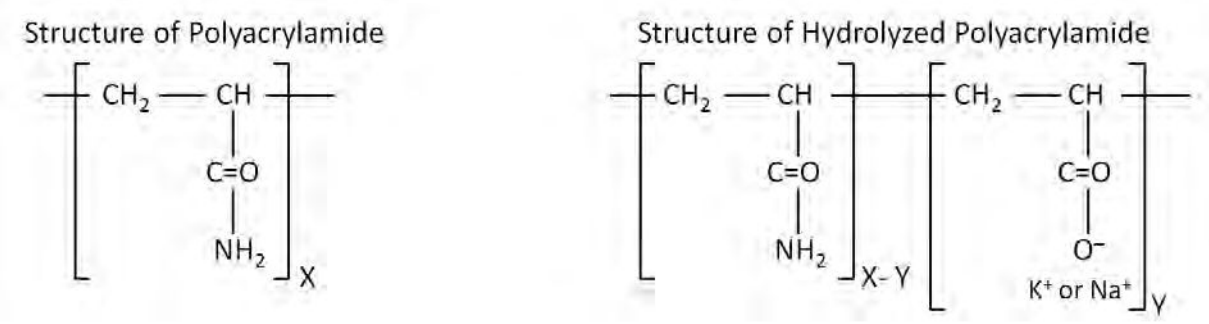

Figure 1.5 – Molecular structure of polyacrylamide (PAM) and partially hydrolyzed polyacrylamide (HPAM) [3]

1.2.1.2 HPAM molecules in aqueous solution

In aqueous solution, HPAM molecule is a flexible chain structure also called random coil in polymer chemistry [16]. It is a polyelectrolyte which induces strong interaction with ions in solution. Due to its flexibility, HPAM solution properties are more sensitive to salt/hardness than uncharged polymers as shown in Figure 1.6. These interactions will be discussed in details in Chapter 2.

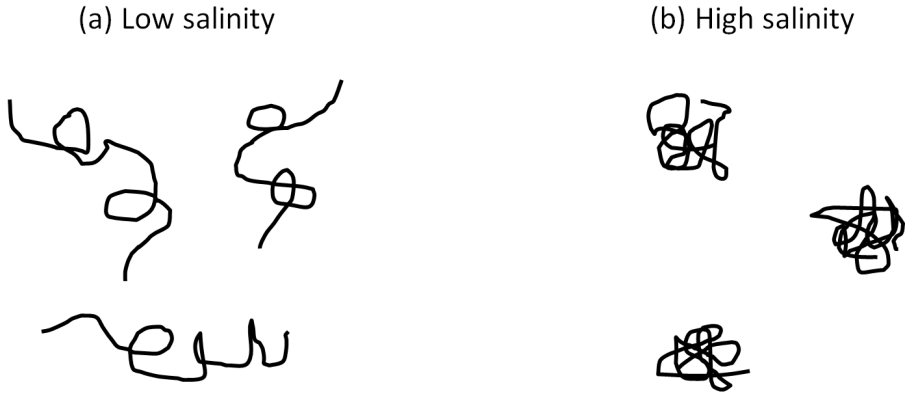

Figure 1.6 – Schematic of the effect of ions in solution on HPAM conformation (for a dilute solution)

1.2.1.3 HPAM solutions in EOR systems

As mentioned earlier, polymer and particularly HPAM operates in oil displacement mechanisms by increasing the macroscopic displacement efficiency. Its application may then be considered for unfavorable mobility ratio waterfloods or in reservoirs with high heterogeneity [16]. Polymers can act through two mechanisms:

- mobility control: polymer viscosity changes fluid flow patterns in the reservoir;
- conformance improvement: reduces the effects of high permeability layers in vertically stratified system which reduces watercut and improves sweep efficiency.

In order to evaluate the improvement brought by the addition of polymer compared to the sweeping obtained by simple water injection (in the case of secondary recovery), it is necessary to introduce the notion of the mobility ratio M [2] which is defined as the ratio between the mobility of the displaced fluid, oil (λ_o) and that of the displacing fluid, water (λ_w), the mobility of a fluid being defined by its ability to flow in a given medium:

$$M = \frac{\lambda_w}{\lambda_o} = \frac{k_{rw}/\eta_w}{k_{ro}/\eta_o} \tag{1.1}$$

Where η is the fluid viscosity and k_r the relative permeability of oil (index o) or water (index w).

When water is injected in a porous medium, a part of oil is not displaced. It is either overstepped by water (digitation effects) or trapped in pores due to their small size and/or the oil's affinity for the rock (capillary effects). The overstepping is mainly due to an "unfavourable" mobility ratio, which is the case when $M > 1$ [15]. In this case, the displacing fluid is moving "faster" than the displaced fluids, the phenomenon of viscous fingering occurs and makes the sweeping ineffective, leading to a very low recovery. When the mobility ratio is less than or equal to 1 ($M \leq 1$) the displacing fluid moves slower, allowing efficient sweeping and thus significant recovery [17]. As a result, by adding polymer, the viscosity of the displacing fluids increases, thereby improving the mobility ratio M.

1.2.2 Surfactant

Surfactants or surface active agents are originally thought of as detergents or wetting agents (reservoir wettability alteration). However, since one of the main parameters influencing oil recovery is oil/brine interfacial tension (IFT), most of the EOR surfactants are mainly used in order to reduce the IFT.

1.2.2.1 Types of surfactants for EOR

Surfactants are amphiphilic molecules, i.e. composed of a hydrophobic group, the "tail" that is often a hydrocarbon chain (straight or branched) and a polar hydrophilic group the "head" [15, 4] as shown in Figure 1.7. Surfactant molecules adsorb at fluid/fluid interfaces which leads to surface properties alteration; in particular, IFT reduction.

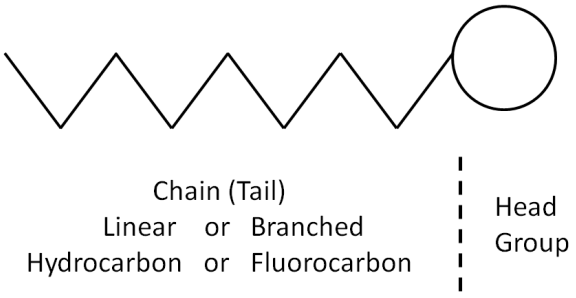

Figure 1.7 – Schematic of surface-active molecule [4]

Surfactants are categorized according to the ionic nature of the head group as anionic, cationic, nonionic, and zwitterionic [18, 16].

- Anionics: the hydrophilic head of the molecules in solutions is negatively charged, such as Sodium Dodecyl Sulfate (SDS) or Sodium DodecylBenzeneSulfonate (SDBS). They are the most common surfactants used in EOR as they present low adsorption on sandstone rocks whose surface charge is negative;

- Cationics: for example, quaternary ammonium salts. Positively charged, they can strongly adsorb onto anionic mineral surfaces (silica, clays) so they are generally not used in sandstones but can be used in carbonates to change wettability from oil-wet to water-wet;

- Nonionics: they generally serve as cosurfactants to improve salinity tolerance of anionic surfactants;

- Zwitterionics: they contain two active positive and negative groups and are temperature and salinity tolerant. They are expensive and therefore are not used in EOR processes.

Some of the most commonly used surfactants in EOR are: Internal Olefin Sulfonate (IOS), Alcohol Ethoxy Sulphate (AES), AlkoxyGlycidylEther Sulfonate (AGES) and AlkylBenzene Sulfonate (ABS).

1.2.2.2 Surfactant solutions in EOR systems

As mentioned before, surfactants are used to reduce the IFT between displacing fluids and oil. IFT is defined as the force per unit length required to create new surface area at the interface between two immiscible fluids [19]. If two immiscible fluids, an aqueous solution and a hydrocarbon phase for example, are brought into contact, and a surfactant is added to the system, surfactant molecules adsorb at the interface, they orient themselves such that the hydrophilic part is directed into the water phase and the hydrophobic part into the oil phase. This mechanism disrupts the fluid structure in the interfacial zone which leads to a rapid decrease of the IFT as the concentration of the surfactant increases up to the critical micelle concentration as shown in Figure 1.8. The CMC being the concentration at which micelles first occur: beyond which the IFT remains constant while the quantity of surfactant increases, which leads to the formation of aggregates (micelles) of surfactant while the concentration of isolated molecules in solution remains constant [20].

After briefly introduction the chemicals used in EOR (polymers and surfactants) and their respective contributions in the improvement of oil's displacement efficiency, we will present in the next section the chemical flooding applied to low permeability reservoirs.

1.3 Chemical flooding in low permeability porous media

In this section, we will focus on the application of chemical EOR in low permeability reservoirs (between 10 and 100mD). First, we will present experience from field application. Then, we will list challenges related to the application of chemical flooding in this range of permeability and cite some suggested solutions from the literature.

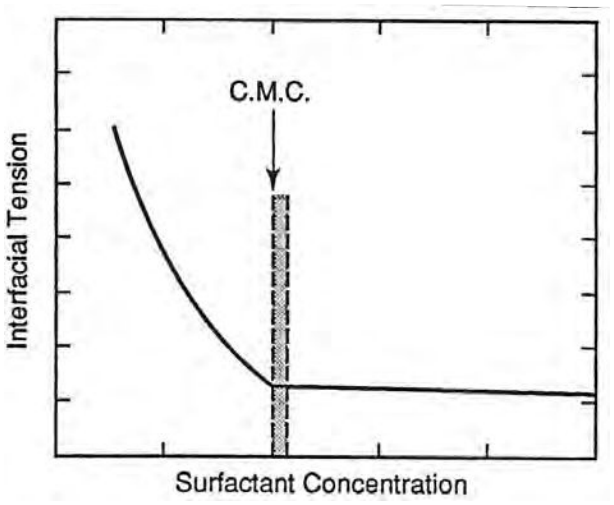

Figure 1.8 – IFT as a function of the concentration of a single-component surfactant [4], with the arrow pointing to the CMC

1.3.1 Experience from field applications

Chemical EOR processes are currently used in low permeability reservoirs, but although several pilots have been successful for chemical injection, transport problems have been observed such as in Big Muddy and Isenhour fields shown in Table 1.1 [14].

Table 1.1 – Chemical EOR projects - tests data [14]

Field	Permeability (md)	Process	Injectivity test	Injectivity issues	Hydraulic fractures	Successful
North Ward Estes	3-47, 25 avg.	A	N	N	N	Y
West Burkburnett/ Wichita County Regular	<159, 53 avg.	SP	N	N	Y	Y
Big Muddy (Pilot)	56 avg.	SP	N	N	N	Y
Big Muddy (Demonstration project)	56	SP	N	Y	N	Y
Isenhour	21	AP	N	Y	Y	Y
Triangle U	3-77 , 15 avg.	W	N	N	N	Y
Slaughter	1-25, 6 avg.	SP	N	Y	N	Y
Bothamsall	6	S	Y	Y	Y	Y
Chao-522	19	S	N	N	N	Y
UNKNOWN	4	SP	N	N	N	Y

Three types of challenges can be encountered when injecting polymers and surfactants in low permeability reservoirs: injectivity and in-depth transport problems, polymers and/or surfactants retention and polymer degradation. In the following section, we will present in details a literature review of challenges related to chemicals flooding in low

permeability porous media.

1.3.2 Related challenges

1.3.2.1 Properties of fluids transport in porous media

Poiseuille flow of a viscous fluid If we consider the flow of a fluid of viscosity η in a capillary tube of radius R , length L as shown in Figure 1.9, the flow velocity for a cylindrical element of length dz and radius r, subject to a pressure gradiant $\frac{dP}{dz} < 0$, is given by Hagen-Poiseuille's law as follows:

$$v(r) = \frac{dP}{dz}\frac{R^2}{4\eta}((\frac{r}{R})^2 - 1) \tag{1.2}$$

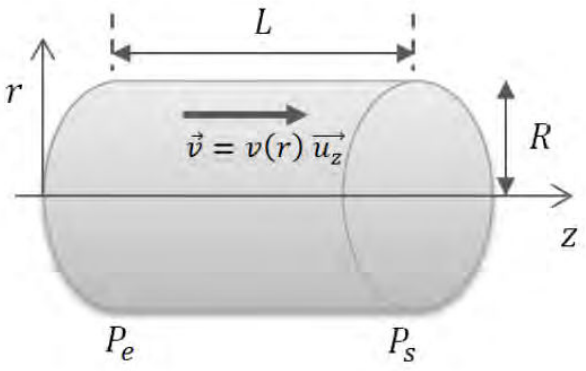

Figure 1.9 – Schematic of the capillary tube

And the flow rate by:

$$Q = \int v(r)dA = \frac{\pi}{8\eta}\frac{\Delta P}{L}R^4 \tag{1.3}$$

Where A is the capillary section: $A = \pi R^2$ and ΔP the pressure drop between the inlet and the outlet of the considered section $\Delta P = P_e - P_s$.

For a porous medium modeled by a set of n parallel capillaries of uniform radius R and identical length L, the flow rate is given by the following equation:

$$Q = n\frac{\pi}{8\eta}\frac{\Delta P}{L}R^4 \tag{1.4}$$

By combining this equation with Equation 3.3 for a porous medium of section S , permeability can be defined by:

$$k = n\frac{\pi R^4}{8S} \tag{1.5}$$

Considering the definition of porosity given earlier, it can be defined in this case by the ratio between the volume occupied by the capillaries and the total volume of the porous

media, written as follows:

$$\phi = \frac{n\pi R^2}{S} \tag{1.6}$$

By combining equations 1.5 and 1.6, porosity ϕ , permeability k and pore radius R are linked by the following formula:

$$R = \sqrt{\frac{8k}{\phi}} \tag{1.7}$$

For a real porous medium, this equation is multiplied by a prefactor α that has been determined by *Chauveteau* [21] and found equal to 1.15 for granular porous media.

Poiseuille's law also helps determine the wall shear rate $\dot{\gamma}_{wall}$ considering the maximum velocity in the middle of the cylinder (at $r = 0$), which can be written:

$$\dot{\gamma}_{wall} = \frac{2V_{max}}{R} = \frac{4 < v >}{R} = \frac{4}{\pi R^3} Q \tag{1.8}$$

With V_{max} and $< v >$ are respectively the maximum and the average flow velocities.

Flow properties of chemicals in porous media Describing the flow of polymer solutions in a porous medium requires the introduction of two dimensionless physical quantities: mobility reduction also called resistance factor R_m and permeability reduction or residual resistance factor R_k .

Mobility reduction is defined as the ratio between the brine mobility $(k/\eta)_{brine}$ and that of the polymer solution $(k/\eta)_{polymer}$ and is assimilated to the apparent viscosity of the polymer solution in the porous medium.

Based on Darcy's law (Eq. 3.3), and considering $\Delta P_{ref\ brine}$ as the reference pressure drop in the porous medium during brine injection, and $\Delta P_{polymer}$ the pressure drop in the porous medium during the injection of a polymer solution (prepared in the same brine) at the same injection rate, the mobility reduction is defined as follows:

$$R_m = \frac{(k/\eta)_{brine}}{(k/\eta)_{polymer}} = \frac{\Delta P_{polymer}}{\Delta P_{ref\ brine}} \tag{1.9}$$

During polymer injection, *Gogarty* [22] showed that a transient phase in which the polymer is retained either by mechanical entrapment or adsorption (mechanisms detailed in Section 1.3.2.3) precedes the pressure stabilization in the porous medium.

The presence of polymer irreversibly retained in the porous medium (a fraction of the initial polymer concentration) induces a permeability reduction R_k, defined as the ration between the reference permeability of the medium and its permeability after polymer injection and is expressed as follows:

$$R_k = \frac{k_{reference}}{k_{post-injection}} = \frac{\Delta P_{post-injection}}{\Delta P_{ref\ brine}} \tag{1.10}$$

Where $\Delta P_{ref\ brine}$ and $\Delta P_{post-injection}$ are respectively the pressure drop during brine

injection before and after polymer injection.

1.3.2.2 Injectivity and in-depth propagation

Problems such as poor injectivity and in-depth propagation can lead to the generation of high pressures and plugging of the core.

According to *Fletcher et al.* [23], the five factors influencing polymer plugging are: volume injected per cross section of area, core permeability, hydrodynamic size of the polymer, core mineralogy and surface state.

Treiber et al. [24] insisted that the hydrodynamic size of the polymer molecule must not exceed the pore-throat size associated with the porous medium. Later on *Sheng* [15] concluded that for low permeability rocks, low molecular weight polymer should be used as the high molecular weight polymer may cause injectivity problems. However, on economics level, the disadvantage of using low molecular weight polymer is that it requires higher concentration for an equivalent viscosity [14].

For polymer, the presence of debris, microgels or any other impurity impacts the injectivity. Filterability tests with different filters and polymer solutions have been carried out and have shown that it is possible to achieve good injectivities for the "cleanest" polymer solutions, i.e. cleaned of all their impurities [25]. Hence the importance of planning a filtration step for polymer solutions before their injection into the porous medium, where the pore diameter of the selected filter should not exceed the average pore radius in the porous medium.

Polymer rheology also plays an important role in the quality of injectivity. Indeed, an increase in polymer viscosity due to elongational deformations in porous media might occur (generally not taken into account initially). In this regard, it has been shown that an optimal polymer viscosity can be found by checking that it is not too high to cause injectivity problems and that the mobility of the polymer solution remains lower than the mobility of deplaced fluids, i.e. residual oil and water [5]. Therefore, the mobility condition to be verified is the following:

$$(\lambda_{rw})_{slug} < (\lambda_{rw} + \lambda_{ro})_{bank} \tag{1.11}$$

Where $(\lambda_{rw})_{slug}$ is the displacing fluid mobility, i.e. the injected formulation, and $(\lambda_{rw} + \lambda_{ro})_{bank}$ that of the displaced fluids: the water and oil supposedly in the form of a bank.

Thus, the mobility of the injected fluid must not exceed the minimum value of the relative mobility of the displaced fluids.

In Figure 1.10 is represented the relative mobility of the formulation for several viscosities as a function of water saturation, where the red line corresponds to the minimum value of the relative mobility of displaced fluids

In the same study, a specific value of polymer concentration was determined, beyond which an early clogging is observed. This critical concentration varies according to the conditions of the porous medium (e.g. mineralogy, permeability) as well as experimental parameters (e.g. salinity, temperature). A compromise must then be found between a viscosity sufficient enough to maintain a good mobility ratio throughout the experiment,

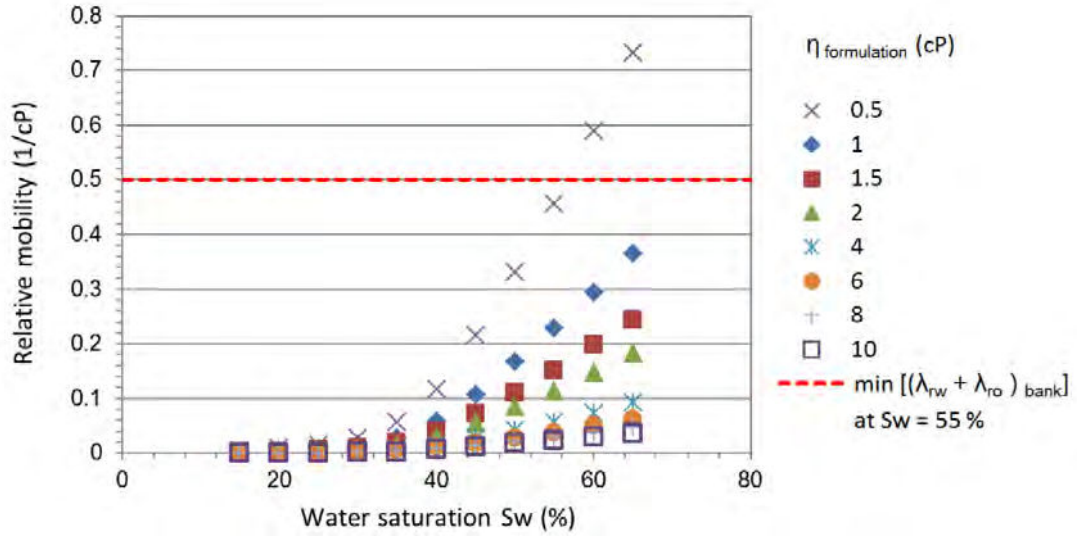

Figure 1.10 – Relative mobility of the formulation slug for different viscosities as a function of water saturation [5]

and a concentration below the critical concentration.

Regarding core properties, it has been shown that injectivity is a function of permeability [23, 26]. In fact, for low permeability reservoirs, several studies [14, 27, 24, 8] recognized plugging risks and injectivity issues. They also noted the importance of the pore structure and size distribution as well as permeability on the injectivity quality.

One of the major challenges impacting the quality of polymer transport in low permeability porous media is permeability reduction R_k. In fact, an increase of permeability reduction with the decrease of permeability has frequently been reported [8, 28].

Injectivity and in-depth propagation problems are often a consequence of permeability change due to polymer retention: adsorption or steric effects.

1.3.2.3 Retention

Chemicals retention is one of the major problems in chemical EOR processes in general and in low permeability reservoirs in particular, due to the small amount of free molecules (not retained in the porous medium) that can play their roles. This requires injecting higher amounts of chemicals, thereby impacting the project's economy and creating a significant potential for injectivity problems.

Polymer

For polymer, among the different types of retention, the most common is adsorption which becomes significant in the presence of clay, then steric effects such as jamming effect or mechanical entrapment of molecules, then hydrodynamic retention in the case of high injection rates [3, 2]. These retention mechanisms are schematized in Figure 1.11 [6].

In typical studies on polymer transport in porous media, retention is quantified by per-

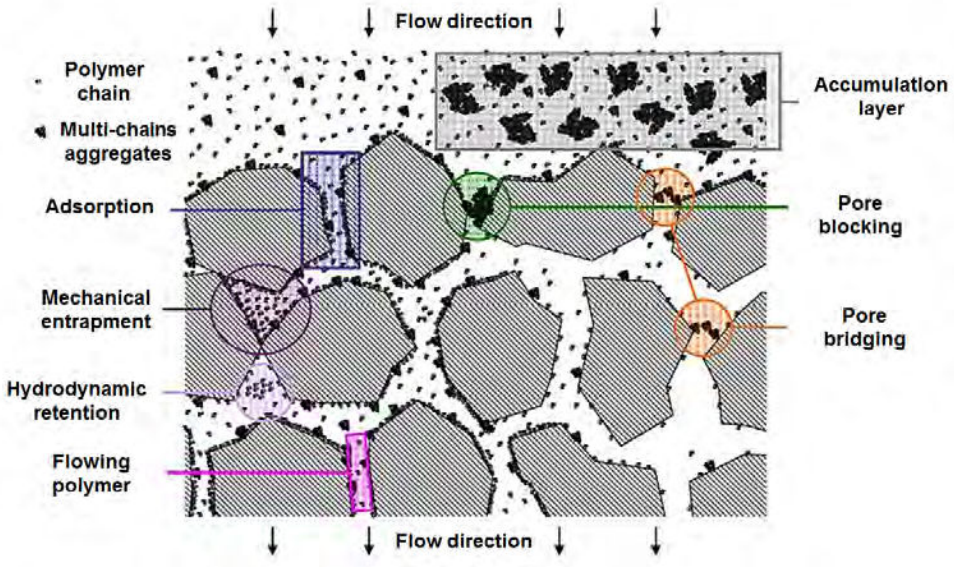

Figure 1.11 – Retention mechanisms potentially involved during polymer injection in a porous medium, adapted from [6]

forming material balance (between the injected and the collected quantity downstream the porous medium). Retention is often associated with the adsorption of polymer on pore surfaces. Actually, adsorption refers to the interaction between polymer molecules and the solid surface by physical adsorption, van der Waals forces, and hydrogen bonding [15] where polymer essentially occupies surface adsorption sites. However, *Lakatos et al.* [29] have shown that there are significant differences between the level of static HPAM adsorption and dynamically retained level in a porous medium. They related the differences to the changes in the specific surface area of consolidated and unconsolidated packs and also the accessibility of certains portions of the pore space. Similarly, *Szabo* [30] showed that HPAM adsorption on silica flour, measured in static bulk adsorption was significantly higher than that on sand pack, estimated using dynamic flow test, as the accessible surfaces in silica flour are higher than that in the sand pack. In addition, when estimating the adsorption by unit of specific surface area, the results from the two types of measurements were almost the same.

Consequently, polymer corefloods cannot be compared to powder adsorption tests such as those that provide adsorption isotherms. In fact, in long injection experiments, the available rock surface is exposed to an "infinite" amount of polymer, since the injected solution is constantly renewed. Under these conditions, the amount of adsorbed polymer in a porous medium is not expected to depend on the injected concentration.

However, *Zhang & Seright* [7] have shown that polymer adsorption increases with injected concentration (Figure 1.12). These results suggest that the injection of a long slug of a dilute polymer solution ($10-100ppm$), long enough to satisfy adsorption, before the injection of the main slug (generally in the semi-diluted or concentrated regime ($100-10000ppm$), could significantly reduce adsorption.

Another parameter influencing polymer adsorption is salinity. In fact, *Martin et al.*

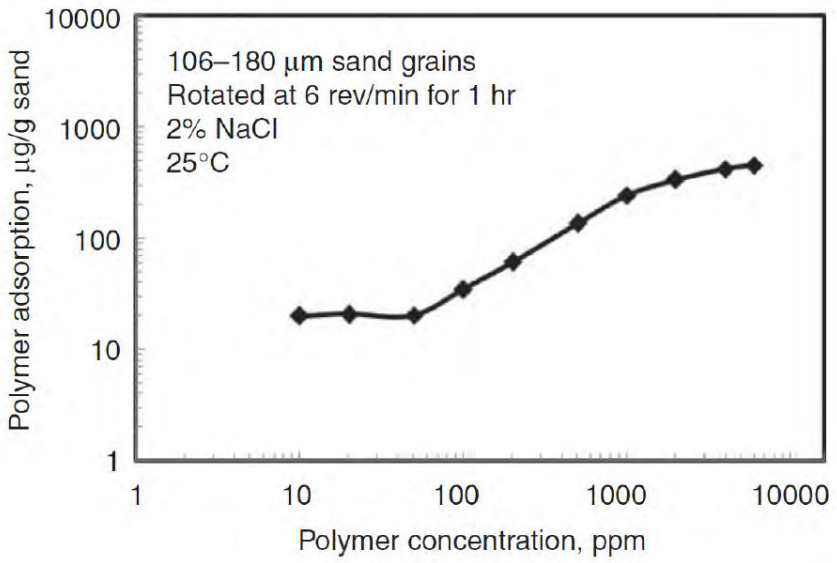

Figure 1.12 – HPAM adsorption as a function of polymer concentration [7]

[31] observed an increase in polymer adsorption with increased salinity ($NaCl$) for different types of polymer. Similarly, *Smith* [32] showed an increase in HPAM adsorption on silica in the presence of divalent calcium ion Ca^{2+}. Actually, the presence of divalent cations leads to the reduction of HPAM molecules' size and also the reduction of the static repulsion between carboxyl groups and silica surfaces.

In general, polymer adsorption is considered irreversible as it does not decrease with the decrease of polymer concentration [30, 33]. Although prolonged exposure to water or brine injection can help desorbing polymer, the rate of polymer retention is generally much higher than the rate of polymer removal.

In the case of mechanical entrapment, studies have highlighted that the significance of this type of retention depends on the pore size distribution [34, 3] thus showing that it is a more likely mechanism for polymer retention in low-permeability formation. Similarly, *Vela et al.* [8] showed that HPAM retention decreases with permeability increase in Berea sandstone as shown in Figure 1.13, suggesting then that mechanical trapping in a low-permeability rock is higher than that in a high-permeability rock.

For hydrodynamic retention, *Chauveteau & Kohler* [35] stated that it is flow rate-dependent as the total level of retention increases when the flow rate is increased. The mechanisms of this retention are not fully understood and generally contribute marginally to the total retained polymer [2].

Surfactant

So far, few surfactants injectivity problems have been reported in the literature. However, strong pressure build-ups were observed during long surfactant injections [36], but the causes are not all yet well known.

The main problem encountered during surfactant injections is retention and more

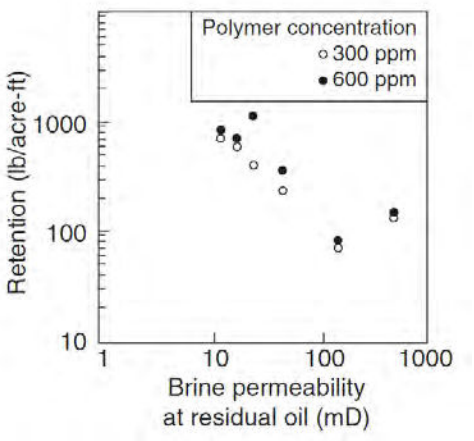

Figure 1.13 – Variation of HPAM retention with initial brine permeability of a Berea sandstone [8]

specifically adsorption. In this regard, it has been shown that increased salinity induces higher adsorption [9] as shown in Figure 1.14. Consequently, the application of a salinity gradient (of lower salinity) would help desorbing the adsorbed surfactant [5].

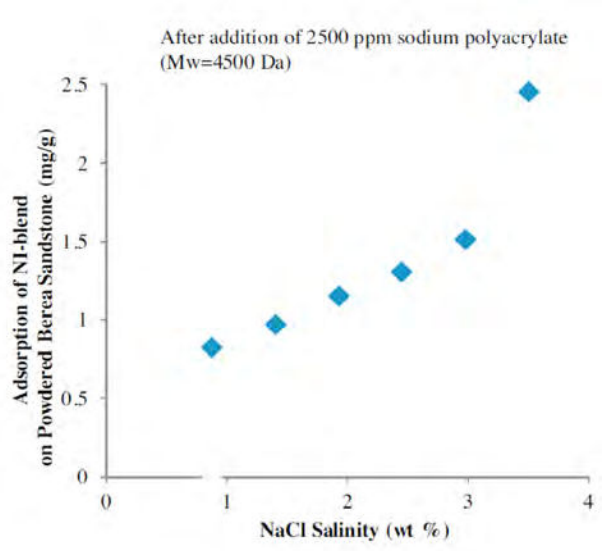

Figure 1.14 – Salinity effect on the adsorption of NI-blend surfactant on Berea sandstone [9]

The surfactant chemistry also plays an important role in reducing adsorption. In fact, for nonionic surfactants, a high degree of ethoxylation could induce an increase in the surface area of the surfactant's polar part, which would reduce adsorption in sandstones [37]. Using time resolved fluorescence techniques, the structure of the adsorbed layer for two nonionic surfactants of different degrees of ethoxylation was analyzed and showed that the size of adsorbed aggregates highly depends on the structure of surfactant's polar part.

In other studies, it has been suggested that the addition of additives such as sodium polyacrylate [9] or silica nanoparticles [38] would significantly reduce adsorption.

1.3.2.4 Degradation

Polymer degradation is defined as the change in its physical and/or mechanical properties (chain splitting for example) caused by more or less aggressive environmental factors such as chemical attack or mechanical stress. Both mechanical and chemical degradations induce a significant decrease in polymer viscosity which leads to poor sweeping of the reservoir.

Mechanical degradation can be attributed to high deformations (high shear rates) due to small pore throats and/or high injection rates, while chemical degradation is generally caused by the presence of iron ions with oxygen in the porous medium [15]. It has been shown that polymers with high molecular weight are most likely to degrade [14], especially mechanically.

In contrast, it has been shown that the application of moderate mechanical degradation of the polymer around the injection well (without significantly affecting viscosity) would lead to an improvement in polymer injectivity [39].

In this study, we will avoid problems of chemical degradation (lack of iron and moderate temperature). As for mechanical degradation problems, they will be controlled by viscosity measurements at the outlet of the porous medium.

1.3.2.5 Rock-polymer interaction

Silica minerals

In their study on polyacrylamide adsorption on siliceous minerals, *Lecourtier et al.* [40] have shown that what governs the adsorption of HPAM on siliceous minerals is a competition between attractive interactions between polymer and minerals surfaces and repulsive electrostatic forces, thus, it is salinity and pH-dependent. For salinities lower than 1 M NaCl, and due to charge screening, an increase in HPAM adsorption with increased salinity has been observed. For pH dependence, they showed a significant decrease in HPAM adsorption with pH increase, which was attributed to the increase in electrostatic repulsion between polymer and surface, since both polymer and the mineral surface charges increase with pH.

Clay minerals

The interaction between polyacrylamide and clay surfaces is very complex as electrostatic, hydration, van der Waals and other forces can operate simultaneously [41]. For neutral polyacrylamide, the main force responsible for the adsorption of polyacrylamide on alumino-silicate is hydrogen bonding. For hydrolyzed polyacrylamide, charge-charge interactions add to the effects of hydrogen bonding to change the amount of adsorbed polymer and adsorption kinetics. In fact, the strong affinity of hydrolyzed polyacrylamide for positively charged surfaces leads to interfacial spreading of the adsorbed molecules. In

the case of complexed polyacrylamide, the presence of chain segments of different charges give the polymer chain an amphoteric character.

In the context of this thesis, a study on clay-polymer suspensions was carried out in terms of particle size, turbidity and eletrophoretic mobility for various clays (kaolinite, illite and smectite) and different polymer concentrations and ionic strengths [42]. Results from this study showed that HPAM shifts the critical coagulation concentration to higher values. In addition, clay-polymer interaction was only slightly influenced by the ionic strength and no major differences were observed with regard to the clay type. Furthermore, the eletrokinetic mobility of the polymer was not affected in the presence of clay, which suggests the incorporation of clay particles into polymer aggregates.

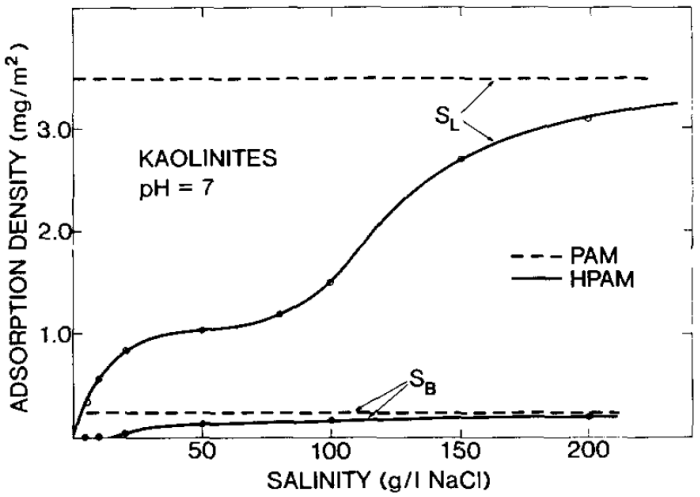

Figure 1.15 – Adsorption densities of PAM and HPAM on lateral and basal surfaces versus salinity [10]

For kaolinite *Lee et al.* [10] have observed for anionic polyacrylamides an increase in the adsorption density on kaolinite lateral surfaces with salinity in two steps as shown in Figure 1.15. The first increase was explained as a result of the screening of electrostatic repulsions between polymer and kaolinite surface where a pseudo plateau is observed around $1\,M$ NaCl. The second increase observed beyond this value, is attributed to cation condensation on the polymer and eventually on kaolinite surface, leading to charge neutralization and thus to an adsorption density equivalent to that of neutral polyacrylamide. The differences in adsorption density on lateral and basal surfaces are due to the weak negative charge of basal surface.

For illite, *Long et al.* [43] have shown that HPAM addition to illite-illite systems leads to strong bridging adhesion force and flocculation between illite particules as well as immediate settling.

1.4 Research motivation and thesis outline

Based on results and conclusions drawn from the literature, several challenges are encountered during the application of chemical EOR using polymer and/or surfactant in low permeability porous media ($10 - 100\ mD$). In fact, chemicals retention as well as poor injectivity and in-depth fluid propagation are frequently observed for these porous media, mainly due to their mineralogy naturally clay-rich and also to their permeability and complex pore structure. These problems involve high risks of formation damage but also present considerable economical and environmental challenges due to the use of large quantities of chemicals. Therefore, the understanding of mechanisms governing this processes is of great importance in order to optimize the use of chemical EOR in this range of permeability.

The main motivation of this study is thus to prioritize the parameters influencing the chemicals transport in low permeability porous media. For that, we will study characteristics of the porous medium (mineralogy, permeability), the injected fluids (salinity, concentration, viscosity) or the injection conditions (temperature, flow rate) according to their degree of influence on fluids transport mechanisms.

To this end, we chose to base our study on synthetic granular porous media composed of quartz sand grains and various clays (kaolinite, illite and smectite). In this way, the experiments can be simplified, the effects of each mineral phase can be better understood and the complexity and heterogeneities as well as lithological and textural variations of natural rocks can be avoided as much as possible. Meanwhile, the fundamental challenge is to ensure the reproducibility of these experiments in order to improve results comparison. In terms of experimental methods, injection tests will be carried out with the development of new procedures allowing working with different porous media and fluids then collect data that can be analyzed afterwards.

First (in Chapter 2), we will study polymer solutions characteristics. For that we will present theoritical backgroung on polymer's physical chemistry, then detail preparation and characterization methods, and finally obtained results that allowed us to select the parameters for injection tests. In Chapter 3, we will present used porous media starting by the characteristics of low permeability porous media, then the preparation and characterization procedure and finally characterization results. The last part, Chapter 4, will be dedicated to polymer injection experiments in porous media. We will first present the experimental set-up and procedure, then experimental observables and finally results analysis.

Chapter 2

Polymer solutions

Contents

In order to study the transport properties of polymers in porous media, we prepared and characterized polymer solutions of different characteristics. In this chapter we will first present theoretical background of polymer solutions physical chemistry, then materials and methods used to prepare and characterize the solutions and finally characterization results and discussion.

2.1 Polymer solutions physical chemistry

Polymers or macromolecules are generally formed by the linear repetition of a group of atoms called monomer. The particularity of polymers, which is responsible for their mechanical and physicochemical properties, is that their configuration is not defined. In fact, depending on the conditions, polymer configuration can take a wide variety of forms [44], varying from a completely coiled to a fully stretched chain. The conformation of polymer chains can vary widely depending on its environment and the flow history. For these reasons, we will present in this section the theoretical principles of the behavior of polymers chains in solution, polymer solutions rheology and general insights on polyelectrolyte solutions.

2.1.1 Polymer chains in solution

In order to analyze the polymer chains behavior in solution, it is important to first introduce concentration regimes.

Dilute regime For the dilute regime, polymer chains are considered to be sufficiently far from each other so that there are no inter-chain interactions. In this regime, the mean size of a polymer chain in solution is characterized by its radius of gyration R_g which is a statistical property defined as the root mean square of the distances between each monomer and the chain's center of mass. It can be defined as a function of N the number of monomer units and b the persistence length of the polymer chain as follows:

$$R_g = \frac{b\sqrt{N}}{\sqrt{6}} \tag{2.1}$$

Since the conformation of a polymer chain is not static but dynamic, it is sensitive to external stresses (thermal, mechanical). It can thus be assimilated to an elastic body that can deform under the effect of external stresses and when these stresses stop, the chain relaxes its deformation and returns to its equilibrium state [45].

Several theoretical models have been developed to describe the dynamic properties of dilute polymer solutions. They can be used to determine the characteristic properties of the polymer in solution such as the diffusion coefficient and the intrinsic viscosity.

Zimm's model [46], among others, takes into account hydrodynamic interactions, i.e. the solvent counterflow caused by the movement of a chain that modifies the movement of other chains. This model helps determine the diffusion coefficient of chains D expressed as follows:

$$D = \frac{k_B T}{\eta_s R_g} \tag{2.2}$$

Where k_B is Boltzmann constant, T the temperature, η_s the solvant viscosity and R_g the radius of gyration of the chain.

In this model, it is implicitly assumed (Kirkwood approximation [47]) that the hydrodynamic behavior of the polymer chain could be described by its static configuration. The diffusion coefficient is actually related to the hydrodynamic size of the polymer chain and is defined according to the Stokes-Einstein equation [48] as follows:

$$D_0 = \frac{k_B T}{f_0} = \frac{k_B T}{6\pi\eta_s R_h} \tag{2.3}$$

In this model, polymer chains behavior is assimilated to that of rigid spheres of hydrodynamic radius R_h , with f_0 the macromolecule friction coefficient. In reality, polymer chains do not exist as hard spheres, so the estimated hydrodynamic radius actually reflects the apparent size of the molecule in solution. Experiments show that the ratio R_h/R_g is equal to 1 in theta solvent, where polymer coils act like ideal chains, and is about 3/5 in good solvent, where polymer coils expand [45]. R_h and D_0 can be determined using Dynamic Light Scattering experiments, a technique detailed in Section 2.2.2.2.

Overlap concentration As the polymer concentration increases, the average distance between two macromolecular coils decreases. Interactions between polymers become stronger and the limit of the dilute regime is reached when the volume fraction occupied by macromolecules, φ , is around 1 [49] considering φ as the hydrodynamic volume:

$$\varphi = \frac{4}{3}\pi \frac{C}{N_A\, M_w} R_h^3 \tag{2.4}$$

Where C is polymer concentration, N_A Avogadro's number and M_w polymer's molecular weight.

At this point, the polymer chains are in contact with each other and by continuing concentration increase, polymer coils interpenetrate. The overlap concentration C^* can then be defined by:

$$C^* = \frac{3N_A M}{4\pi R_h^3} \tag{2.5}$$

Semidilute regime When the concentration is higher than C^*, the macromolecules are in contact and the solution is considered semidilute. The transition from dilute to semidilute regime is in general not sudden but progressive. This regime can be subdivided into two additional regimes: the nontangled and the entangled semidilute regime separated by a second critical concentration noted C^{**} . Generally, the ratio between the two critical concentrations C^{**} and C^* is estimated to be around 10 [49].

In Figure 2.1, a schematic representation of polymer solution in the different concentration regimes is shown.

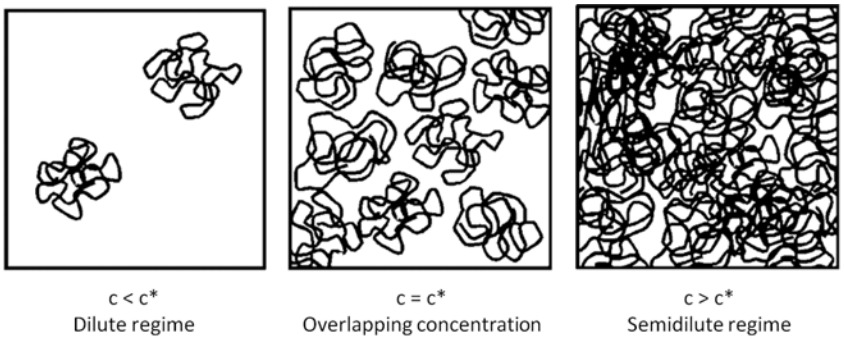

Figure 2.1 – Behavior of polymer chains in solution as a function of concentration [11]

As mentioned in Chapter 1 (Section 1.2.1), in this work, we focus on the study of HPAM. In the following section, we will present general background on polyelectrolyte solutions that are of interest for our study.

2.1.2 Polyelectrolyte solutions

2.1.2.1 Rheology

In general, three regimes are used to describe the rheological behavior of polymers: the Newtonian regime where viscosity is independent of shear rate, the shear thinning regime where viscosity decreases as the shear rate increases and the shear thickening regime where viscosity increases with shear rate increase.

In the particular case of HPAM, due to its relatively high flexibility, this polymer is likely to deform when subjected to shear rate. By analyzing the rheological properties of HPAM solutions in dilute and semidilute regimes, and in particular the variations of their viscosity with shear rate, two deformation regimes can be distinguished:

The Newtonian regime which corresponds to low shear rates where macromolecules are in their statistical coil conformation and are subjected to rotation without change in conformation. In this regime, viscosity is independent of shear rate.

The shear thinning regime which corresponds to high shear rates where macromolecules are either deformed or oriented along the flow direction. The size of polymer coils decreases, which leads to a decrease in viscosity as the shear rate increases. The shear thinning effect is particularly pronounced for polymers of high molecular weight.

These two regimes are observed in particular in pure shear flows, e.g. rheometer, where the shear rate is perpendicular to the flow direction. In the case of elongational flows, e.g. flow in porous media, the shear rate can also be parallel to the flow direction and the deformation can be very high for high flexibility polymers. A total stretching of polymer chains can be reached when macromolecules are subjected to elongational deformations for a sufficient period of time, exposing a larger number of monomers to flow which increases monomer-solvent friction and thus the solution's viscosity [39]. A third regime is then observed in the range of high shear rates: **the shear thickening regime**.

For polymer solutions, in addition to viscosity, relative viscosity η_r is an important parameter in enhanced oil recovery operations. It is defined as the ratio between polymer solution viscosity $\eta_{polymer}$ and that of its solvent, brine in this case η_{brine} :

$$\eta_r = \frac{\eta_{polymer}}{\eta_{brine}} \tag{2.6}$$

In order to study the conformation of polymer chains in solution, the intrinsic viscosity $[\eta]$ can be introduced to characterize the polymer. Intrinsic viscosity is expressed in cm^3/g and represents the ratio of the volume swept by the swollen macromolecules over its mass. It can hence be considered as the reciprocal of a "density in solution". It is practically determined by the Huggins equation [50] which links the reduced specific viscosity $\eta_{spr} = \frac{\eta_r - 1}{c}$ to the intrinsic viscosity as follows:

$$\eta_{spr} = [\eta] + K_H [\eta]^2 c + O\left(c^2\right) \tag{2.7}$$

Where K_H is the Huggin's constant and c the polymer concentration.

Huggins constant characterizes polymer-polymer and polymer-solvent interactions and provides an indication of the solvent quality. When K_H is small, the chains are stretched, thus occupying high volume whereas for high K_H the chains occupy a smaller volume. In theta conditions, $K_H = 0.5$. In the case of a good solvent, $K_H < 0.5$ and in contrast, when the solvent is of poor quality $K_H > 0.5$. It should be noted that high K_H values ($K_H > 1$) can be obtained experimentally when there are strong attractive interactions between polymer chains [51].

The intrinsic viscosity is determined from viscosity measurements extrapolated to zero concentration (dilute regime) as follows:

$$[\eta] = \lim_{c \mapsto 0} \eta_{spr} \tag{2.8}$$

For a dilute suspension of hard spheres, the intrinsic viscosity can be related to the spheres density ρ by Einstein's law:

$$\eta_r = 1 + 2.5\rho + O(\rho^2) => [\eta] = \frac{2.5}{\rho} \tag{2.9}$$

It is also possible to deduce the average molecular weight M of a macromolecule based on the intrinsic viscosity of the solution using the *Mark-Houwink-Sakurada* law [52]:

$$[\eta] = KM^{\alpha} \tag{2.10}$$

where K and α are the Mark-Houwink parameters that characterize the particular polymer-solvent system at a given temperature.

Polyelectrolytes are composed of monomeric units that include an ionizable group, i.e. a group that can dissociate in aqueous solutions into a cation or anion fixed to the chain and a mobile counter-ion having the opposite charge [11]. Presence of charges changes the polymer condition in a qualitative manner and leads to different solution properties. In particular, factors such as salinity and temperature can significantly affect solution's viscosity.

2.1.2.2 Effects of salinity

For HPAM for example, when dissolved in water the conter-ion (in our case Na^+) dissipates in water and backbone charges repel each other leading them to stretch occupying a certain hydrodynamic volume and resulting in a solution with higher viscosity compared to water's viscosity [15].

When a monovalent salt (e.g. $NaCl$) is added, polymer viscosity decreases as the salt cations $Na+$ neutralizes the carboxyl groups charges in HPAM side chains. This charge screening causes the reduction of repulsion within the carboxyl groups which decreases the hydrodynamic volume leading to a viscosity decrease.

When divalent salts (e.g. $CaCl_2$, $MgCl_2$) are added, the effect is more complex. The screening effect is more significant than that of monovalent species, as the divalent ions bind more tighly to the polyelectrolyte due to their higher charge and polarizability [2]. In the presence of divalent cations, the trends can be reversed as higher viscosities may be observed due to the electrostatic bridging interactions between chains.

2.1.2.3 Effect of temperature

For temperature, it has been shown that the polymer solution apparent viscosity decreases with temperature. In fact, as the temperature increases, polymer chains activity seems to be enhanced and the friction between molecules to be reduced. Thus, the flow resistance is reduced and the viscosity decreases. [15]

In the following sections, we will first present materials and methods used to prepare and characterize polymer solutions used in this study, then characterization results obtained for different parameters, in particular salinity.

2.2 Materials and methods

2.2.1 Preparation

The preparation of polymer solutions consists of dissolving polymer powder in brines of various characteristics.

2.2.1.1 Brines

Salts used in this study for brine preparation are sodium chloride ($NaCl$) and calcium chloride ($CaCl_2, H_2O$) respectively provided by *Fisher Chemical* and *Merck KGAa*. Salts are first dissolved in distilled water, the solution is then filtered using a Millipore filter of $0.22\mu m$ estimated pore diameter and degassed under vacuum and agitated for at least $30min$.

Brines used are defined by two parameters: ionic strength I and hardness R^+ .

Ionic strength I is a chemical parameter used to evaluate the activity of ions in aqueous solution. It is expressed in mol/L and is defined by:

$$I = \sum_i C_i z_i^2 \tag{2.11}$$

With C_i the molar concentration of the ion i and z_i its charge.

Hardness can be defined as the mass fraction of divalent cations in solution expressed in percentage (%):

$$R^+ = \frac{\sum divalent\ cations}{\sum total\ cations} = \frac{Ca^{2+}}{Na^+ + Ca^{2+}} \tag{2.12}$$

In the following, brines will be noted $SI - R+$. For example, a brine of an ionic strength $I = 1mol/L$ and a hardness $R^+ = 20\%$ will be noted $S1 - 02$.

2.2.1.2 Polymer solutions

For this study, the polymer used is a conventional partially hydrolyzed polyacrylamide (HPAM) Flopaam 3130S provided by *SNF-Floerger*. This polymer is among the EOR polymers with the lowest molecular weight (M_w between 3 and $5MDa$) and is hence adapted for application in reservoirs with permeability lower than 100mD. The degree of hydrolysis of this polymer (fraction of carboxylates) is between 27 and $32\%mol$.

HPAM solutions are prepared by gradually adding polymer powder to the brine under high agitation, then left overnight under minimum agitation to allow a good dissolution of the polymer without degradation.

Before its injection in the porous media, polymer solutions are filtered in order to remove debris and microgels. Filtration is carried out under imposed flow rate conditions using a volumetric pump with a SPI-Pore filter having a pore diameter of $1\mu m$ and at a rate of $70mL/h$, corresponding to an interstitial velocity of $50m/day$. The choice of the pore diameter was made so as not to exceed the average pore radius in the porous medium, estimated between 1.2 and $1.8\mu m$ for permeabilities between 50 and $100mD$ (Equation 1.7). The viscosity of the polymer solutions was checked during filtration to ensure that the process induces no viscosity loss as shown in Figure 2.2.

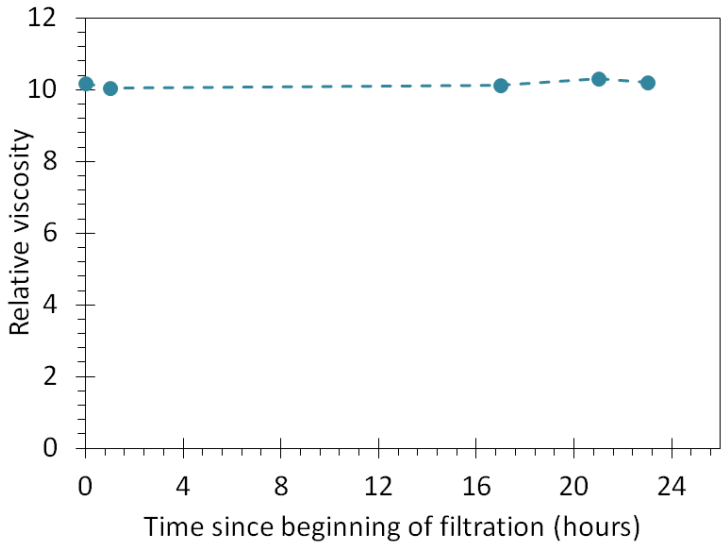

Figure 2.2 – Evolution of a polymer solution's relative viscosity during filtration (brine S1-0)

2.2.2 Characterization

To characterize the fluids, we mainly focused on the evaluation of the density in solution and inter-chain interactions using viscosity measurements as well as the qualitative assessment of the hydrodynamic size.

2.2.2.1 Viscosity measurements

For viscosity measurements, we used a LS300 viscosimeter developed by *ProRheo* and designed to measure low viscosities at low shear rates. Measurements were conducted using a Couette-like geometry, shown in Figure 2.3, at a temperature of $40°C$ - which is the chosen temperature for coreflood experiments.

Figure 2.3 – Couette geometry: stator on the left and rotor on the right

For our solutions, measurements consist of performing, for a duration of $20min$, logarithmic shear ramps (ascending then descending in steps) for a shear rate range of 1 to

$100s^{-1}$, and measuring corresponding viscosity.

2.2.2.2 Dynamic Light Scattering

In addition to viscosity measurements, the hydrodynamic size of the polymer has been qualitatively estimated using Dynamic Light Scattering (DLS). DLS is a non-destructive technique based on the fluctuation of the light scattering induced by the Brownian motion of colloidal particles [53].

The method, as shown in Figure 2.4, is that a laser beam passes through the suspension and interacts with particles in solution.

The detector records, for a fixed angle of diffusion θ , the temporal fluctuations of the scattered light intensity I . Then, the correlator builds the temporal autocorrelation function of scattered light intensity G_2 , written as follows:

$$G_2(\Delta t; q) =< I_{(t)} I_{(t+\Delta t)} > \tag{2.13}$$

Where <> indicates time average, $I(t)$ and $I(t + \Delta t)$ the scattered light intensity at time t and $t + \Delta t$ respectively, and q the wave vector.

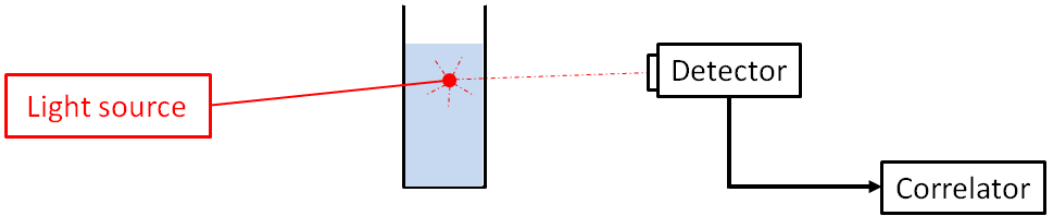

Figure 2.4 – Schematic of DLS method

According to Siegert's theorem [54], the autocorrelation function of the scattered light intensity is a function of the module of the standard aurocorrelation function of the electric field g_1 :

$$G_2(\tau, q) = \alpha + \beta g_1^2(\tau, q) \tag{2.14}$$

With α the baseline, β the correlation factor and τ the relaxation time.

The wave vector q is dependent on the diffusion angle θ and is written:

$$q = \frac{4\pi}{\lambda_0} n \sin\frac{\theta}{2} \tag{2.15}$$

Where n is the refractive index of the medium and λ_0 the wavelength of the light source in vacuum.

For a dilute suspension of Brownian and monodisperse particles, the relaxation of the electric field's autocorrelation function results in an exponential decay:

$$g_1(\tau) = exp(-Dq^2\tau) \tag{2.16}$$

For polydisperse suspensions, g_1 can be divided into a sum of decreasing exponentials:

$$g_1(\tau) = \sum_i A_i \exp(-D_i q^2 \tau) \tag{2.17}$$

Where A_i is the contribution in scattered light intensity of the particles of population i. [55]

For a suspension of spherical particles free of interactions and sedimentation, Stokes-einstein equation (Equation 2.3) is used to determine the hydrodynamic radius of a particle R_h based on its diffusion coefficient D_0.

In this study, DLS experiments were performed using an experimental set-up provided by *Cordouan Technologies*. The sample is illuminated by a laser beam (wavelength $\lambda_0 = 657nm$) and the intensity of the light scattered by particles in solution over time is collected at a fixed angle (90°) by an Avalanche Photodiode Detector (APD). Temperature was kept constant at $20°C$.

2.3 Characterization results

For viscosity measurements, in order to reproduce the brines used in EOR operations, namely: formation, fresh and sea waters, brines of different characteristics were used. Table 2.1 summarizes used parameters. For polymer, studied concentrations vary between 0.1 and $5g/L$.

Brine	[NaCl] (g/L)	[$CaCl_2$, $2H_2O$] (g/L)	TDS (g/L)	R^+ (%)	I (mol/L)
S1-0	60	0	60	0	1.03
S1-005	55.2	4.2	59.4	5	1.03
S1-02	42	15.15	57.15	20	1.03
S01-0	6	0	6	0	0.10
S01-005	6	0.44	6.44	5	0.10
S001-0	0.6	0	0.6	0	0.01
S001-005	0.55	0.04	0.59	5	0.01
S001-02	0.42	0.15	0.57	20	0.01

Table 2.1 – Summary of brine parameters used in viscosity measurements

Viscosity results presented in this section are based on the characterization carried out using the LS300 viscosimeter.

2.3.1 Relative viscosity

We first analyzed relative viscosity η_r. The flow curves of polymer solutions at different concentrations for two examples of brine, lowest $S001-0$ and highest salinity $S1-0$ among used brines, are shown in Figure 2.5.

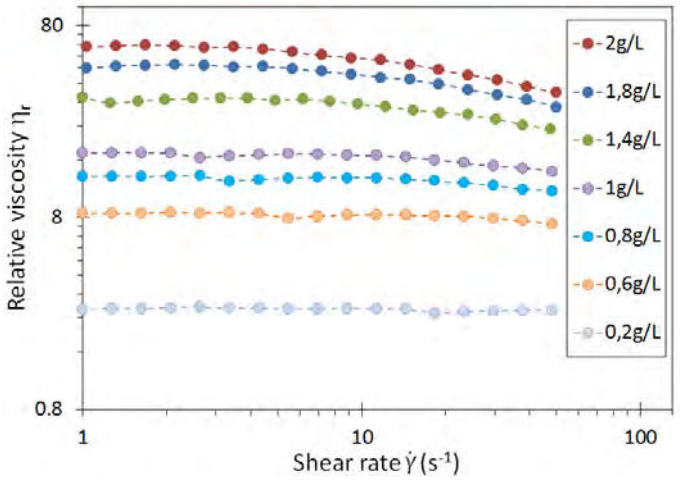

(a) S001-0

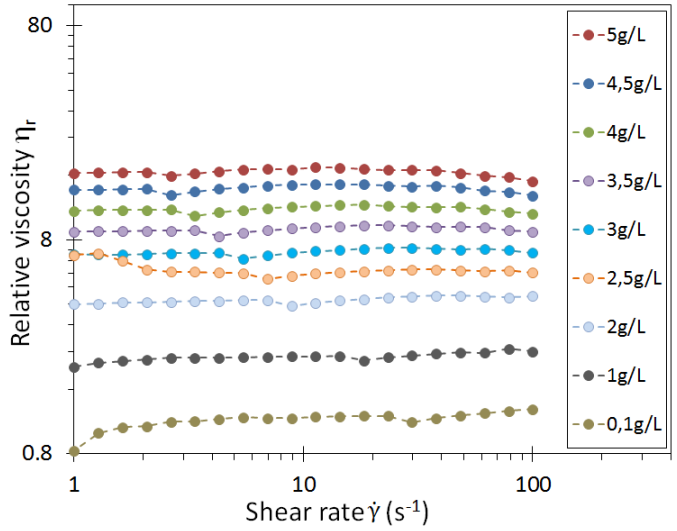

(b) S1-0

Figure 2.5 – Flow curves of HPAM Flopaam 3130S at different concentrations for two different brines

By comparing the different curves, the first observation is that for the same brine, there is an increase in the relative viscosity with polymer concentration These results are not surprising since the increase in polymer concentration leads to an increase in viscosity. For the same concentration, a decrease in relative viscosity with shear rate is observed beyond a threshold value, highlighting that the presence of two regimes can be identified: Newtonian, where viscosity remains constant with shear rate, and shear-thinning, where viscosity decreases with shear rate. This shear-thinning feature is one of the main characteristics of HPAM.

When comparing the two Figures 2.5 (a) and (b), a decrease in viscosity with increasing salinity is observed. To properly visualize this effect, it can simply be noted that for a concentration of $2g/L$ of polymer, the relative viscosity of the solution in $S1-0$ brine

is around 4 while in $S001-0$ it is about 62. This effect along with the shear-thinning feature are much more visible at high concentration and low salinity.

In order to select solutions for coreflood experiments, viscosities of the different polymer solution were compared. We investigated relative viscosity at the Newtonian plateau η_{r0} which corresponds, in the flow curve, to the low shear viscosity plateau before shear-thinning.

Figure 2.6 presents the evolution of relative viscosity at the Newtonian plateau as a function of polymer concentration for each brine.

In this figure, we notice that viscosity decreases with ionic strength increase, and for the same value of ionic strength, viscosity decreases with hardness. We can conclude that an increase in total salinity leads to a decrease in viscosity, which is in agreement with HPAM behavior in presence of salts (cf. Section 2.1.2.2)

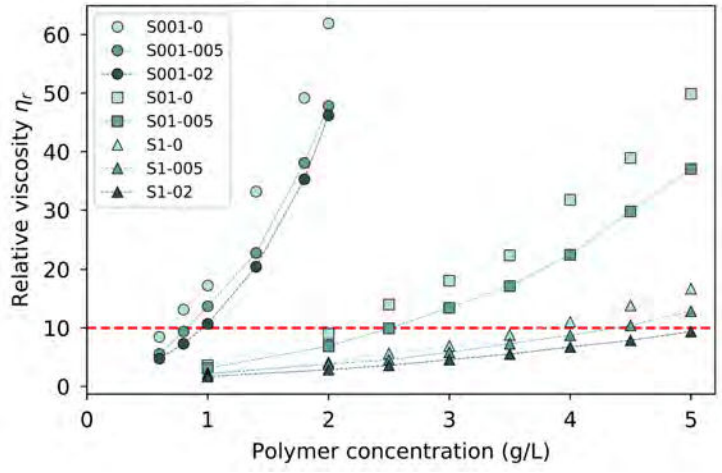

Figure 2.6 – HPAM 3130S relative viscosity as a function of polymer concentration for different brines. The red line represents the relative viscosity used for corefloods, $\eta_{r0} = 10$

However, this result does not provide information about the differences in polymer chains conformation with regard to salinity and hardness, nor how to distinguish effects due to the addition of sodium from those due to divalent cations, in this case calcium. Therefore, we studied another parameter: intrinsic viscosity $[\eta]$.

2.3.2 Intrinsic viscosity

For each polymer solution, we represented the reduced specific viscosity η_{spr} as a function of polymer concentration, and we deduced, based on Equation 2.8, the intrinsic viscosity (value when polymer concentration tends to zero). Figure 2.7 shows an example of this representation for a polymer solution prepared in brine $S1-0$.

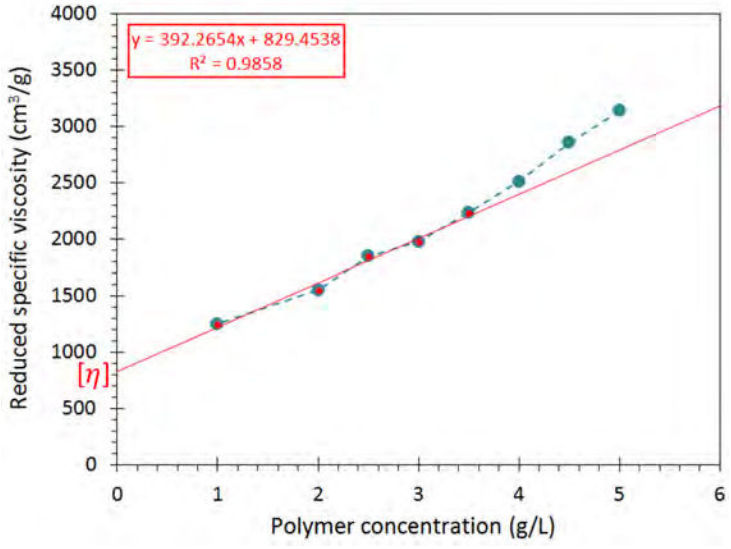

Figure 2.7 – HPAM 3130S reduced specific viscosity as a function of polymer concentration, in brine S1-0. The red line represents the Huggins formula at order 1

The red line represents the linear regression (cf. Equation 2.7) for low concentrations, providing an estimation of the intrinsic viscosity, in this case equal to: $829 \pm 45 cm^3/g$. Huggin's constant K_H in this case is equal to 0.57 which is determined based on the linear regression of the equation corresponding to order 1 of Huggins formula ($\eta_{spr} = [\eta] + K_H [\eta]^2 c$). Table 2.2 summarizes estimated intrinsic viscosities and Huggin's constants for the studied solutions.

Brine	Intrinsic viscosity $[\eta]$ (cm^3/g)	K_H
S001-0	6530 ± 400	0.24
S001-05	5650 ± 1100	0.34
S001-02	3070 ± 1700	0.61
S01-0	960 ± 170	1.71
S01-005	1030 ± 80	0.95
S1-0	830 ± 45	0.57
S1-005	890 ± 20	0.30
S1-02	450 ± 15	1.21

Table 2.2 – Summary of estimated intrinsic viscosities and Huggin's constant for the different HPAM Flopaam 3130S polymer solutions

In order to investigate separatly the effects of ionic strength and hardness, we first studied the evolution of intrinsic viscosity with ionic strength I for fixed hardnesses then its evolution with hardness R^+ for fixed ionic strengths, shown respectively in Figures 2.8 (a) and (b).

In Figure 2.8 (a), we can see that for a fixed hardness, the intrinsic viscosity decreases strongly with ionic strength and stabilizes at a threshold value of ionic strength $I =$

$0.1mol/L$ for both hardnesses 0 and 5%. This decrease was expected as the added salt screens the polymer side chains charges which lead to a decrease in hydrodynamic volume, meaning a higher "density" and thus a lower intrinsic viscosity (intrinsic viscosities from $6530cm^3/g$ in $S001-0$ to $830cm^3/g$ in $S1-0$). For Figure 2.8 (b), we notice that for both ionic strengths 0.01 and $1.03mol/L$, the intrinsic viscosity decreases significantly with hardness. In this case, the screening effect was also significant ($830cm^3/g$ in $S1-0$ to $450cm^3/g$ in $S1-02$) as the divalent cations (Ca^{2+} in this case) bind more tightly to the polyelectrolyte due to their double charge (bridging effect) and polarizability which results in denser polymer chains [15]. We can conclude that the increase in ionic strength as in hardness induces a decrease in intrinsic viscosity. Results obtained for only two points, on both figures, are not conclusive.

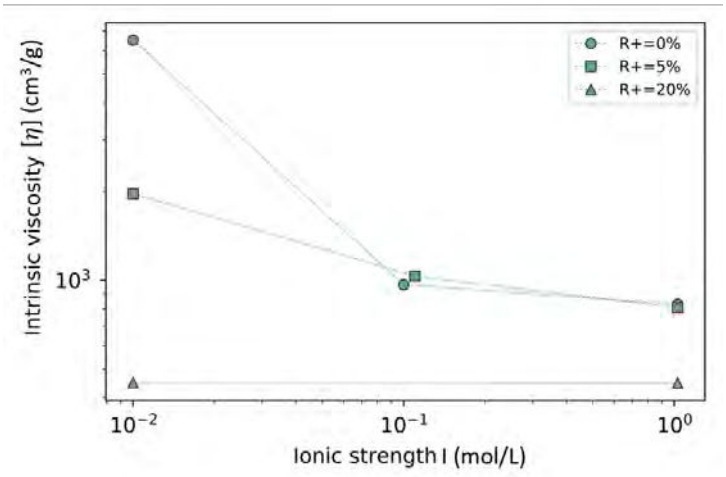

(a)

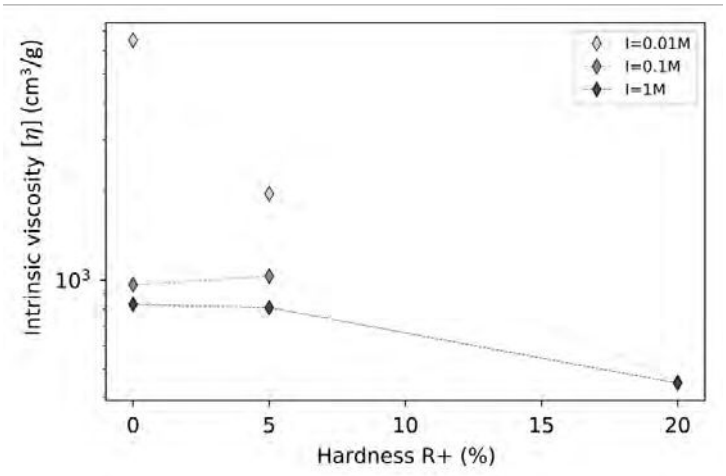

(b)

Figure 2.8 – Evolution of intrinsic viscosity of HPAM Flopaam 3130s solutions, with (a) ionic strength for fixed hardnesses and (b) hardness for fixed ionic strengths

2.3.3 Hydrodynamic size

For DLS experiments, impacts of ionic strength and hardness were studied using three brines: $S001-0$, $S1-0$ and $S1-02$. The three selected brines were characterized at a very low concentration $0.25g/L$ which is below overlap concentration C^*, in order to be in the dilute regime (cf. Section 2.1.1). Polymer solutions were pre-filtered as described in Section 2.2.1.2 and the temperature was set at $20°C$.

DLS results always indicated that hydrodynamic sizes of the solutes were roughly of the order of $300nm$, but unfortunately, due to the polydispersity in size of the polymer solutions, they cannot be translated in precise hydrodynamic sizes. They can however be discussed using the raw autocorrelation functions. Obtained results as shown in Figure 2.9, are presented in terms of the autocorrelation function as a function of sampling time for each polymer solution.

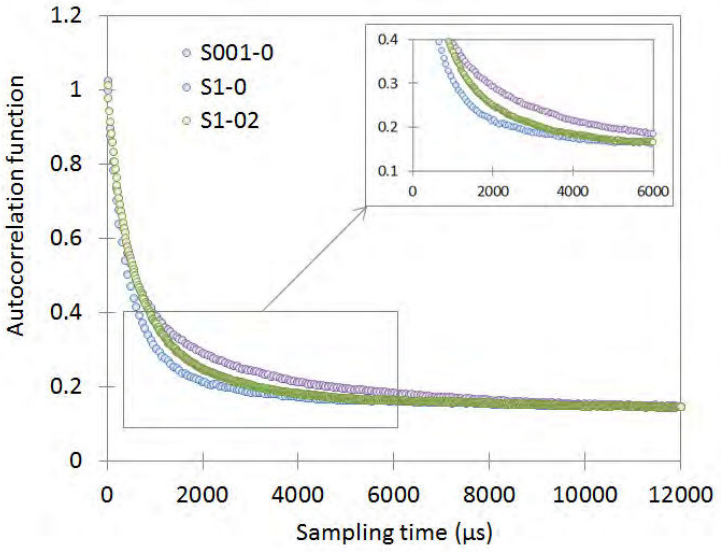

Figure 2.9 – Autocorrelation function as a function of sampling time from DLS measurements for three HPAM Flopaam 3130S solutions in $S001-0$, $S1-0$ and $S1-02$ brines

A shift towards higher decay rates is clearly observed when the salinity was increased from $S001-0$ to $S1-0$. This corresponds to larger diffusion coefficients and hence to smaller hydrodynamic sizes and is consistent with a higher "density" in solution of the chains in $S1-0$ than in $S001-0$. When hardness is increased from $S1-0$ to $S1-02$, on the contrary, a shift towards larger hydrodynamic sizes is observed. These observations confirm viscosity results considering the values of the Huggins constant (K_H). K_H significantly increases from $S1-0$ ($K_H = 0.57$) to $S1-02$ ($K_H = 1.21$). This suggests that attractive interactions between chains exist in hard brine (likely because of the bridging effect entailed by the divalent cations Ca^{2+}). The viscosity and DLS results suggest that, in $S1-02$, solutes made of multiple, but dense, polymer chains are present.

2.4 Selected solutions

In order to study the impacts of ionic strength and hardness during polymer injection tests, three polymer solutions were selected:

- A soft brine with very low salinity $S001-0$
- A soft brine with high salinity $S1-0$
- A hard brine with high salinity $S1-02$

A fixed relative viscosity was chosen $\eta_r = 10$, and due to the salinity differences in the selected brines, polymer concentrations varied as shown in Table 2.3 which summarizes the characteristics of selected solutions.

Brine	Ionic strength (mol/L)	Hardness (%)	TDS (g/L)	Polymer concentration (g/L)
S001-0	0.01	0	0.6	0.7
S1-0	1.03	0	60	3.8
S1-02	1.03	20	57.15	5.2

Table 2.3 – Summary of the characteristics of selected polymer solutions

Chapter conclusion

In this chapter, we focused on polymer solutions. First, we presented some theoretical background on the physical chemistry of polymer solutions such as the behavior of polymer chains in solution, solutions rheology and a focus on electrolytes. Then, we presented the processes of preparation and characterization of these solutions. Characterization results derived from viscosity measurements and DLS highlighted two major effects:

i) increasing ionic strength leads to an increase in polymer chains density and a decrease in their hydrodynamic volume

ii) increasing hardness leads to an increase in both density and hydrodynamic volume of polymer chains suggesting eventual bridging between the chains and calcium cations Ca^{2+}.

Finally, brines with different ionic strengths (0.01 and $1 mol/L$) and hardnesses (0 and 20%) were selected to study these effects in injection tests.

Chapter 3

Porous media

Contents

This chapter will be dedicated to the preparation and characterization of low permeability granular porous media of different mineralogies. First, we will present general characteristics of porous media, then materials and methods used to prepare and characterize them and finally characterization results and discussion.

3.1 Characteristics of low permeability porous media

3.1.1 Porous media properties

A porous medium is made of a solid phase and pores through which fluids can flow (when connected to each other). This representation is defined on a macroscopic scale using several parameters such as: porosity, permeability and specific surface area.

Porosity

Porosity is most often expressed in (%) and is defined as follows:

$$\phi = \frac{pores\ volume}{total\ volume} = \frac{V_p}{V_t} \tag{3.1}$$

Rock saturation for a given fluid is defined as the porosity fraction occupied by that fluid. For example, the water saturation of a porous medium, S_w , is written:

$$S_w = \frac{V_w}{V_p} \tag{3.2}$$

V_w being the volume occupied by water.

Specific Surface Area (SSA)

Also known as mass area, specific surface area is one of the most important porous media properties, especially for studying surfaces phenomena such as adsorption and depletion.

It is defined as the geometrical surfaces separating the porous space and the solid part, per gram of solid (expressed in m^2/g). It can be determined using different methods such as nitrogen adsorption to derive the amount of nitrogen molecules needed to cover the surface with one monolayer. The estimation of the specific surface area is conventionally calculated by applying the BET approach (based on the work of *Brunauer, Emmett and Teller* [56]).

Permeability

The flow of a fluid in a porous medium is only possible thanks to the interconnection of the voids that constitute its porous network [57]. Permeability k is defined as the material's ability to allow the fluid to flow through a connected network.

Darcy's law links the flow rate $Q\ (m^3/s)$ of a fluid flowing in a porous medium of section $S\ (m^2)$ and length $L\ (m)$ under the effect of a pressure gradient $\Delta P\ (Pa)$ by the permeability $k\ (m^2)$ of the porous medium and the viscosity $\eta\ (Pa.s)$ of the fluid flowing, such as:

$$Q = k\,\frac{S}{\eta}\,\frac{\Delta P}{L} \tag{3.3}$$

Permeability is commonly expressed in Darcy D or miliDarcy mD, with:

$$1\ Darcy = 0.97 \times 10^{-12}\ m^2$$

3.1.2 Low permeability porous media characteristics

Low permeability porous media (between 10 and $100mD$) are characterized by typically small pores (from 0.1 to $10\mu m$) [58], and very tortuous path. Even when "large" pores exist, their efficiency is controlled by the size of the pore throats that limit fluid access [59].

Moreover, these porous media have generally high specific surface area due to authigenic clay content which also contributes enormously in decreasing the permeability.

3.1.2.1 General clay structure

The properties of a clay mineral are derived from its chemical composition, geometric arrangement of atoms and ions, and the electrical forces that bind them together [60, 61]. Based on the generalizations of Pauling [62] for the structure of the micas and related layer minerals, the atomic structures of clay minerals have been widely studied.

For most clays, two structural units are involved in the atomic lattices [12]. The first unit consists of two sheets of closely packed oxygens or hydroxyls in which aluminum, iron, or magnesium atoms are embedded in octahedral coordination: equidistant from six oxygens or hydroxyls as shown in Figure 3.1.

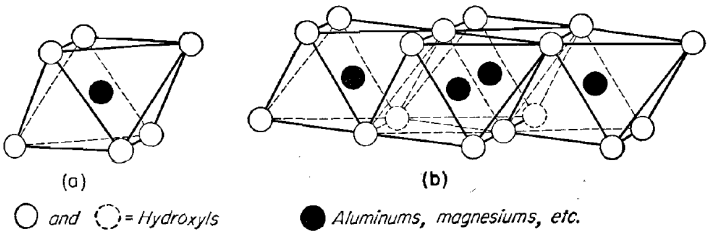

Figure 3.1 – Sketch of (a) single octahedral unit and (b) sheet structure of the octahedral units [12]

The second unit is built of silica tetrahedrons. In each tetrahedron a silicon atom is equidistant from four oxygens. The silica tetrahedral groups are arranged in a hexagonal network, which is repeated indefinitely to form a sheet of composition $Si_4O_6(OH)_4$ as

shown in Figure 3.2.

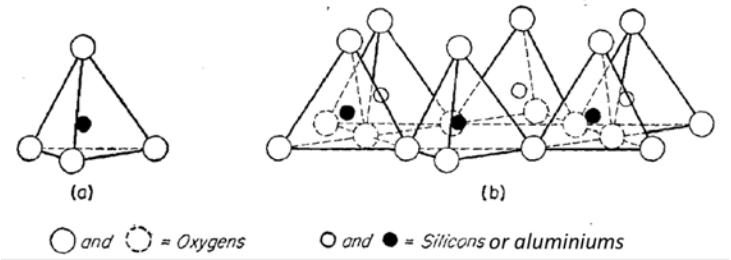

Figure 3.2 – Sketch of (a) single silica tetrahedron and (b) sheet structure of silica tetrahedrons arranged in a hexagonal network [12]

Most frequently, three types of clay can be found in low permeability sandstones: kaolinite, illite and smectite [58].

3.1.2.2 Kaolinite

Kaolinite $Al_2Si_2O_5(OH)_4$ generally forms from the weathering of feldspars and is one of the simplest clay minerals. It is a 1:1 layer mineral, as described in several references [63, 64, 65], and its structure, shown in Figure 3.3, is composed of a single silica tetrahedral sheet and a single alumina octahedral sheet combined so as the tips of silica tetrahedrons and one of the octahedral sheet form a common layer [12].

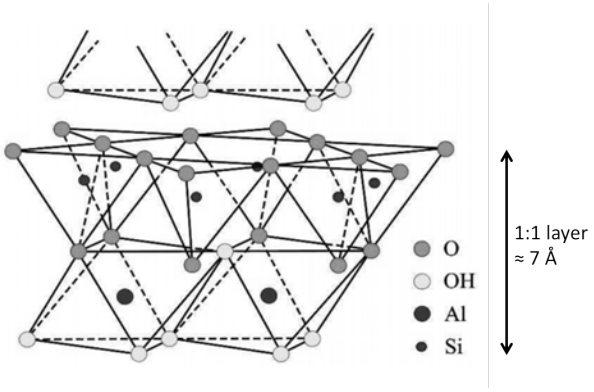

Figure 3.3 – Crystal structure of kaolinite [12]

As there are no substitutions in the tetrahedral and octahedral sheets, kaolinites are uncharged clay minerals. In kaolinite, the 1:1 layers are held together by van der Waals bonds between the basal oxygens of the tetrahedral sheet and the hydroxyls of the octahedral sheet of adjacent layers whereas the layers are held together tightly by hydrogen bonding, restricting expansion in water and limiting the reactive area to external surfaces [66].

3.1.2.3 Illite

Illite is a 2:1 layer mineral in which the basic structural unit is a layer composed of two silica tetrahedral sheets with a central octahedral sheet. Its structure is shown in Figure 3.4 and its general formula is $K_y Al_4(Si_{8-y}, Al_y)O_{20}(OH)_4$ (usually with $y \sim 0.7$). $K+$ charge density y prevents illite from swelling. Consequently, the interlayer cations (K^+, Ca^{2+} and Mg^{2+}) are not exchangeable and prevent the intrusion of polar ions into the clay structure [67, 68].

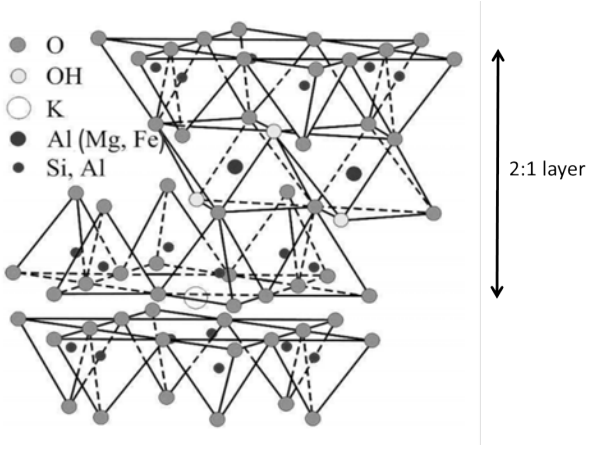

Figure 3.4 – Crystal structure of illite [12]

3.1.2.4 Smectite

Smectite is a dioctahedral 2:1 mineral. Its general formula is $(\frac{1}{2}Ca, Na)(Al, Mg, Fe)_4(Si, Al)_8O_{20}(OH)_4 nH_2O$ and its structure is shown in Figure 3.5. The low Mg^{2+}/Fe^{2+} substitution of Al^{3+} in octahedral and Al^{3+} substitution of Si^{4+} in tetrahedral leads to low charge density. This allows water molecules to enter in the interlayer allowing the expansion of the crystal lattice as the mineral hydrates [12].

Besides the hydration characteristics of its interlamellar space, the structure and chemical composition of smectite clays are responsible for some unique properties such as large chemically active surface area, high cation exchange capacity and in some cases the ability to strongly modify the flow behavior of fluids [69].

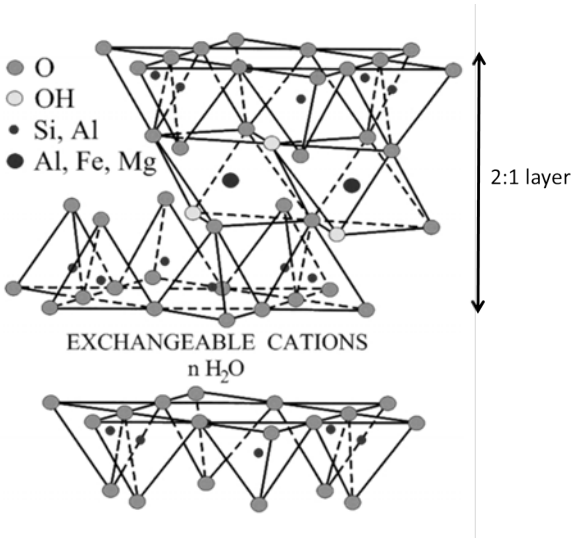

Figure 3.5 – Crystal structure of smectite [12]

3.2 Materials and methods

3.2.1 Preparation

3.2.1.1 Porous media mineralogies

In this study, we focused on four mineralogies. The first one is a reference porous medium made of quartz only. For the remaining types, we studied three types of clay separately: kaolinite, illite and smectite. In the following, the porous media will be noted as follows:

- **MP1** : quartz
- **MP2** : quartz + kaolinite
- **MP3** : quartz + illite
- **MP4** : quartz + smectite

For the first porous medium, in order to obtain low permeabilities, two quartz of different sizes (Figure 3.6) were used.

The first one, $GA39$, is a natural sand extracted from Fontainebleau area and provided by *SIFRACO*. It contains about 99% silicon dioxide (SiO_2), its density is $2.65 g/m^3$ and its average particle size is $100 \mu m$ as shown in Figure 3.7. Before use, fines and impurities such as iron (0.2%) were removed from $GA39$ by performing repeated washes in caustic soda solution (to remove fines by increasing electrostatic repulsion between fines and particles) and in hydrochloric acid solutions (to dissolve iron impurities). The quartz is then placed to dry in an oven at $60°C$. It is weighted regularly and the drying process is considered complete when the mass no longer varies.

(a) (b)

Figure 3.6 – (a) quartz GA39; (b) quartz BCR-067

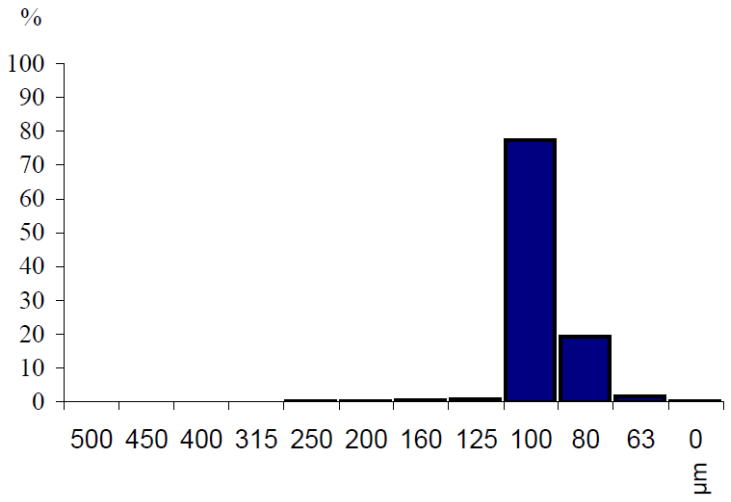

Figure 3.7 – Particle size distribution provided by SIFRACO

The second sand, $BCR-067$, is a reference quartz provided by *SIGMA-Aldrich* with an average particle size of about $10\mu m$. $BCR-067$ is laboratory purity grade as supplied and is hence used without further purification.

For kaolinite, we used $KGa-1$ which comes from Washington County, Georgia, USA and is provided by the *Clay Mineral Society (CMS)*. Given its purity [70], kaolinite was used with no particular treatment.

For illite, the one used in this study is Illite du Puy ($I77$) provided by *Argile du Velay* and for smectite, we used Wyoming montmorillonite ($MX80$) provided by *CETCO France*. Both illite and smectite were purified before use in LIEC (affiliation laboratory of the thesis). The purification consisted in decarbonation using acetic acid to remove carbonates (insoluble in water) followed by repeated washes in soda then ultrapure water before centrifugation. At the end of the purification process, the clays were lyophilized.

3.2.1.2 Preparation procedure

The first step in the prepration of porous media is mixing the appropriate grain proportions to achieve the same permeability for all types of porous media (between 50 and 100mD).

To study the impact of mineralogy, the proportion of the three clays used was set to a fixed value while the quartz proportions were varied in order to obtain the same permeabilities. The clays chosen proportion is 8%wt to approach real cases of low permeability sandstone oil reservoirs (2 to 10% clay content). In Table 3.1 are listed the proportions of quartz used for the different lithologies.

Lithology	**Quartz content (wt-%)**		**Clay type**	**Clay content (wt-%)**
	GA39	**BCR-067**		
MP1	70	30	/	/
MP2	84	8	**KGa-1**	
MP3	78	14	**I77**	8
MP4	86	6	**MX80**	

Table 3.1 – Particles proportions used for the different lithologies

To avoid particle segregation due to the presence of particles having different sizes and to improve the mixtures homogeneity, a rotary agitator, shown in Figure 3.8, is used for the dry-mixing of minerals. Agitation is maintained for a minimum of 8$hours$. The preparation is then put in an oven at 60°C for a minimum of 8hours to ensure it is completely dry and avoid any humidity effect (capillary bridges between the particles).

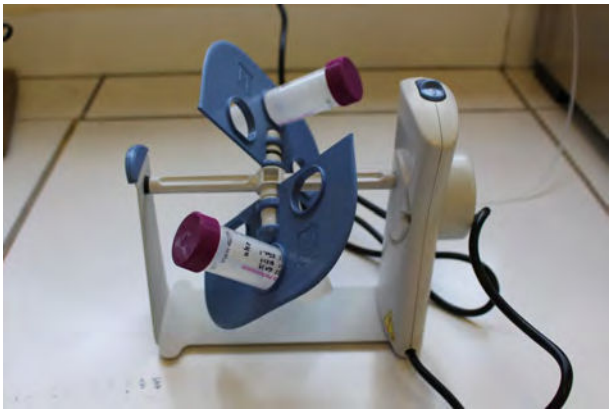

Figure 3.8 – Rotary agitator

The sand and clay grain mixture is then manually dry packed in cylindrical cells made of PEEK having on both ends pistons equipped with Nylon nets with aperture of 10μm (Figure 3.10). The cell dimensions are 10cm length and 1.5cm diameter.

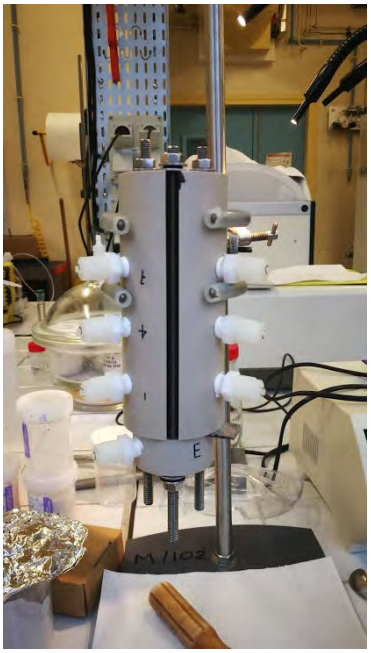

Figure 3.9 – Arrangement of the cell during packing

The arrangement of the cell during packing is shown in Figure 3.9. The procedure consists of adding progressively a small amount of the mixture and vibrating the cell after each addition by tapping it using a wooden stick.

Different intermediate connection taps allow the measurement of differential pressure in the sections $0-1cm$, $1-4cm$, $4-7cm$ and the total section $0-10cm$; the differential pressure in the section $7-10cm$ being deduced from the results measured in the other sections.

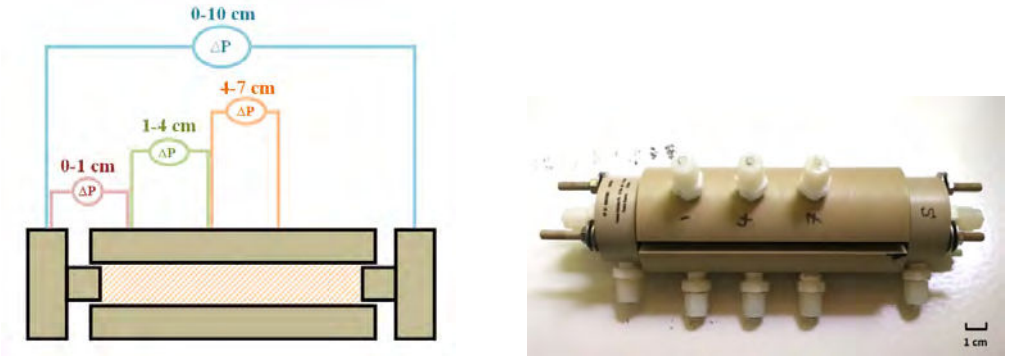

Figure 3.10 – Schematic and illustration of the PEEK cell for granular porous media

The intermediate pressure taps are connected to differential pressure sensors, of ranges 60, 2500 and $20000mbar$, provided by *ABB*. They are calibrated and adjusted so that there are two sensors of different measurement ranges per section in order to improve the measurements quality and better estimate uncertainties. The interests of the intermediate

pressure taps layout are first to be able to check the porous medium homogeneity during permeability measurements, then to follow the progression of the injected fluids front during coreflood experiments and in case of clogging to detect the section presenting the problem.

3.2.2 Porosity and pore volume

Porosity and pore volume (PV) of the porous medium, were determined by gravimetry, tomography and conductimetry.

Gravimetry In this method, the mass and dimensions of the cell are simply determined before and after the porous medium packing, which allows calculating porosity $\phi(\%)$ and pore volume $PV(mL)$ of the porous medium, using following equations:

$$\phi = (1 - \frac{V_s}{V_t}) \tag{3.4}$$

$$PV = V_t\phi \tag{3.5}$$

Where V_s and V_t are respectively the volume of the solid fraction and the total volume, defined by:

$$V_s = \frac{m_{PM}}{\rho_s} \tag{3.6}$$

$$V_t = \pi(\frac{d_{PM}}{2})^2 L_{PM} \tag{3.7}$$

With m_{PM}, d_{PM} and L_{PM} the porous medium mass, diameter and length respectively and ρ_s its minerals density.

Tomography Computerized Tomography scan (CT-scan) is used to provide the porous medium porosity profile and an estimation of its average porosity. Using a medical scanner Discovery 750HD provided by *GEHD*, the procedure consists of scanning the cell with an X-ray beam, after which a detector measures the attenuation of the rays transmission which varies depending on the density of the passed through material. During this process, the cell is automatically moved in order to scan all the sections, with an image acquisition interval of $0.625mm$ (Figure 3.11), and the reconstruction of the obtained images constitutes the spectral profile. The porosity profile is then obtained by the use of a correlation based on two coefficients which are determined by analyzing the spectral profiles and porosities of reference porous media (in this case: a sandstone).

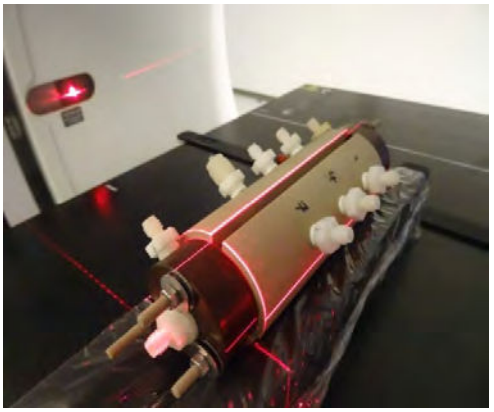

Figure 3.11 – Scanning of the cell containing the porous medium

Conductimetry Pore volume can also be obtained by conductimetry. This method consists of injecting a brine, called tracer, of a different salinity (higher or lower) than the brine used for the porous medium saturation, and measuring the evolution of the conductivity of the outlet solution during injection using an on-line conductimeter. The one used for our experiments is provided by *GE Healthcare Bio-Sciences AB* (reference Monitor pH/C-900). The pore volume PV is calculated by deducting from the cumulated volume V_C the dead volumes V_D in the tubings and those at the inlet and outlet of the porous medium: $PV = V_C - V_D$.

3.2.3 Permeability

For the four studied types of porous media, the clay and quartz contents are adjusted in order to obtain a permeability around $50 - 100mD$.

For permeability determination, the porous medium is first saturated with brine (solvent of the polymer solution to be injected in the medium). After that, the injection rate is increased then decreased over a range of injection rates from 0.8 to $150mL/h$, while keeping each injection rate long enough to achieve the differential pressures stabilization in the different sections of the porous medium. Three cycles are carried out in order to obtain a permeability profile that is representative of the porous medium (one cycle corresponding to an increase followed by a decrease in injection rates). As high injection rates can potentially change the granular porous medium structure by inducing particle displacement, this three cycles method allows ensuring that the medium is fully stabilized during the permeability measurement. In addition, a Millipore filter of $0.22\mu m$ pore diameter is placed downstream of the porous medium and connected to pressure sensors to ensure that there is no pressure increase that would indicate accumulation of fine particles coming from the porous medium.

3.2.4 Specific Surface Area determination

The determination of the specific surface area is done via physical adsorption of gases at liquid nitrogen temperature. The samples are first degassed (at $110°C$), the measurement

is then carried out using point by point manometry, on a BEIsorp II device provided by *BEL JAPAN*. The specific surface area of a mixture is estimated from the amount of nitrogen adsorbed regarding its pressure at the boiling temperature of liquid nitrogen and under atmospheric pressure. The isotherms obtained are then analyzed according to the BET model for the specific surface area estimation [56], and by applying the De Boer t-plot model [71] for the accessible microporosity to nitrogen.

3.2.5 Scanning Electron Microscopy (SEM) observation

Scanning electron microscopy (SEM) is a microscopy technique allowing the visualization of samples' surface and shape. This technique is used as a part of porous media characterization to visualize their shape and structure, evaluate their homogeneity and get an idea about the organization of particles of different size. The electron beam scans the sample's surface which retransmits some electrons, then a detector synchronously captures the signal induced by this beam to form a reconstructed image, which is the cartography of that signal. The equipment used in our study is a high vacuum conventional SEM provided by *Zeiss SMT* (reference EVO MA10). It allows observing the surface topography using secondary electron (SE) imaging and images with atomic number contrast using back scattered electron (BSE) imaging. Moreover, it allows EDS analysis for mineral identification. For results analysis, obtained images are processed using *JMicroVision* or *ImageJ* softwares.

The preparation of the sample of granular porous media for SEM analysis involves several steps: sampling, lyophilization, resin impregnation, cutting, grinding and finally polishing. The sample is extracted at the end of the coreflood experiment using a copper tool with a diameter around $0.7cm$. It is sampled by slow rotation of the copper tool to preserve as best as possible the medium structure. Once extracted, the sample is lyophilized (rapid freezing at $-80°C$ followed by a complete vacuum dehydration of the sample to preserve its structure). The sample is then impregnated with a mix of resin and hardener, placed under vacuum for about $20min$ then left to dry in open air for a minimum of $48hours$ (Figure 3.12).

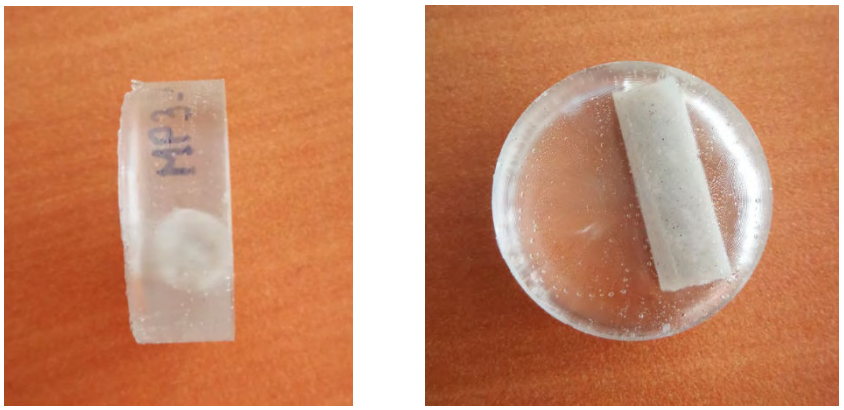

Figure 3.12 – Example of a sample impregnated with resin, before cutting (left: side view, right: top view)

After hardening, the sample is cut and ground in order to obtain a flat surface. It is then gradually polished with Silicon Carbide (SiC) abrasives with grains size from $15\mu m$ to $1\mu m$. The surface is observed at each polishing step using a binocular microscope: polishing is completed when no more scratches are visible on the sample's surface. Finally, a metallization is performed: a thin carbon layer is deposited on the sample's surface using an evaporator metallizer provided by *Quorium Technologies* (reference Q150 R ES).

3.3 Characterization results

3.3.1 Basic petrophysical characterization

3.3.1.1 Porosity and pore volume

Porosity profile using CT-scan was obtained once for each lithology on dry samples (before brine or polymer injection) to assure porosity homogeneity along the samples. An example of the porosity profile using CT-scan obtained for a porous medium containing quartz only (MP1-2) is given in Figure 3.13. The obtained profile shows that porosity varies between 29.7% and 31.3%. The last section, and also the top section during packing (cf. Figure 3.9), has a higher porosity than the rest of the porous medium which is consistent since it is the least packed of all sections. Obtained results give the mean porosity and show the overall homogeneity of the porous medium. The corresponding mean porosity $\phi_s = 30 \pm 1\%$ is in good agreement with the porosity determined by the gravimetric method: $\phi_g = 32 \pm 1\%$. For all porous media, porosity was determined by gravimetry.

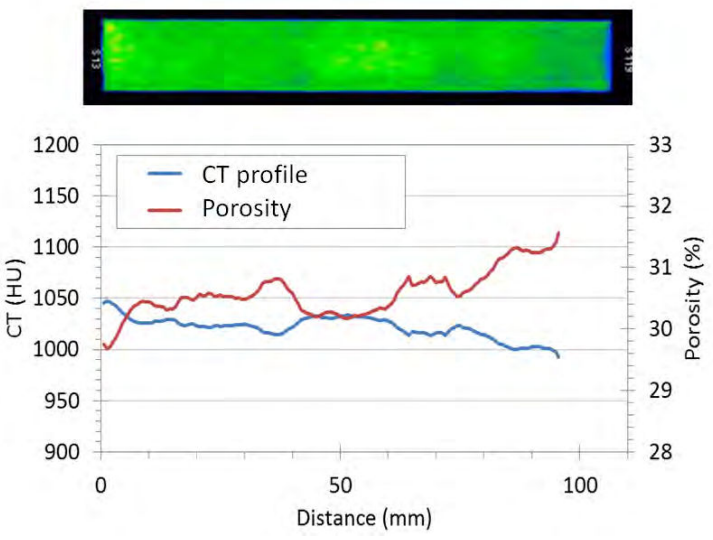

Figure 3.13 – Porosity profile and CT-scan image of MP1-2

For pore volume, conductimetry was carried out for some of the porous media. An example of the obtained tracer curve is shown in Figure 3.14, where the pore volume was estimated around $5.6mL$ with dead volumes estimated around $3.6mL$. However, due to

the small pore volume of used porous media compared to the dead volumes, estimated pore volumes based on conductimetry were not always accurate. Moreover, the pore volume estimated by gravimetry was found around $5.4mL$ which is consistent with conductimetry results. For these reasons, only pore volumes determined using gravimetry were considered for the rest of the study.

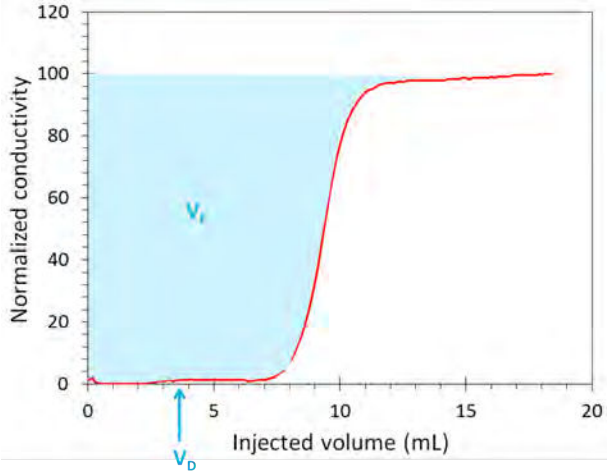

Figure 3.14 – Tracer curve obtained for the porous medium MP1-2

3.3.1.2 Permeability

For each porous medium, permeability cycles were carried out with the same brine used for saturation. Permeability profiles were obtained for the different sections of the porous medium as shown in the example given in Figure 3.15 for porous medium MP1-2.

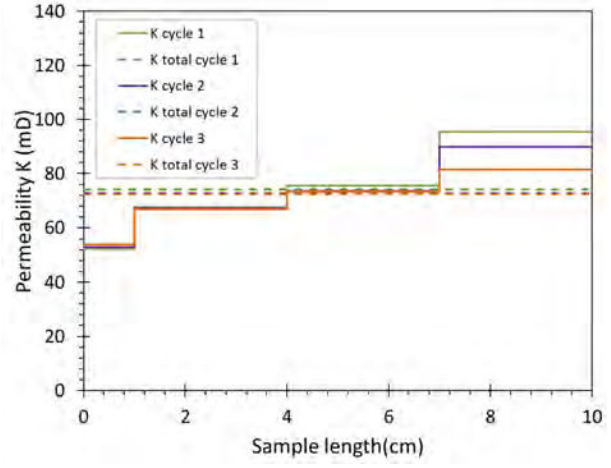

Figure 3.15 – Permeability profiles of MP1-2

The porous medium is globally homogeneous, with no remarkable differences between the three permeability cycles except for the last section where the permeability gets higher. The corresponding mean permeability is around $k = 72 \pm 4mD$. Permeability profiles in

this figure show that the sections $(0-1cm)$ and $(7-10cm)$ have permeabilities that are respectively lower and higher than the mean permeability value, which is probably due to the packing procedure, which is consistent with the porosity profile shown in Figure 3.13.

In Figure 3.16 are presented the permeability profiles of the different studied porous media, with different brines, which shows that they are all in the range of the fixed permeability $(50-100mD)$, except two porous media where the permeability is slightly higher in the first section. It should be noted that, for these porous media, no fine particles have been accumulated in the filter placed downstream (introduced in Section 3.2.3), as no increase in the differential pressure has been observed.

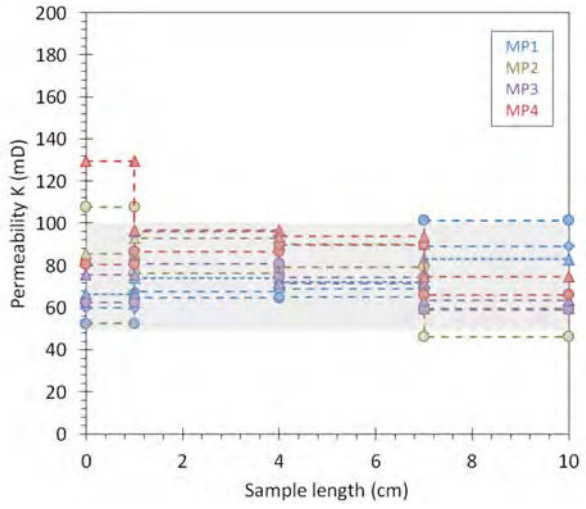

Figure 3.16 – Permeability profiles of the different porous media

3.3.1.3 Specific surface area

Results obtained from specific surface area measurements are summarized in Table 3.2 for the different minerals used in this study. Quartz present very low values of specific surface area compared to clays, with illite having higher specific surface area than kaolinite and smectite. It should be noted that the studied minerals have no detectable microporosity.

Minerals	Specific surface area (m^2/g)
GA39	0.08 ±0.05
BCR-067	0.60 ±0.1
KGa-1	7.80 ±0.2
I77	128.0 ±0.5
MX80	76.0 ±0.2

Table 3.2 – Results obtained from specific surface area measurements

The values of specific surface area of the porous media are presented in Table 3.3 and were calculated based on the measurements given in Table 3.2 and the minerals proportions presented in Table 3.1.

Porous medium	**Specific surface area** (m^2/g)
MP1	0.24
MP2	0.72
MP3	10.4
MP4	3.6

Table 3.3 – Estimated specific surface area for the different porous media

3.3.1.4 Summary: main properties of the porous media

Table 3.4 summarizes the characteristics of studied porous media. It shows that obtained permeabilities were all in the chosen permeability range.

As it can be seen in this table, very similar petrophysical characteristics for all the porous media were achieved using this method in our case: a porosity around $31.3 \pm 1.8\%$, pore volume of $5.5 \pm 0.3mL$ and a permeability around $50 - 100mD$.

However, for porous media with clay, a change in permeability has been observed for low salinity brines. As shown in Table 3.4, a slight change in permeability was observed for lithology 2 (with kaolinite content) as the permeability is lower with decreasing salinity. For the third and fourth lithologies with illite and smectite content, it was not possible to carry out the experiment using the brine $S001 - 0$ as the permeabilities obtained were very unstable and of values below $6mD$ resulting in a permeability decrease of around 90%. These results are not surprising and are consistent with clay dispersion and/or pore bridging usually observed with low salinity brines.

Porous medium		**Brine**	**Porosity**	**Pore Volume**	**Permeability**	**SSA**
Type	Label		(%)	(mL)	(mD)	(m^2/g)
Quartz	MP1-1	S001-0	31.4	5.5	71	0.24
	MP1-2	S1-0	31.0	5.4	72	
	MP1-3	S1-02	31.9	5.5	75	
Quartz + kaolinite	MP2-1	S001-0	31.0	5.4	52	0.72
	MP2-2	S1-0	31.1	5.4	66	
	MP2-3	S1-02	31.3	5.5	78	
Quartz + illite	MP3-1	S1-0	29.8	5.2	69	10.4
	MP3-2	S1-02	29.5	5.2	75	
Quartz + smectite	MP4-1	S1-0	32.4	5.7	80	3.6
	MP4-2	S1-02	33.1	5.8	90	

Table 3.4 – Summary of the characteristics of studied porous media

3.3.2 Microscopic structural characterization

The microscopic structure of studied porous media was characterized using SEM observation (detailed in Section 3.2.5). The observations were carried out for all of the studied porous media in the different brines used. In this section, first we will present the impact of polymer flow using a comparison between the porous media structure before and after

polymer flood experiments (the experiments will be presented in details in Chapter 4). Then, a finer analysis of SEM images will be carried out for each type of porous media.

3.3.2.1 Impact of polymer flow

Table 3.5 shows a comparison between the structure of porous media before and after polymer injection, first for $MP3$ containing quartz + kaolinite in brine $S001-0$, at different scales, then $MP4$ containing quartz + smectite in brine $S1-0$. Kaolinite structure and repartition before and after polymer flood is similar, which can be confirmed at different scales. Smectite aggregates also seem to have similar features before and after polymer injection. Both observations show that globally the polymer injection does not change the microscopic structure of the porous media.

Porous media	**Brine**	**Condition**	
		Before polymer injection	**After polymer injection**
quartz + kaolinite	S001-0	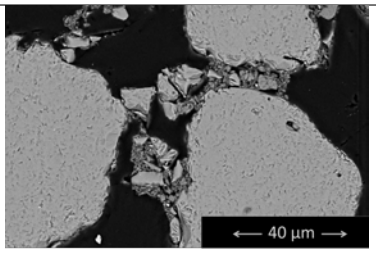	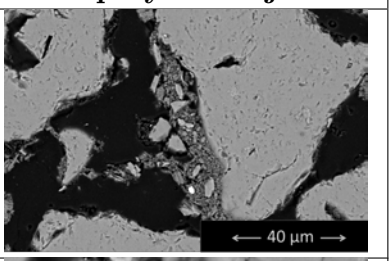
		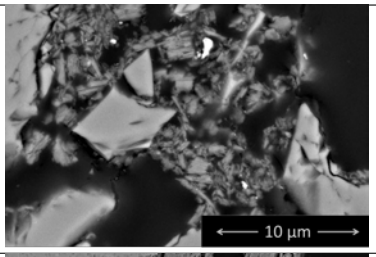	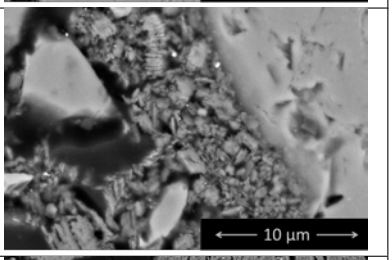
quartz + smectite	S1-0	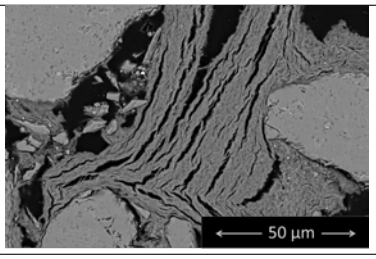	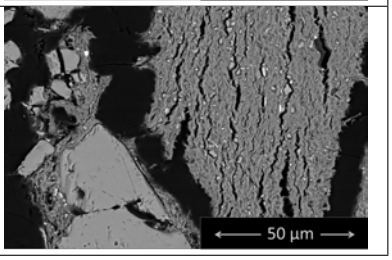

Table 3.5 – Comparison between SEM images of porous media before and after polymer injection (for quartz + kaolinite and quartz + smectite)

Since polymer injection does not impact the initial structure of the porous media, results can be discussed on the basis of SEM observations performed at the end of injection tests. Sampling for SEM being destructive, SEM observations cannot be carried out before polymer injection without having to change the porous medium.

Therefore, for the study of the microstructure of porous media in the next section, we will focus on the structural changes resulting from the change in salinity and mineralogy.

3.3.2.2 Quartz and clays grains structure

In the following, the microstructure of porous media will be analyzed with regard to involved minerals. The identification of each mineral has been done using EDS analysis.

Quartz

Obtained SEM images confirm the homogeneity of the quartz porous medium as shown in Figure 3.17. By analyzing the SEM image of the first porous medium for example, the calculated proportions, 70% for quartz $GA39$ and 30% of $BCR-067$, are in agreement with the proportions used in the mixture (Table 3.1) and show a good repartition of the small particles towards bigger sand grains. The figure also shows the difference in size between $GA39$ and $BCR-067$ mentioned before (Section 3.2.1.1), with the small particles being of different sizes and shapes. Obtained images show that the sampling procedure does not destructure the porous medium. The images are therefore representative of the porous medium structure.

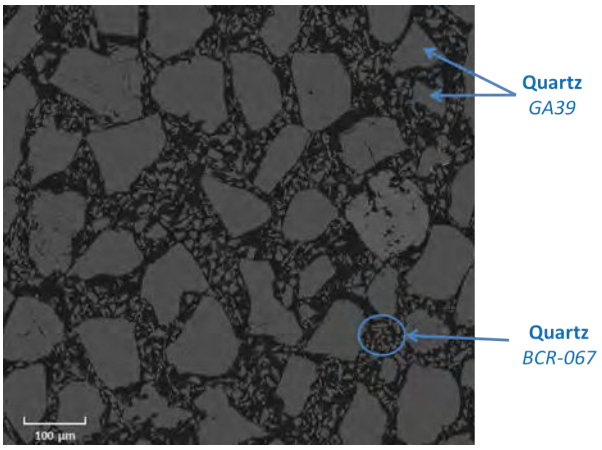

Figure 3.17 – SEM image obtained for a quartz-only porous medium ($MP1-2$, brine $S1-0$), with quartz grains in gray and porosity in black

In the following, the porous media structure of each mineralogy will be presented at different scales.

Kaolinite

Figure 3.18 shows the repartition of quartz and kaolinite particles, the latter being smaller and well separated. Table 3.6 shows SEM images of both quartz and quartz + kaolinite porous media for low and high salinity brines. No changes has been observed with regard to salinity: in low ($S001-0$) and high ($S1-02$) salinities the porous media structures are similar. This result is not surprising as kaolinite is not a particularly charged clay in our experiments conditions, and the permeabilities were only slightly changed with salinity (cf. Table 3.4).

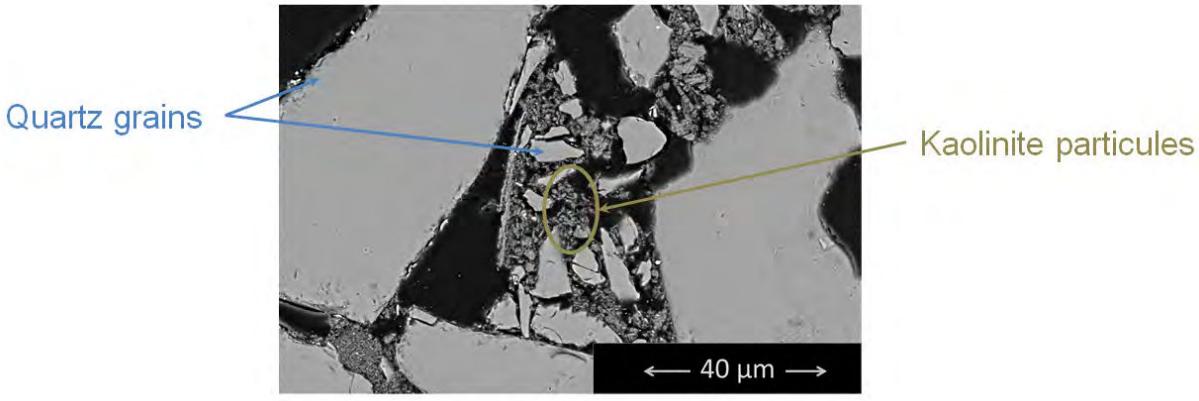

Figure 3.18 – Quartz grains and kaolinite particules in a quartz + kaolinite porous medium ($MP2-3$, brine $S1-02$)

Quartz	**Quartz + kaolinite**	
S1-0	**S001-0**	**S1-02**
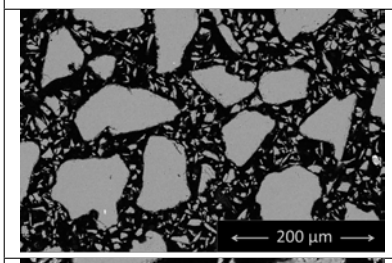	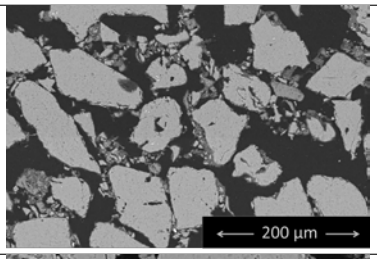	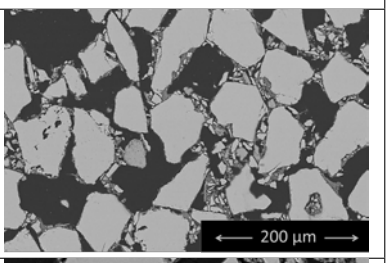
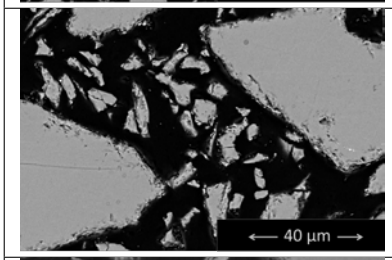	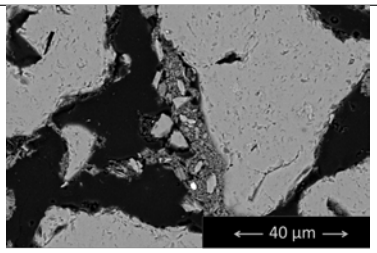	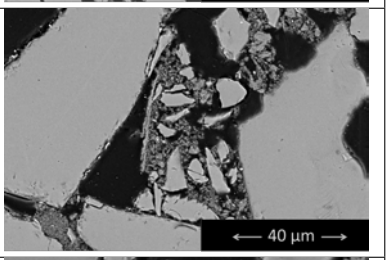
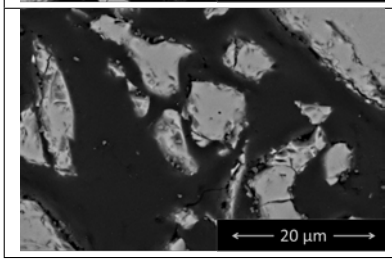	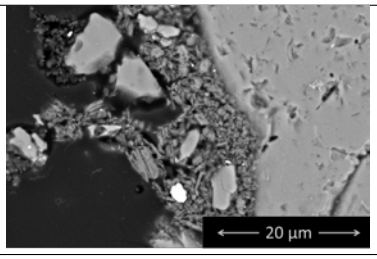	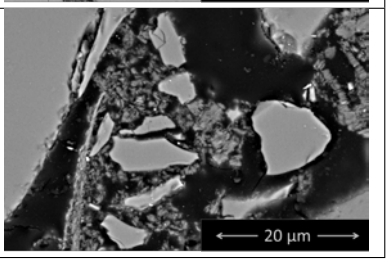

Table 3.6 – Comparison between SEM images of quartz only and quartz + kaolinite porous media

Illite

For porous media containing illite, Table 3.7 shows that unlike kaolinite, illite was highly

affected by salinity. In low salinity ($S001-0$), illite aggregates having the shape of elongated filaments were formed reducing drastically the porous medium pore throats which explains the sharp decrease in permeability shown in Table 3.4 making it impossible to carry out the experiment. In contrast, in high salinity brine ($S1-0$), it is interesting to notice that illite forms large compact aggregates whose size is close to that of quartz $GA39$ grains. This difference in behavior between the two salinities confirms that the observations made on porous media with clay content are not due to the packing procedure but rather to the structure of the porous medium in the presence of different solutions.

Quartz	**Quartz + illite**	
S1-0	**S001-0**	**S1-0**
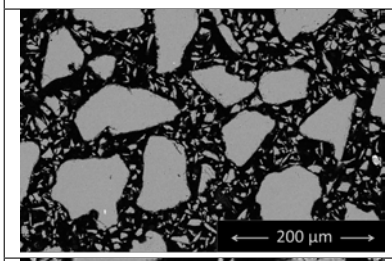	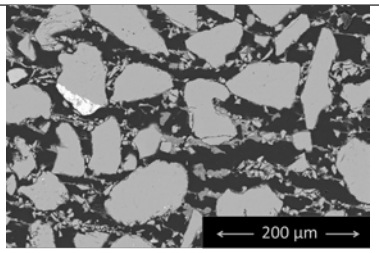	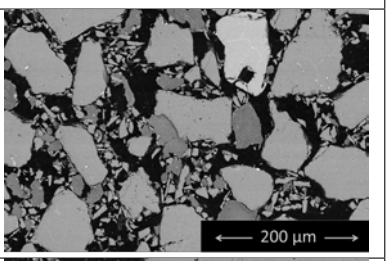
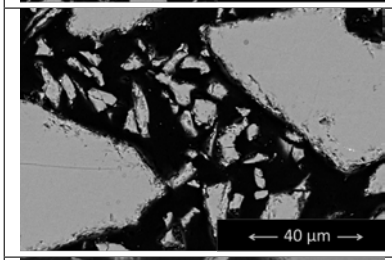	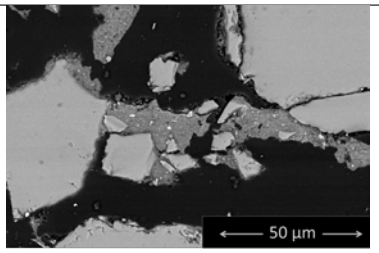	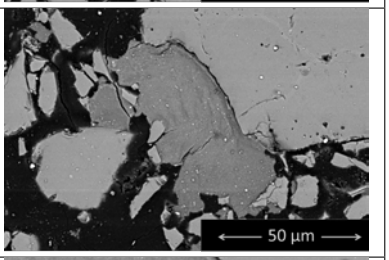
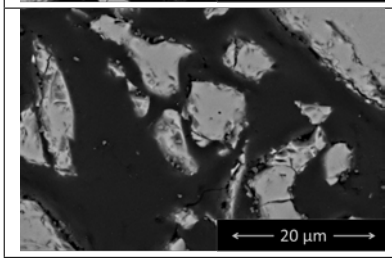	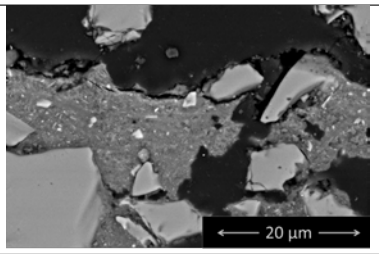	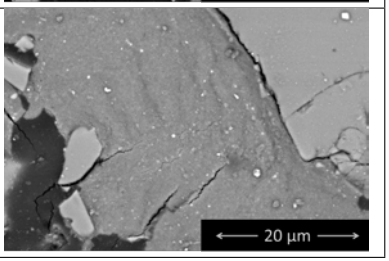

Table 3.7 – Comparison between SEM images of quartz only and quartz + illite porous media

Smectite

Table 3.8 shows that with regard to salinity, smectite's behavior is similar to illite's. For low salinity ($S001-0$), smectite particles seem to envelop quartz grains and form a sort of bridges between grains. In this salinity, a sharp decrease has been observed in the porous medium permeability. For high salinity ($S1-0$), SEM images (Table 3.8) show that smectite aggregates were formed with the presence of micrometric voids inside of smectite's aggregates in opposite to illite's.

Quartz	**Quartz + smectite**	
S1-0	**S001-0**	**S1-0**
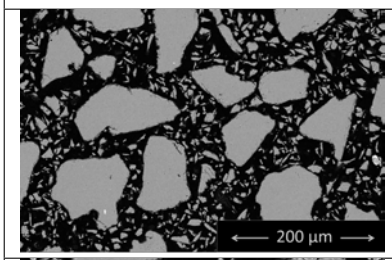	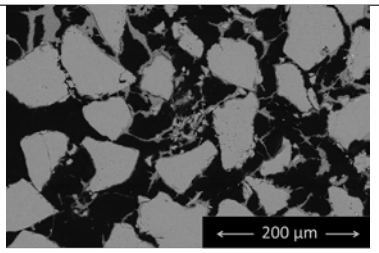	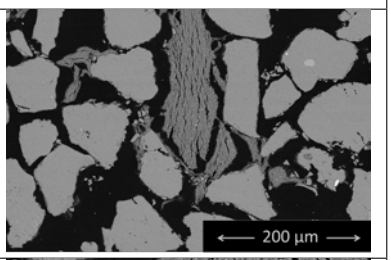
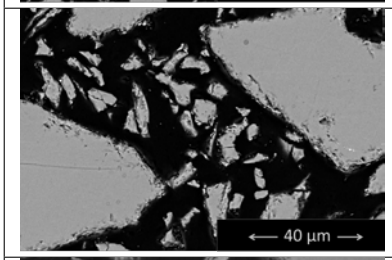	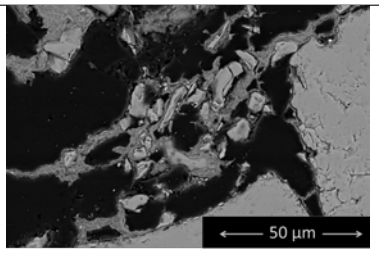	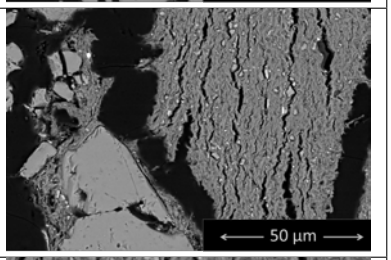
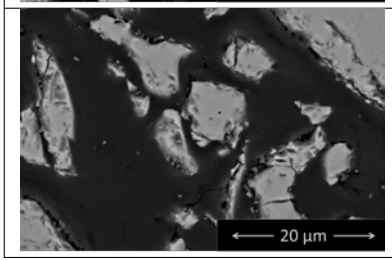	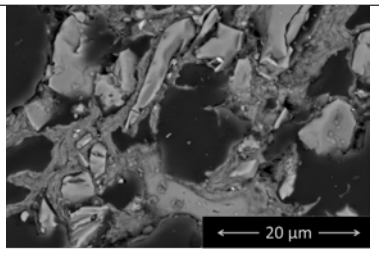	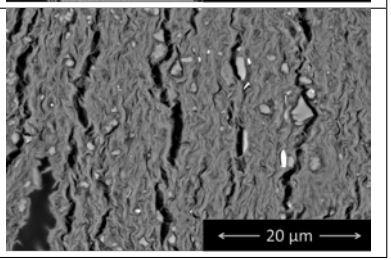

Table 3.8 – Comparison between SEM images of quartz only and quartz + smectite porous media

SEM observations allowed the visualization of the porous media microstructure where several differences have been noted according to mineralogy and salinity. Indeed, for $MP2$, the change in salinity impacts very little the structure of the porous media. In contrast, for $MP3$ and $MP4$, salinity significantly change the porous media's microstructures. Moreover, in these porous media, the formation of clays aggregates, of a size similar to that of quartz grains, has been observed in high salinity brines. These differences are likely to have a significant impact on the transport of polymer solutions.

Chapter conclusion

In this chapter, we focused on porous media. First, we presented basic background on porous media properties and low permeability porous media characteristics. Then, we described materials and methods used for porous media preparation and characterization. Finally, characterization results were presented.

We showed the importance of the preparation of porous media with different mineralogical composition, quartz and quartz + clay (kaolinite, illite and smectite), with very similar petrophysical properties (porosity $31.3 \pm 1.8\%$, pore volume $5.5 \pm 0.3mL$ and permeability $50 - 100mD$) and different specific surface area.

Afterwards, microscopic structural characterization using SEM observation was presented, showing the structural change resulting from mineralogy on one hand, and salinity on the other. Indeed, for illite and smectite, SEM images highlighted the distinctive structure of the porous media in low salinity and revealed the formation of clay aggregates at high salinity.

Chapter 4

Transport of polymer in porous media

Contents

After introducing polymer solutions and porous media in the previous chapters, we will present in this chapter the transport properties of polymer in porous media. For that, we will first describe materials and methods used for injection experiments (also called corefloods) then we will present corresponding results and discussion regarding the impacts of salinity and clay content.

4.1 Materials and methods

In this section, we will detail materials and methods used for corefloods. First, we will describe the experimental set-up and the injection protocol. Then, we will present the observables.

4.1.1 Experimental set-up

The set-up used for this study is shown in Figure 4.1. It was implemented during the first months of the thesis and is based on a standard set-up used for experiments in unconsolidated porous media, developed at IFP Energies nouvelles. Some changes have been made in order to adapt to our experiments such as the introduction of filters that we will present in details in Section 4.1.1.3.

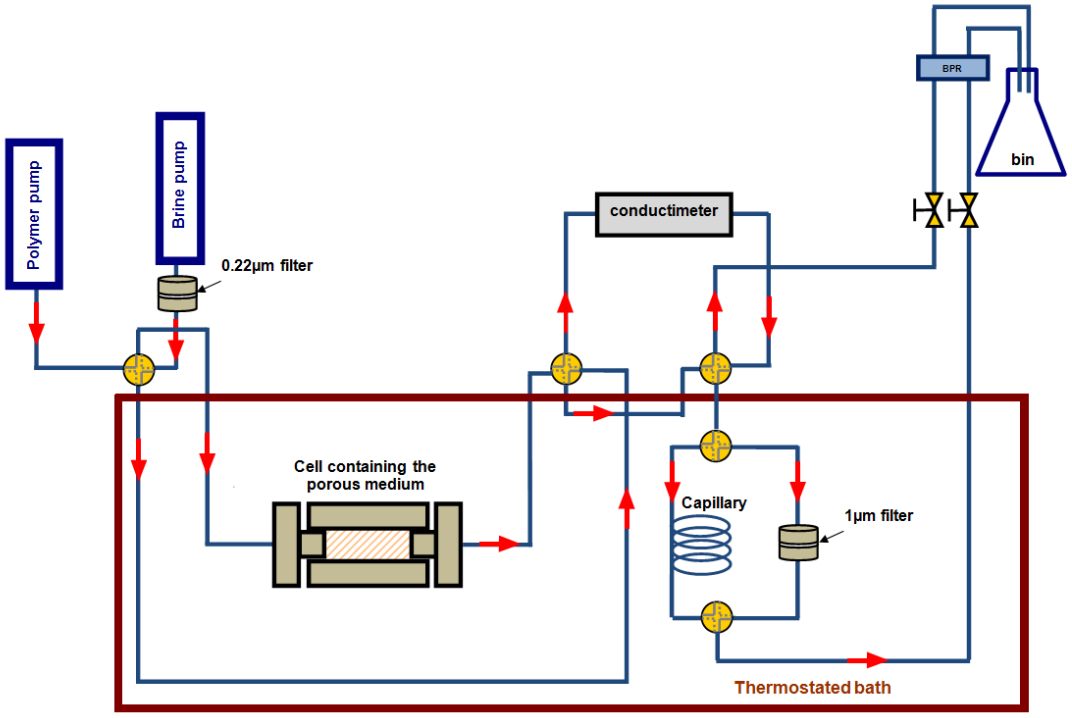

Figure 4.1 – Schematic of the experimental set-up

The experimental set-up consists of two pumps, one for the polymer solution and one for the brine, followed by a cylindrical PEEK cell (previously introduced in Section 3.2.1.2)

containing the porous medium with differential pressure sensors, a by-pass tube to bypass the porous medium, a conductimeter downstream of the porous medium (introduced in section 3.2.2), placed in parallel with a filter all placed in a temperature-regulated bath. In all the set-up the pressure is maintained around $250mbar$ using a counter-pressure. In the following, we will detail the elements which are not yet introduced, in particular: the pumps, the capillary tube, the filters and the temperature-regulated bath.

4.1.1.1 Pumps

In order to control the injection rate, two pumps were used. They are provided by *Chandler Engineering* and *Ametek Oil& Gas* (reference: Quizix QX Series). They are double cylinder pumps allowing continuous flow: while one cylinder is delivering fluid, at constant rate or constant pressure, the other quickly refills and pre-pressurizes to match the pressure of the first cylinder. It should be noted that these pumps do not induce polymer degradation.

The pumps are connected to the set-up through a four-ways valve (marked in yellow in Figure 4.1) which alternately allows the passage of one of the two fluids.

4.1.1.2 Capillary tube

In order to track viscosity evolution of polymer solutions before and after each experiment and also detect fluids breakthroughs during corefloods, a capillary tube was placed downstream the porous medium as shown in Figure 4.1. The capillary used is $1.5m$ long, with a $500\mu m$ internal diameter made of Polyether ether ketone (PEEK) and provided by *Cluzeau Info Labo*. The fluid to be characterized is injected in the capillary tube at several injection rates $Q(mL/h)$ (stepwise descendant ramp) for which the differential pressure $\Delta P(mbar)$ is measured using pressure sensors connected to the ends of the capillary tube.

To obtain viscosity from the differential pressure measurements, the method consists in conducting a brine reference measurement by injecting the brine used to prepare the polymer solution at several injection rates Q_{brine} for which the differential pressures $(\Delta P)_{brine}$ are measured. The linearity of the pressure sensors allows writing: $\Delta P_{brine} = aQ_{brine}$. Afterward, the polymer solution is injected in the capillary tube following the same procedure.

Thanks to Hagen-Poiseuille's law (Equation 1.3) polymer and brine viscosities can be written:

$$\eta_i = \frac{\Delta P_i}{Q_i}\, n\frac{\pi}{8}\,\frac{R^4}{L}; i = polymer, brine \tag{4.1}$$

The ratio between $\eta_{polymer}$ and η_{brine} gives the following equation:

$$\frac{\eta_{polymer}}{\eta_{brine}} = \frac{\Delta P_{polymer}}{Q_{polymer}}\frac{Q_{brine}}{\Delta P_{brine}} \tag{4.2}$$

The polymer solution viscosity $\eta_{polymer}$ is then obtained as a function of the injection rate $Q_{polymer}$, the differential pressure $\Delta P_{polymer}$ and the brine viscosity η_{brine} measured using the LS300 rheometer:

$$\eta_{polymer} = \frac{\Delta P_{polymer}}{a\ Q_{polymer}}\ \eta_{brine} \tag{4.3}$$

4.1.1.3 Filters

Two filters were mainly used in injection experiments. The first one is a $0.22\mu m$ *Millipore* filter at the outlet of the brine pump used to remove possible impurities in the injected brine. The second one is a $1\mu m$ *SPI-Pore* polycarbonate filter placed downstream of the porous medium and used for polymer solutions filtration, presented in details in Section 2.2.1.2.

4.1.1.4 Temperature-regulated bath

For representativeness of oil reservoirs, we have chosen a temperature of $40°C$ for injection experiments. For that, part of the experimental set-up (cell, by-pass, capillary and filter holders) is immersed in a temperature-regulated bath consisting of a water tank, a temperature sensor for temperature monitoring over time and a bath regulator equipped with a heating coil supplied by *LAUDA* (reference Ecoline Staredition E200). In order to limit evaporation, plastic balls were placed on the water surface.

4.1.2 Injection protocol

In order to simulate in-depth flow in an oil reservoir during EOR operations, the injection rate Q chosen for this study was set at $0.8mL/h$, corresponding to an interstitial velocity V_i of $0.3m/day$: $Q = V_i\phi\pi R^2$, with ϕ the porous medium porosity and R the core radius, in our case equal to $0.75cm$, and an estimated shear rate of $20s^{-1}$ for a permeability around $100mD$ using Equation 1.8.

For polymer corefloods, polymer injection was performed in typically two stages ("two slugs method"). Initially, the porous medium was saturated with the brine to be used in each given experiment. First, a polymer slug at the same salinity was injected until the stabilization of the differential pressures, followed by a brine injection to displace the polymer retained reversibly. Then, a second polymer slug was injected. At the end of the second slug, the injection rate was increased up to $30mL/h$ and then stepwise decreased in order to simulate the velocities around injection wells. Brine was finally injected until differential pressure stabilization, and the same series of injection rate variation was then applied for the brine. During the injection process, the polymer's viscosity was monitored before each slug using the capillary tube, in order to detect the polymer breakthrough and to make sure the polymer was not degraded over time. The duration of a typical coreflood is between two and three weeks.

4.1.3 Observables

4.1.3.1 Mobility and permeability reduction

The raw observables are differential pressures. They help ensuring the good propagation of polymer solutions in the porous medium and detecting the beginning of clogging when injectivity problems potentially occur.

From differential pressures, the first observables, mobility reduction R_m and permeability reduction R_k, are obtained. R_m and R_k definitions are given in Section 1.3.2.1. Mobility reduction R_m is linked to permeability reduction R_k as follows:

$$R_m = \frac{(k_{reference}/\eta)_{brine}}{(k_{injection}/\eta)_{polymer}} = \eta_{r_{app}} * R_k^{inj} \tag{4.4}$$

Where $k_{injection}$ and R_k^{inj} are respectively the permeability and the permeability reduction during polymer injection, and $\eta_{r_{app}}$ the apparent relative viscosity of the injected polymer solution.

4.1.3.2 Polymer irreversible retention and IPV

For low retention cases such as in polymer flood, monitoring polymer concentration downstream the porous media is unreliable. For this reason, we use the two slugs method. It allows estimating the irreversible polymer retention and the Inaccessible Pore Volume (IPV) by analyzing the successive breakthroughs of the tracer (obtained by conductimetry) and the polymer slugs (by the use of the capillary tube placed at the outlet of the porous medium).

As shown schematically in Figure 4.2, polymer irreversible retention $\Gamma_{retention}$, (expressed in $\mu g/g$: micrograms of polymer retained per gram of rock) is quantified based on the shift between the injected polymer volumes at breakthrough of the first and the second slug respectively V_{BT1} and V_{BT2}, such as:

$$\Gamma_{retention} = (V_{BT1} - V_{BT2})\, C_{pol}/m_{PM} \tag{4.5}$$

Where, C_{pol} and m_{PM} are respectively polymer concentration and porous medium mass.

It is important to note that in most cases, where no clogging occurs, retention is often associated with adsorption considered to be its major component.

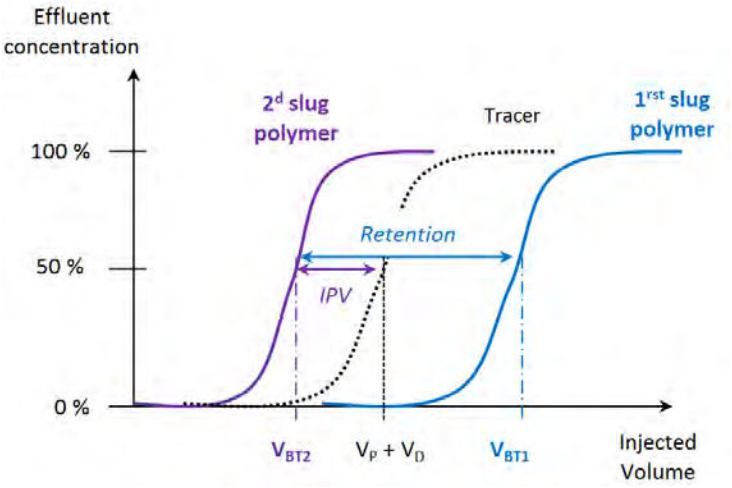

Figure 4.2 – Schematic of the two slugs method breakthrough curves for retention and IPV determination

For IPV , it is defined as the fraction of the porosity that is inaccessible to polymer and that can therefore be considered as a dead volume. IPV can be estimated from the shift between the second slug and the tracer breakthrough, such as:

$$IPV = V_p + V_D - V_{BT2} \tag{4.6}$$

With V_p and V_D respectively the pore volume and dead volumes.

To better understand the principle of this consideration, Figure 4.3 from the work of *Dawson and Lantz* [13], schematizes the position of the polymer solution's breakthrough for four situations according to adsorption (in the case where retention = adsorption) and IPV values.

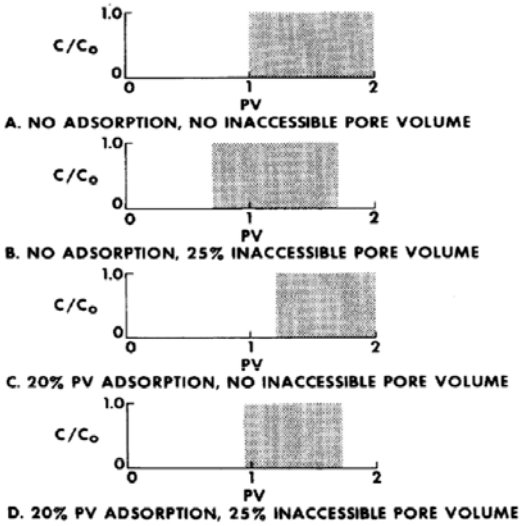

Figure 4.3 – Ideal polymer breakthrough curves according to adsorption and IPV values [13]

When there is no adsorption/retention nor IPV (Figure 4.3 - A), the polymer solution exits after the injection of one pore volume. The presence of IPV (Figure 4.3 - B), causes the polymer solution to exit early due to a fraction of the pore volume inaccessible for the polymer solution, thus, the breakthrough curve is shifted forward by the amount of the inaccessible pore fraction. Adsorption on the other hand (Figure 4.3 - C) causes the delay of the polymer breakthrough. A combination of both effects (Figure 4.3 - D), makes it hard to predict when the polymer breakthrough will occur.

4.1.3.3 Adsorbed layer thickness and density

Permeability reduction is often considered as a result of the formation of a polymer adsorbed layer on the pore surface. It is then possible to calculate this adsorbed layer's thickness, ε_h , considering the porous medium as a bundle of capillaries all of radius r_h, as shown in Figure 4.4, where r_h stands for an estimation of the pore throat's hydrodynamic radius.

Considering the formation of an adsorbed layer of thickness ε_h, frome Equation 4.1 applied to one capillary tube, the flow rate Q, before and after polymer injection, writes:

$$Q = \pi \frac{\Delta P_{ref\ brine}}{L} \frac{r_h^4}{8\eta} \tag{4.7}$$

$$Q = \pi \frac{\Delta P_{post-injection}}{L} \frac{(r_h - \varepsilon_h)^4}{8\eta} \tag{4.8}$$

The ratio between these two equations gives:

$$(\frac{r_h}{r_h - \varepsilon_h})^4 = \frac{\Delta P_{post-injection}}{\Delta P_{ref\ brine}} = R_k \tag{4.9}$$

After simplification, ε_h writes:

$$\varepsilon_h = r_h(1 - (R_k)^{-1/4}) \tag{4.10}$$

And r_h:

$$r_h = \alpha\ (8k/\phi)^{1/2} \tag{4.11}$$

k being the initial permeability of the porous medium, ϕ its porosity and α a prefactor that has been determined by *Chauveteau* [21] and found equal to 1.15 for granular porous media.

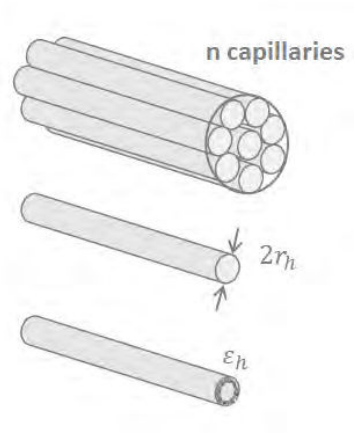

Figure 4.4 – Schematic of the porous medium considered as a capillary bundle and the adsorbed layer

The adsorbed layer's density ρ_{ads} can be defined as a function of polymer irreversible retention $\Gamma_{retention}$, specific surface area of the porous medium SSA and the adsorbed layer thickness ε_h as follows:

$$\rho_{ads} = \frac{\Gamma_{retention}}{SSA * \varepsilon_h} \tag{4.12}$$

4.2 Results and discussion

As mentioned earlier, injection tests aim at studying the transport of polymer solutions in low permeability porous media. In this section, we will first present results obtained from the different corefloods, then, we will discuss these results with regard to the effects of salinity and clay type.

4.2.1 Typical outcomes of each injection test

The first result obtained from corefloods are the differential pressures $\Delta P(mbar)$ measured in each section of the porous medium to evaluate the quality of polymer solution's propagation. An example of the differential pressures obtained for the porous medium $MP2-3$ (quartz + kaolinite) in brine $S1-02$ as a function of injected pore volumes is given in Figure 4.5. The differential pressures increase and stabilize successively in the different sections, which shows that the polymer solution propagates well in the porous medium during the first and the second slug with no apparent plugging trends. Interestingly, for the first slug, differential pressures stabilization is reached after the injection of 2 pore volumes whereas for the second slug it is reached after the injection of only 1 pore volume. Polymer retention is the reason behind the stabilization delay in the first slug. During the second slug, the retention is satisfied leading to stabilization after around the injection of 1 pore volume.

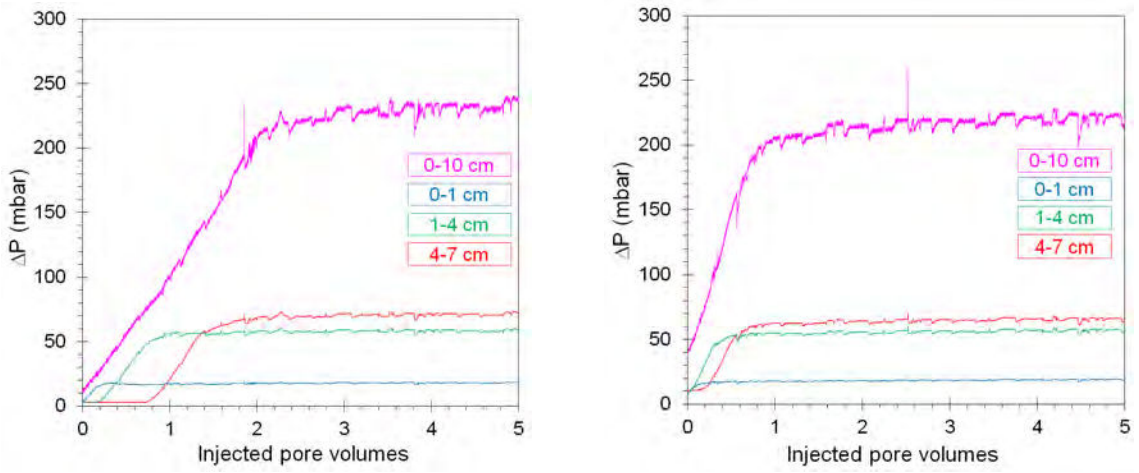

Figure 4.5 – Differential pressures measured for each section of the porous medium $MP2-3$ in brine $S1-02$ during the first (a) and the second slug (b)

Secondly, mobility reductions R_m obtained in the different sections of the porous medium were studied as a function of injected pore volumes. An example is given in Figure 4.6 for the same experiment as above ($MP2-3$ in brine $S1-02$).

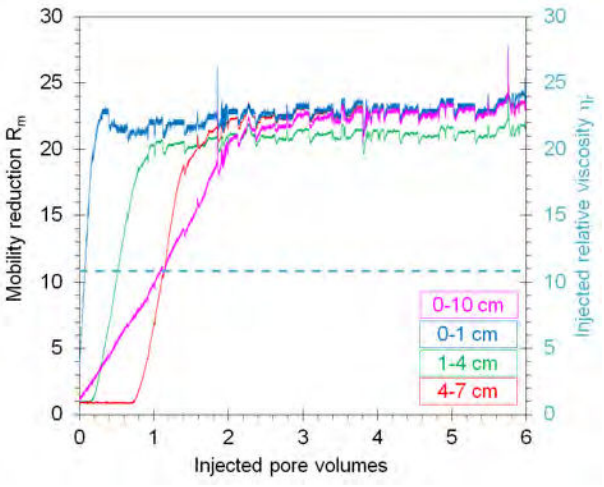

Figure 4.6 – Mobility reductions in the different sections of the porous medium $MP2-3$ in brine $S1-02$ during the first polymer slug, the dashed line corresponds to the value of the injected relative viscosity

It can be seen that mobility reductions increase and stabilize progressively around 21.5 ± 1.5 which confirms the good propagation of the polymer solution in the porous medium. Moreover, R_m values are higher than the injected polymer's relative viscosity $\eta_r = 10$. According to Equation 4.4 linking R_m to R_k, this result could be explained either as a consequence of elongational deformations of polymer potentially leading to an

increase in viscosity (very unlikely at low velocity) or as a result of the reversible and irreversible permeability reduction occurring during polymer injection.

Mobility reduction was also studied as a function of interstitial velocity. In fact, at the end of the second slug in each coreflood, the injection rate Q was increased up to $30mL/h$ and then stepwise decreased in order to simulate the velocities around injection wells. In Figure 4.7, values of mobility reduction are plotted as a function of interstitial velocity V_i. For intermediate sections, an increase in mobility reduction with increased velocity is observed, with a total increase of around 45% between the lowest and the highest velocity. This increase is either due to elongational deformations at higher shear rates leading to viscosity increase with velocity increase or to permeability reduction increase as the injected relative viscosity is constant.

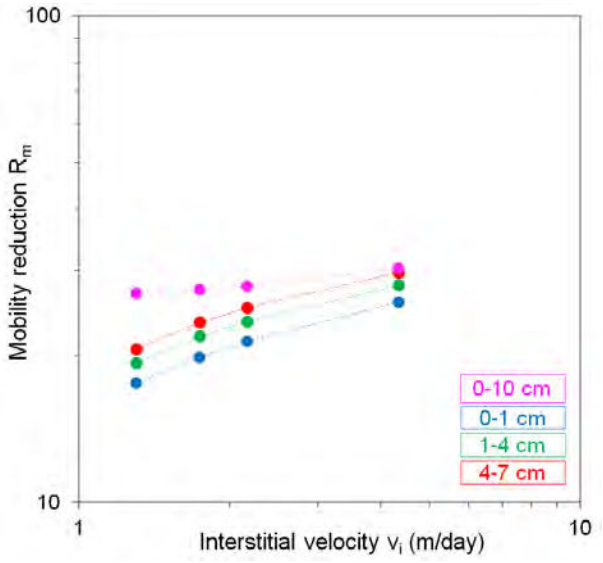

Figure 4.7 – Mobility reductions as a function of interstitial velocity (porous medium $MP2-3$ in brine $S1-02$)

At the end of the second polymer slug and the end of the following brine injection, we proceeded, as mentioned in 4.1.2, to a variation of the injection rate in order to study the permeability reduction R_k as well as the adsorbed layer thickness ε_h and their evolution with the injection rate.

Figure 4.8 presents permeability reduction and adsorbed layer thickness as a function of the interstitial velocity for the same experiment presented so far ($MP2-3$ in brine $S1-02$). In this experiment, a total increase of 220% for R_k (from 4 to 12.8), and 24% for ε_h (from 0.8 to $0.98\mu m$) was observed between the lowest and the highest interstitial velocity.

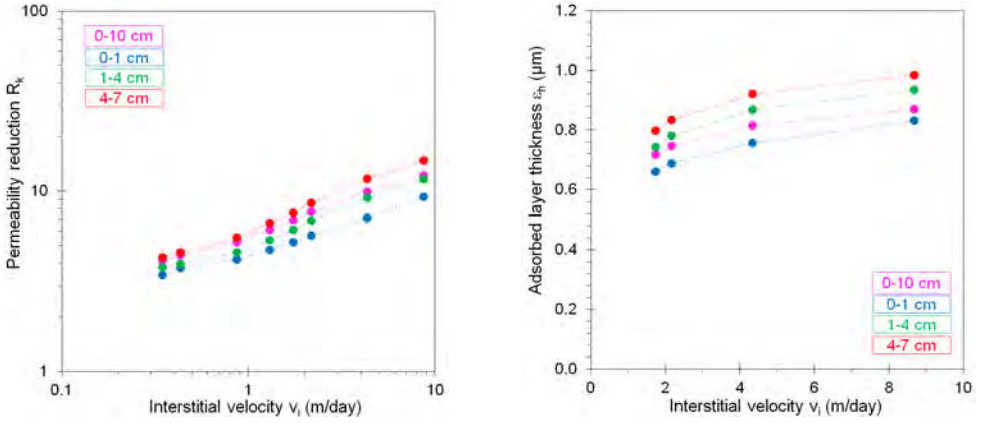

(a) (b)

Figure 4.8 – Permeability reduction (a) and adsorbed layer thickness (b) as a function of interstitial velocity (porous medium $MP2-3$ in brine $S1-02$)

In order to evaluate the retention of polymer in the porous medium as well as the IPV, the shift between the breakthroughs of the two polymer slugs and between the tracer and the second polymer slug are studied as explained in Section 4.1.3. An example is given in Figure 4.9 for the obtained curves corresponding to the injection test carried out in the porous medium $MP2-3$ using brine $S1-02$. In this figure, a dashed line was fixed at 1 pore volume, using the pore volume value obtained by gravimetry.

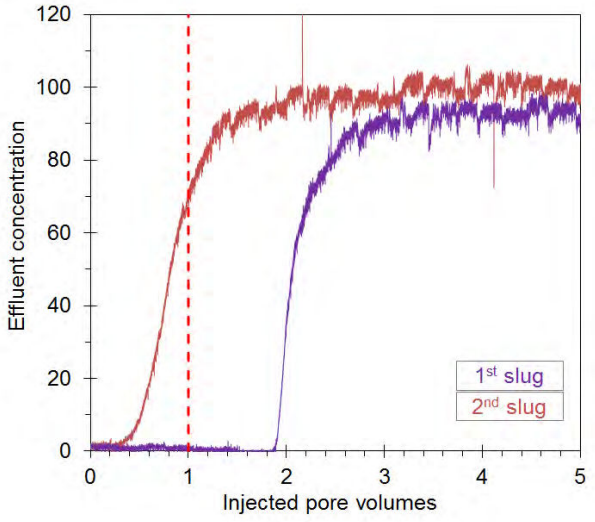

Figure 4.9 – Breakthroughs of the two polymer slugs of the injection test in porous medium $MP2-3$, brine $S1-02$, the red dashed line being fixed at 1 pore volume

For this example, polymer retention was estimated at $1110 \pm 30 \mu g/g$ (μg of polymer per g of rock), while the IPV was estimated at $18 \pm 2\%$ meaning that approximately 18% of the porous volume is not "visited" by the injected polymer solution.

However, in most cases, the error related to IPV estimation was high due to the porous medium's small porous volume and the high dead volumes in the setup. For this reason, we decided not to discuss our results in terms of polymer IPV.

For the rest of this report, we will present and discuss coreflood results based on the values obtained in the intermediate section $4-7cm$ as the results in the different sections are quite similar except for the first section $0-1cm$ where entry effects can complicate the discussion.

4.2.2 Overview of the results

Table 4.1 summarizes the results obtained for coreflood experiments performed during this PhD, including plateau values of mobility reduction R_m, permeability reduction R_k, polymer irreversible retention $\Gamma_{retention}$ (by unit mass and by unit SSA), adsorbed layer thickness ε_h and estimated adsorbed layer density ρ_{ads}. These results concern for each type of porous media, three corefloods in three different brines (except for illite and smectite where the experiments in brine $S001-0$ could not be conducted as mentioned in 3.4).

An additional experiment was carried out in porous medium $MP3$ with illite content (referred to as $MP3-1b$ in Table 4.1) using the exact same experimental conditions as the one carried out in $MP3-1$, in order to confirm the repeatability of the experiment. The results of both experiments were remarkably close with polymer retention values of 370 ± 20 and $340 \pm 20 \mu g/g$ respectively in $MP3-1$ and $MP3-1b$ as well as almost perfectly superimposed mobility reduction curves, shown in Figure 4.10.

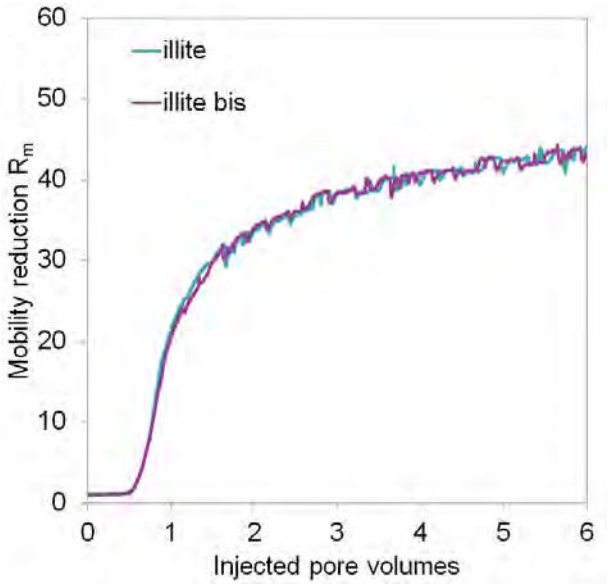

Figure 4.10 – Mobility reduction as a function of injected pore volumes (porous media $MP3-1$ and $MP3-1b$, brine $S1-0$)

As explained earlier (Section 2.4), for corefloods, polymer solution of the same relative viscosity $\eta_r = 10$ were injected, thus resulting in different concentrations. In order to study the impact of polymer concentration on experiments results, an additional injection

test was carried out in a porous medium containing quartz only (referred to as $MP1-3b$ in Table 4.1) using brine $S1-02$. This experiment allowed two comparisons: the first one being the impact of the change in polymer concentration (from 5.2 to $3.8g/L$ corresponding to relative viscosity values of 9.6 and 6.5 respectively) for the same brine $S1-02$ and which revealed very litte to no change in polymer retention (100 ± 40 and $140 \pm 30\mu g/g$ respectively) and in mobility reduction values (15.5 and 12 respectively). These results show that in our case (long polymer slug) the parameters governing polymer transport in porous media are salinity and mineralogy, with no significant impact of polymer concentration, hence our initial choice of injecting solutions of the same relative viscosity rather than the same polymer concentration. The second comparison being the impact of hardness (from brine $S1-0$ to $S1-02$) using the same polymer concentration $3.8g/L$, which confirmed the hardness effect leading to higher polymer retention but with similar mobility and permeability reduction values.

Porous medium	**Label**	**Brine**	C_{pol} (g/L)	R_m	R_k	ε_h (μm)	$\Gamma_{retention}$ $(\mu g/g)$	$\Gamma_{retention}$ $(\mu g/m^2)$	ρ_{ads} $(\mu g/cm^3)$
Quartz	MP1-1	S001-0	0.7	6.0 ± 0.2	1.05 ± 0.1	<0.03	<5	<20	-
	MP1-2	S1-0	3.8	11.0 ± 1.0	2.2 ± 0.1	0.30 ± 0.02	40 ± 20	170	550
	MP1-3	S1-02	5.2	15.5 ± 0.5	2.7 ± 0.1	0.29 ± 0.02	100 ± 40	420	1440
	MP1-3b	S1-02	3.8	12.0 ± 0.2	2.1 ± 0.05	0.28 ± 0.05	140 ± 30	580	2070
Quartz + Kaolinite	MP2-1	S001-0	0.7	15.6 ± 1.0	2.3 ± 0.1	0.28 ± 0.05	125 ± 5	170	620
	MP2-2	S1-0	3.8	22.5 ± 0.5	1.8 ± 0.1	0.27 ± 0.02	550 ± 25	760	2830
	MP2-3	S1-02	5.2	22.0 ± 1.0	4.2 ± 0.2	0.75 ± 0.05	1110 ± 30	1540	2060
Quartz + Illite	MP3-1	S1-0	3.0	40.0 ± 2.0	8.1 ± 0.4	0.75 ± 0.01	370 ± 20	40	52
	MP3-1b	S1-0	3.0	40.0 ± 2.0	8.0 ± 0.8	0.75 ± 0.04	340 ± 20	32	46
	MP3-2	S1-02	4.2	20.0 ± 2.0	7.9 ± 0.4	0.80 ± 0.05	930 ± 30	90	110
Quartz + Smectite	MP4-1	S1-0	3.0	26.0 ± 2.0	5.9 ± 0.1	0.70 ± 0.01	250 ± 20	70	100
	MP4-2	S1-02	4.2	27.0 ± 3.0	9.2 ± 1.3	0.80 ± 0.05	830 ± 30	230	290

Table 4.1 – Summary of coreflood results

4.2.3 Discussion

Coreflood results presented in Table 4.1, will be discussed in this section: first with regard to salinity impact (change in ionic strength and hardness), then regarding clay type impact.

4.2.3.1 Impact of salinity

As mentioned before, for each porous medium, coreflood experiments were carried out using brines with various ionic strength and hardnesses. Figure 4.11 shows the variation of mobility reduction with injected pore volumes for different brines obtained in each type of porous media.

Two families of porous media can be identified: the first one $MP1$ and $MP2$ in Figures 4.11 (a) and (b) respectively, and the second one is $MP3$ and $MP4$ shown in Figures 4.11 (c) and (d) respectively.

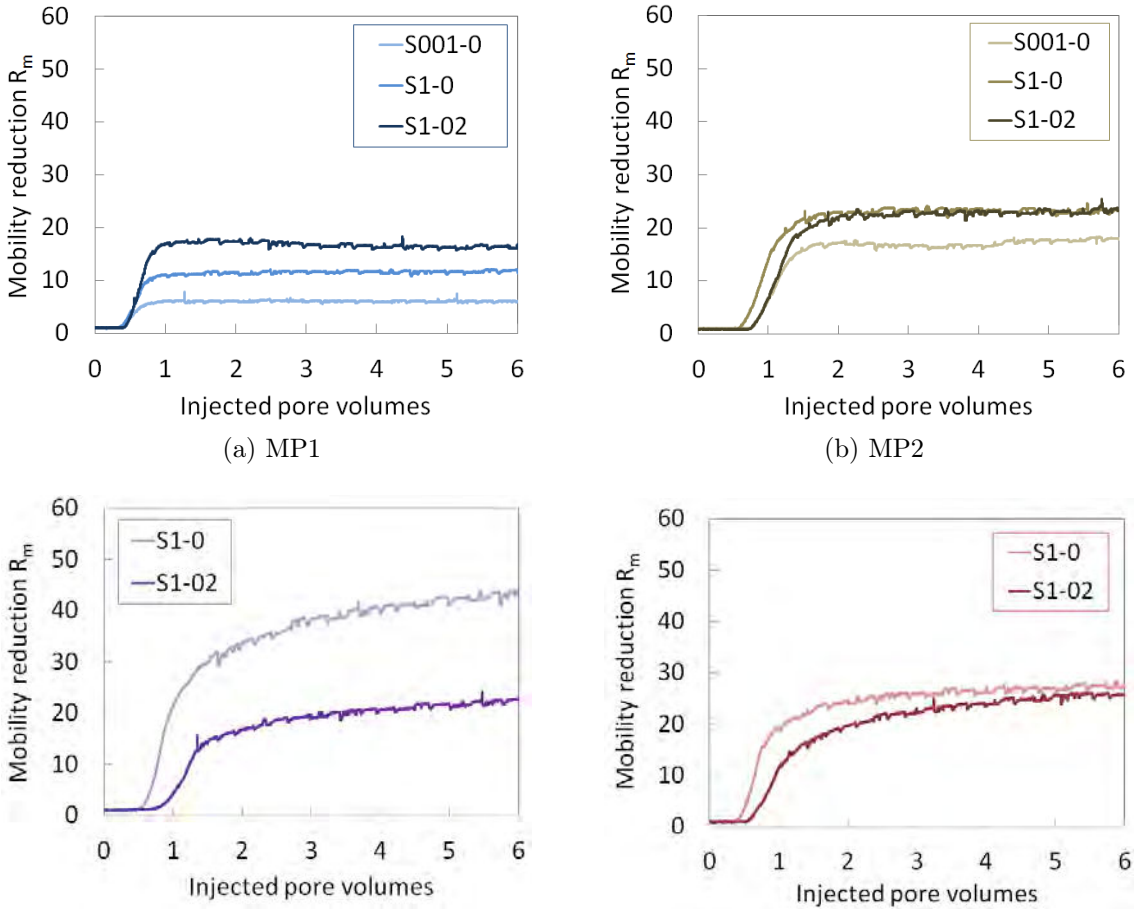

(a) MP1

(b) MP2

(c) MP3

(d) MP4

Figure 4.11 – Mobility reduction as a function of injected pore volumes for (a) $MP1$ (b) $MP2$ (c) $MP3$ and (d) $MP4$ for different brines

For the first family, the polymer solution propagates and stabilizes rapidly. In $MP1$, composed of quartz only, there is a strong salinity dependence as mobility reduction R_m increases with increased ionic strength (comparing $S001-0$ and $S1-0$) and increased hardness (comparing $S1-0$ and $S1-02$) for the same ionic strength. For $MP2$, containing quartz and kaolinite, mobility reduction increases with the increase of total salinity, but presents no hardness dependence. For the second family, a difficult and slow stabilization is observed suggesting poor in-depth transport of polymer solutions with complex salinity dependence. In $MP3$, containing quartz and illite, higher mobility reduction was observed in the absence of hardness ($S1-0$). For $MP4$, composed of quartz and smectite, no significant change was observed in mobility reduction with the increase of hardness.

For almost all experiments, R_m values were higher than the injected polymer's relative viscosity $\eta_r = 10$. According to Equation 4.4 linking R_m to R_k, this result could be explained as a consequence of both the reversible and irreversible permeability reduction occurring during polymer injection.

For polymer irreversible retention and permeability reduction R_k, Table 4.1 shows an increase with the increase of ionic strength and hardness for all the studied types of porous media.

For the clay-free porous media, $MP1$, results show a very low irreversible retention($< 5\mu g/g$) in $S001-0$ with R_k close to 1, which is consistent with a very low adsorption of the polymer as expected from unscreened electrostatic repulsions between the surface and the polyelectrolytes. When salinity was increased (in brine $S1-0$), irreversible retention became measurable ($40 \pm 20\mu g/g$) and R_k increased to 2.2. This is clearly the signature of a higher affinity of the polymer for the quartz surface due to the screening of electrostatic repulsions. The increase of hardness (brine $S1-02$) led to a slight increase in polymer retention ($100 \pm 40\mu g/g$) and permeability reduction (2.7).

In contrast, for the porous media with kaolinite, $MP2$, retention was already high ($125 \pm 5\mu g/g$) in $S001-0$, which indicates that attractive interactions exist between the kaolinite particles and the polyelectrolytes. Polymer retention kept increasing with ionic strength and hardness and permeability reduction reached 4.2 in brine $S1-02$.

For $MP3$ and $MP4$ containing illite and smectite respectively, polymer irreversible retention and permeability reduction both increased with hardness.

As usually described in the literature, a discussion in terms of adsorbed layer thickness ε_h and density ρ_{ads} can be conducted. Figure 4.12 shows the impact of ionic strength and hardness on ε_h and ρ_{ads} for the studied types of porous media.

In $MP1$ (Figure 4.12 (a)), at the lowest salinity $S001-0$ due to the very low permeability reduction 1.05, the modeling approach shows no formation of an adsorbed layer. When ionic strength is increased, brine $S1-0$, a polymer adsorbed layer is formed: its hydrodynamic thickness should be around $0.30\mu m$ and its density around $550\mu g/cm^3$. When hardness was increased (in brine $S1-02$), results show that as R_k was not much affected the thickness of the adsorbed layer remained close to $0.3\mu m$. This suggests that the polymer adsorbed layer was much denser. As quartz surface affinity for polymer does not change (same ionic strength) when hardness is increased, this is very likely the consequence of bridging effects between negatively charged acrylate units on the polyelec-

trolytes and calcium ions. This interpretation is consistent with the intrinsic viscosity that drops from $830cm^3/g$ in $S1-0$ to $450cm^3/g$ in $S1-02$ (cf. Table 2.2): the polymer chains are intrinsically denser in presence of calcium, it is hence not surprising that they form a denser adsorbed layer on the quartz surfaces.

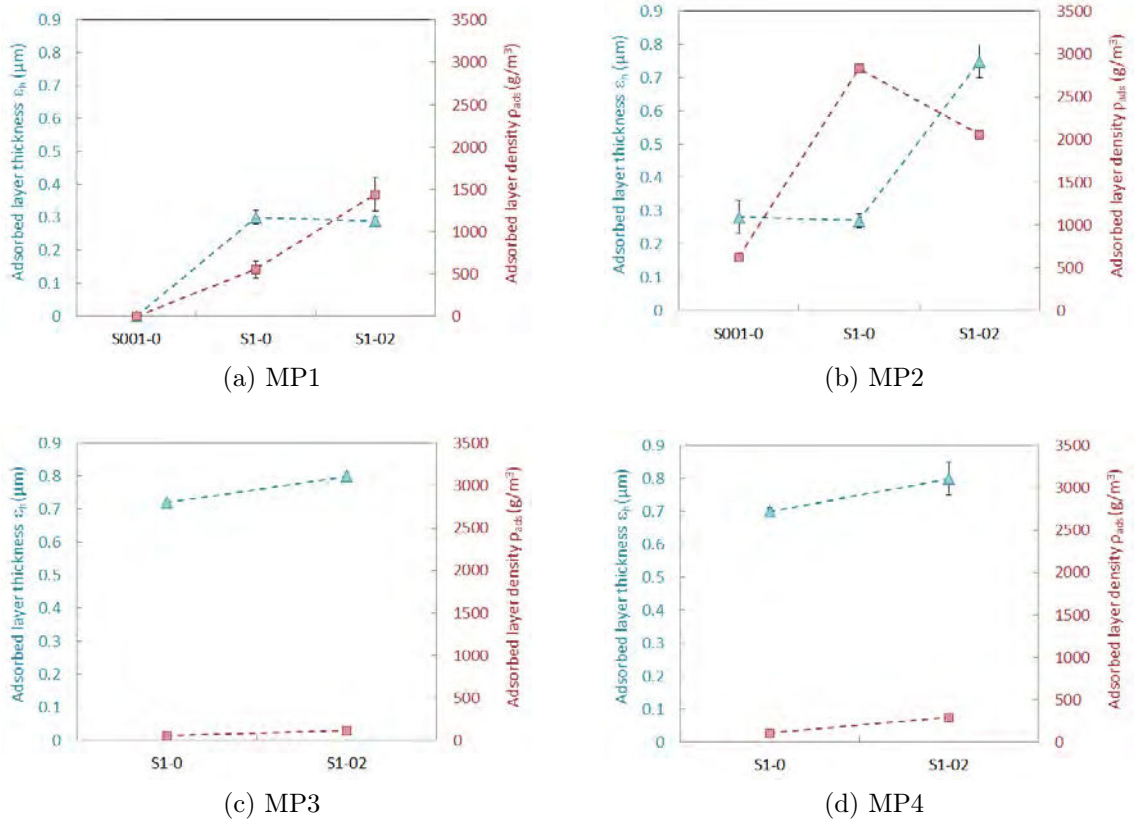

(a) MP1 (b) MP2

(c) MP3 (d) MP4

Figure 4.12 – Adsorbed layer thickness and density for different brines in porous media (a) $MP1$ (b) $MP2$ (c) $MP3$ and (d) $MP4$

For $MP2$ (Figure 4.12 (b)), even at low salinity $S001-0$, results showed the formation of an adsorbed layer with a thickness of about $0.30\mu m$ with a density of $620\mu g/cm^3$. When salinity was increased, with brine $S1-0$, as for the clay-free porous media, charge screening enabled polymer adsorption on the quartz surface but probably also enhanced the interaction between polymer and kaolinite. This resulted in a very high density of the equivalent adsorbed layer ($2830\mu g/cm^3$). When hardness was introduced, with brine $S1-02$, the thickness of the equivalent adsorbed layer increased to $0.75\mu m$ with a density decreasing to about $2000\mu g/cm^3$. The increase of the adsorbed layer thickness as well as the decrease in its density suggest that there are less polymer molecules per unit of surface. This result suggests that for this porous medium, the affinity of the polyelectrolytes for the kaolinite surface was significantly increased in presence of calcium and that the macromolecules tend either to acquire a stretched conformation or to create a multilayer. Those two hypothesis are not consistent with the polymer conformation observed in viscosimetry (Section 2.3.2) and DLS (Section 2.3.3) in presence of divalent cations nor

with kaolinite nature that presents no permanent charges. Moreover, SEM observations presented previously (Section 3.3.2.2) showed surface chemical heterogeneities in porous media due to the presence of quartz and kaolinite grains, which explains why the analysis in terms of a mean uniform adsorbed layer is not relevant for this type of porous media. Indeed, this approach considers the porous medium to be a set of n identical capillary tubes, whereas in $MP2$, two types of grains are present in the porous medium (quartz and kaolinite) which results in different interactions with polymer.

For porous media with illite $MP3$ and smectite content $MP4$ (Figures 4.12 (c) and (d) respectively), no significant change is observed in the adsorbed layer thickness and density with hardness.

4.2.3.2 Impact of mineralogy

Figure 4.13 presents mobility reduction as a function of injected pore volumes for different types of porous media in different brines.

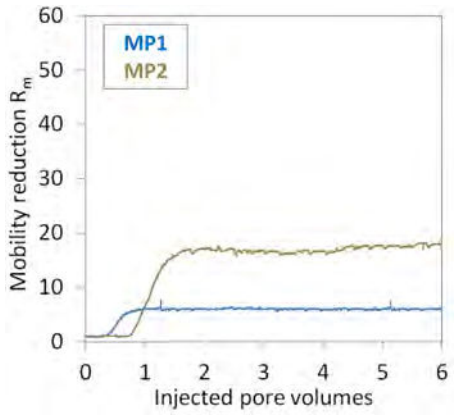

(a) S001-0

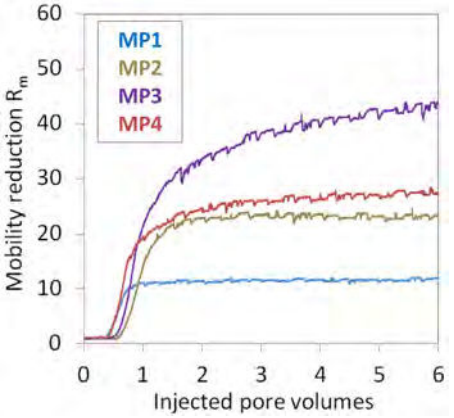

(b) S1-0

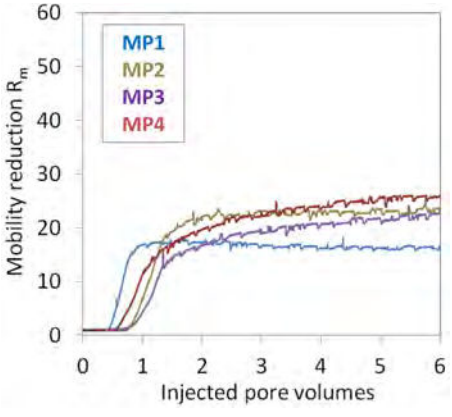

(c) S1-02

Figure 4.13 – Mobility reduction as a function of injected pore volumes for brines (a) $S001-0$ (b) $S1-0$ and (c) $S1-02$ for different types of porous media

For all brines, mobility reduction values in clay-rich porous media are higher than the one obtained in quartz only. In brine $S1-0$ (Figure 4.13 (b)), R_m value in $MP3$, with illite content, is much higher than the rest of porous media with difficult and low stabilization trends, whereas $MP2$ and $MP4$, with respectively kaolinite and smectite content, showed close R_m values despite their different nature. In presence of hardness (Figure 4.13 (c), brine $S1-02$), close R_m values and trends with injected pore volumes were observed in the three clay-rich porous media, $MP2$, $MP3$ and $MP4$.

As shown in SEM images in Tables 3.7 and 3.8, clay aggregates formation was observed for $MP3$ and $MP4$. These observations suggest that polymer diffusion in illite and smectite aggragates may be responsible for the slow stabilization trends of mobility reduction in these porous media. Moreover, the nature of illite aggregates, noticeably dense, could explain why these trends are more pronounced in $MP3$ than it is in $MP4$ where aggregates seemed less dense and partially accessible to polymer.

Figure 4.14 presents obtained permeability reduction values in the different corefloods. In contrast to polymer retention results, R_k values were not significantly increased in the presence of kaolinite compared to quartz only. However, porous media with illite and smectite showed high values of permeability reduction compared to porous media with kaolinite and quartz only. Results obtained in $S1-0$, 8.1 for illite and 5.9 in smectite, explain the differences in mobility reduction obtained in these two porous media and confirm that permeability reduction can be responsible for the differences between injected relative viscosity and measured mobility reduction. In the presence of hardness, brine $S1-02$, permeability reduction was significantly increased in the three clay-rich porous media, reaching up to 9.2 in $MP4$ which suggests that after polymer flood, permeability becomes 9 times lower that reference permeability.

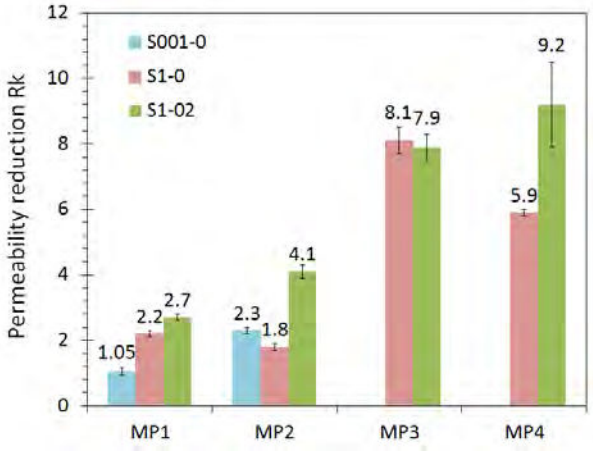

Figure 4.14 – Permeability reduction for different types of porous media in different brines

For polymer irreversible retention, Figure 4.15 shows the different results obtained in the studied porous media. First of all, there is a sharp increase of polymer retention in presence of clays compared to obtained values in quartz only, e.g. retention values up to ten times higher in $MP2$ than $MP1$ for the same brine $S1-02$ (from 100 to 1110$\mu g/g$).

Besides, within the three clay-rich porous media, $MP2$ with kaolinite content showed the highest values of retention compared to $MP3$ and $MP4$ with illite and smectite content, despite its SSA being the lowest (cf. Table 3.2).

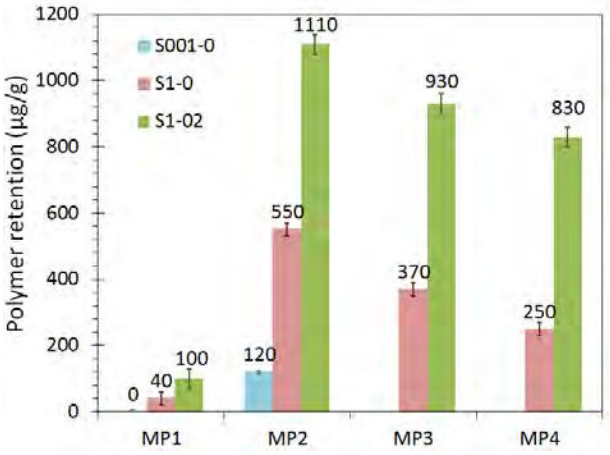

Figure 4.15 – Polymer irreversible retention for different types of porous media in different brines

Analysis in terms of retention per unit of SSA is presented in Figure 4.16, where we observe surprisingly low polymer retention values, as expressed by unit of SSA (40 and $90\mu g/m^2$ for illite, 70 and $230\mu g/m^2$ for smectite, respectively for $S1-0$ and $S1-02$) are associated with high values of Rk (8.1 and 7.9 in illite, 5.9 and 9.2 in smectite, respectively for the two brines).

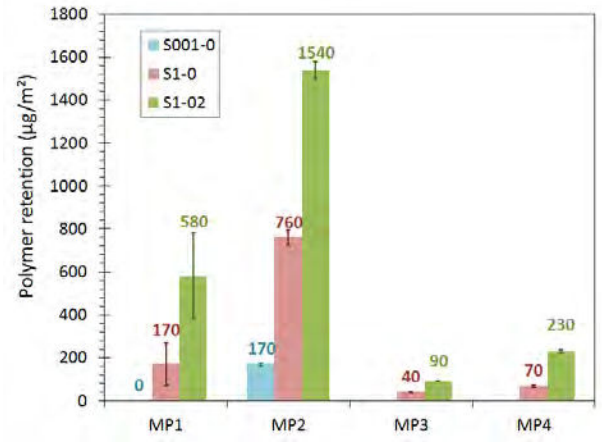

Figure 4.16 – Polymer irreversible retention per unit of SSA for different types of porous media in different brines

Finer analysis of SEM images presented in Tables 3.7 and 3.8 for porous media containing illite and smectite shows that the formation of clay aggregates induces that a significant fraction of the clay surfaces are inaccessible for the polymer. In fact, the nature and form of these aggregates result in the consideration of an effective SSA that

appears to be lower than the measured one as the polymer molecules only interact with the outer surface of clay aggregates. Polymer retention mechanism is very likely adsorption on grain surface in $MP2$, while it appears to be both adsorption on the outer clay aggregates surface and steric retention in both $MP3$ and $MP4$ explaining plugging trends observed in Figure 4.13. These findings suggest that the measured specific surface area is not relevant in the case of illite and smectite and confirm that the interpretation in terms of adsorbed layer is not to be considered in these porous media.

Chapter conclusion

In this chapter, we studied the transport properties of polymer solutions in low permeability porous media. First, we described materials and methods used for injection experiments. Then, after presenting typical outcomes of each injection test, we presented an overview of obtained results. Finally, corefloods results were discussed: first, with regard to the impact of salinity, then that of mineralogy.

Injection tests were carried out in four types of quartz-based porous media involving three different clays: kaolinite, illite and smectite. Injected polymer solutions were prepared in three different brines $S001-0$, $S1-0$ and $S1-02$ with different polymer concentrations allowing the injection of a fixed relative viscosity of $\eta_r = 10$.

Corefloods observables were: mobility reduction R_m, polymer irreversible retention, permeability reduction R_k and adsorbed layer thickness ε_h and density ρ_h.

The first discussion allowed highlighting the impact of ionic strength and hardness on the transport properties of polymer in the studied porous media, showing that globally an increase in ionic strength leads to increasing mobility reduction, polymer retention and permeability reduction, and that the presence of Ca^{2+} divalent cations leads to a sharp increase in polymer retention and permeability reduction in all porous media, whereas its effect on mobility reduction appears to be more complex.

The second discussion shed some lights on the impact of mineralogy on polymer flow through porous media, assessing that the presence of clays leads to a sharp increase in polymer irreversible retention and mobility reduction. Besides, within the clay-rich porous media, illite and smectite show comparable behaviors in terms of mobility reduction, polymer retention as well as permeability reduction. Surprisingly, kaolinite shows the highest value of polymer retention despite its nature (non swelling with no permeanent charge) and its low specific surface area compared to illite and smectite.

Analysis in terms of adsorbed layer thickness and density showed good consistency with viscosity and DLS measurements for quartz, but was not consistent for porous media with clay content due to surface chemical heterogeneities. Besides, measured specific surface area in these porous media, especially with illite and smectite content, seems to be different and much higher than polymer accessible surfaces. This result was highlighted in SEM observation with the formation of clay aggregates which significantly impacts polymer transport as polymer molecules seems to interact only with the outer surface of these aggregates.

Conclusions and perspectives

Chemical EOR, particularly polymer flood, is one of the most promising processes used to improve oil recovery. However, its application to reservoirs of relatively low permeability (between 10 and $100mD$) remains challenging given injectivity problems and high polymer retention. In this thesis, we studied the transport properties of polymer solutions in controlled low permeability porous media with regard to the impacts of salinity and mineralogy.

The polymer selected for this study is a partially hydrolyzed polyacrylamide (HPAM) of low molecular weight usually used in chemical EOR processes. Polymer solutions were prepared in brines of various properties and were characterized through viscosity measurements and hydrodynamic size estimation. This characterization allowed discussing the impacts of ionic strength and hardness on polymer chains' density in solution and inter-chain interactions. It showed that the increase of ionic strength leads to an increase in density and a decrease in hydrodynamic size due to charge screening, whereas the increase of hardness (presence of Ca^{2+} divalent cations) leads to denser chains and also higher hydrodynamic size suggesting attractive interactions between polymer chains, thanks to Ca^{2+} bridging.

For porous media, we chose to carry out our study on granular porous media with controlled mineralogy. On this basis, we were able to work on reproducible porous media with

similar petrophysical properties while controlling the type and amount of used minerals. Therefore, sand-clay packs were prepared using quartz and three types of clay: kaolinite, illite and smectite in equal amounts with a permeability fixed between 50 and 100mD. Porous media were characterized in terms of their petrophysical properties (porosity, pore volume, permeability and specific surface area) and microscopic structures using Scanning Electron Microscopy observation. Characterization results showed that all porous media were in the same permeability range, with different specific surface area values. Moreover, SEM observations showed a change in their microscopic structure resulting from their difference in mineralogy on one hand, and salinity on the other. Interestingly, it highlighted the distinctive structure of the porous media in presence of illite and smectite in low salinity and revealed the formation of clay aggregates at high salinity.

In order to study the transport properties of polymer solutions in low permeability porous media, injection tests were carried out using HPAM solutions in the different mineralogies. Corefloods observables were mainly: mobility reduction, polymer irreversible retention and permeability reduction. Obtained results were discussed regarding the impacts of salinity and mineralogy. The first discussion allowed highlighting the impact of ionic strength and hardness on the transport properties of polymer in the studied porous media, showing that for most porous media an increase in ionic strength leads to increasing mobility reduction, polymer retention and permeability reduction (except for illite where a decrease in mobility reduction was observed with hardness increase). The presence of Ca^{2+} divalent cations leads to a sharp increase in polymer retention and permeability reduction in all porous media, whereas its effect on mobility reduction appears to be more complex. The second discussion shed some lights on the impact of clay type on polymer flow through porous media, assessing that the presence of clays leads to a sharp increase in polymer irreversible retention and mobility reduction. Besides, within the clay-rich porous media, illite and smectite show comparable behaviors in terms of mobility reduc-

tion, polymer retention as well as permeability reduction. Surprisingly, kaolinite shows the highest value of polymer retention despite its nature (non swelling with no permeanent charge) and its low specific surface area compared to illite and smectite.

Analysis in terms of adsorbed layer thickness and density showed good consistency with viscosity and DLS measurements for quartz, but was not consistent for porous media with clay content due to surface chemical heterogeneities. Besides, measured specific surface area in these porous media, especially with illite and smectite content, seems to be different and much higher than polymer accessible surfaces. This result was highlighted in SEM observation with the formation of clay aggregates which significantly impacts polymer transport as polymer molecules seems to interact only with the outer surface of these aggregates.

The outcomes of this work should help guiding EOR operations in terms of the feasibility of polymer flooding in clayey reservoirs of permeabilities below $100mD$ as it showed that high permeability reduction does not always imply high polymer retention. Besides, it pointed out that the interpretation in terms of mean adsorbed layer (classical bundle model approach) is not always valid for clay rich formations as the measured specific surface area are different and seems to be much higher than polymer effectively accessible surfaces.

Alongside this study, experiments on clay-polymer aqueous suspensions were carried out in the attachment laboratory of the thesis (Laboratoire Interdisciplinaire des Environnements Continentaux). Clay-polymer suspensions were studied in terms of particle size, turbidity and electrophoretic mobility for various clay and polymer concentrations and different ionic strengths. This study showed that HPAM shifts the critical coagulation concentration to higher values. Clay-polymer interaction was only slightly influenced by

the ionic strength, and no major differences were observed with regard to the clay type. Furthermore, the electrokinetic mobility of the polymer was not affected in the presence of clay, which suggests the incorporation of clay particles into polymer aggregates. In addition, BET adsorption experiments were also carried out on samples after polymer injection showing no significant difference in polymer-rock interaction based on clay type.

In order to complete our study, surfactant injection tests were carried out in the different types of porous media using brine $S1-0$ (high ionic strength, absence of divalent cations) and the combination of two surfactants: anionic Internal Olefin Sulfonate (IOS) and nonionic AlkoxyGlycidylEther Sulfonates (AGES), both widely used in EOR processes. Results of the corefloods, showed high surfactant adsorption as well as significant plugging trends for porous media with clay content compared to quartz only. It would be interesting to study in depth these results and also complete them with injection experiments combining polymer and surfactant, and in the presence of oil.

Bibliography

[1] James Sheng. *Modern chemical enhanced oil recovery: Theory and practice*. Gulf Professional Pub, Amsterdam and Boston, 2011.

[2] Antoine Thomas. *Essentials of polymer flooding technique*. Wiley, Hoboken NJ USA, first edition edition, 2019.

[3] Eric Delamaide, Rene Tabary, and David Rousseau. Chemical eor in low permeability reservoirs. In *SPE EOR Conference at Oil and Gas West Asia*. Society of Petroleum Engineers, 2014.

[4] K. S. Sorbie. *Polymer-Improved Oil Recovery*. Springer Netherlands, Dordrecht and s.l., 1991.

[5] Marc Bavière, editor. *Basic concepts in enhanced oil recovery processes*, volume 33 of *Critical reports on applied chemistry*. Elsevier Applied Science, London, 1991.

[6] G. Paul Willhite and Jose G. Dominguez. Mechanisms of polymer retention in porous media. In *Improved Oil Recovery by Surfactant and Polymer Flooding*, pages 511–554. Elsevier, 1977.

[7] Jorge Avendano. *Viscoélasticité et récupération améliorée du pétrole*. PhD thesis, Université Paris-Est, 2012.

[8] Don W. Green and G. Paul Wilhite. *Enhanced Oil Recovery*. SPE, Richardson, TX, 2nd ed. edition, 2018.

[9] Tharwat Fouad Tadros. *Applied surfactants: Principles and applications*. Wiley-VCH, Weinheim, 2005.

[10] H. T. Davis and L. E. Scriven. Stress and structure in fluid interfaces. In I. Prigogine and Stuart Alan Rice, editors, *Advances in chemical physics*, volume 33 of *Advances in Chemical Physics*, pages 357–454. John Wiley, New York and Chichester, 2007.

[11] J. M. Cases and F. Villieras. Thermodynamic model of ionic and nonionic surfactants adsorption-abstraction on heterogeneous surfaces. *Langmuir*, 8(5):1251–1264, 1992.

[12] Guy Chauveteau. Molecular interpretation of several different properties of flow of coiled polymer solutions through porous media in oil recovery conditions. In *SPE Annual Technical Conference and Exhibition*. Society of Petroleum Engineers, 1981.

[13] W. B. Gogarty. Mobility control with polymer solutions. *Society of Petroleum Engineers Journal*, 7(02):161–173, 1967.

[14] A.J.P. Fletcher, S. P. Lamb, and P. J. Clifford. Formation damage from polymer solutions: Factors governing injectivity. *SPE Reservoir Engineering*, 7(02):237–246, 1992.

[15] L. E. Treiber and S. H. Yang. The nature of polymer plugging and a wellbore treatment to minimize it. In *SPE Enhanced Oil Recovery Symposium*. Society of Petroleum Engineers, 1986.

[16] Randall S. Seright, J. Mac Seheult, and Todd Talashek. Injectivity characteristics of eor polymers. *SPE Reservoir Evaluation & Engineering*, 12(05):783–792, 2009.

[17] C. Marliere, N. Wartenberg, M. Fleury, R. Tabary, C. Dalmazzone, and E. Delamaide. Oil recovery in low permeability sandstone reservoirs using surfactant-polymer flooding. In *SPE Latin American and Caribbean Petroleum Engineering Conference*. Society of Petroleum Engineers, 2015.

[18] A. Zaitoun and N. Kohler. The role of adsorption in polymer propagation through reservoir rocks. In *SPE International Symposium on Oilfield Chemistry*. Society of Petroleum Engineers, 1987.

[19] F. D. Martin. Laboratory investigations in the use of polymers in low permeability reservoirs. In *Fall Meeting of the Society of Petroleum Engineers of AIME*. Society of Petroleum Engineers, 1974.

[20] Saul Vela, D. W. Peaceman, and E. I. Sandvik. Evaluation of polymer flooding in a layered reservoir with crossflow, retention, and degradation. *Society of Petroleum Engineers Journal*, 16(02):82–96, 1976.

[21] Z.-W. Pang, J.-L. Li, H.-B. Liu, and Y. Li. Polymer viscosity loss in injection and production processes. *Chemical Flooding Symposium-Research Results during the Eighth Five-Year Period (1991-1995)*, I. Petroleum Industry Press:385–394, 1998.

[22] G. Dupuis. *Polymères associatifs pour la récupération améliorée des hydrocarbures: Synthèses, caractérisation et injectivité en milieux poreux modèles*. PhD thesis, Université de Pau et des Pays de l'Adour, 2010.

[23] I. Lakatos, J. Lakatos-Szabó, and J. Tóth. Factors influencing polyacrylamide adsorption in porous media and their effect on flow behavior. In Dinesh O. Shah, editor, *Surface Phenomena in Enhanced Oil Recovery*, pages 821–842. Springer US, Boston, MA, 1981.

[24] Miklos T. Szabo. An evaluation of water-soluble polymers for secondary oil recovery - parts 1 and 2. *Journal of Petroleum Technology*, 31(05):553–570, 1979.

[25] Guoyin Zhang and Randall Seright. Effect of concentration on hpam retention in porous media. *SPE Journal*, 19(03):373–380, 2014.

[26] F. D. Martin, M. J. Hatch, J. S. Shepitka, and J. S. Ward. Improved water-soluble polymers for enhanced recovery of oil. In *SPE Oilfield and Geothermal Chemistry Symposium*. Society of Petroleum Engineers, 1983.

[27] Frank W. Smith. The behavior of partially hydrolyzed polyacrylamide solutions in porous media. *Journal of Petroleum Technology*, 22(02):148–156, 1970.

[28] Ph Gramain and Ph Myard. Adsorption studies of polyacrylamides in porous media. *Journal of Colloid and Interface Science*, 84(1):114–126, 1981.

[29] M. T. Szabo. Laboratory investigations of factors influencing polymer flood performance. *Society of Petroleum Engineers Journal*, 15(04):338–346, 1975.

[30] G. Chauveteau and N. Kohler. Polymer flooding: The essential elements for laboratory evaluation. In *SPE Improved Oil Recovery Symposium*. Society of Petroleum Engineers, 1974.

[31] Mohammed T. Al-Murayri, Abrahim A. Hassan, Mohammad B. Abdullah, Abdulla M. Abdulrahim, Claire Marlière, Sabrina Hocine, René Tabary, and Guillaume P. Suzanne. Surfactant/polymer flooding: Chemical-formulation design and evaluation for raudhatain lower burgan reservoir, kuwait. *SPE Reservoir Evaluation & Engineering*, 2018.

[32] Hadi ShamsiJazeyi, Rafael Verduzco, and George J. Hirasaki. Reducing adsorption of anionic surfactant for enhanced oil recovery: Part i. competitive adsorption mechanism. *Colloids and Surfaces A: Physicochemical and Engineering Aspects*, 453:162–167, 2014.

[33] Fabíola D.S. Curbelo, Vanessa C. Santanna, Eduardo L. Barros Neto, Tarcílio Viana Dutra, Tereza N. Castro Dantas, Afonso A. Dantas Neto, and Alfredo I.C. Garnica. Adsorption of nonionic surfactants in sandstones. *Colloids and Surfaces A: Physicochemical and Engineering Aspects*, 293(1-3):1–4, 2007.

[34] Mohammad Amin Bagrezaie and Peyman Pourafshary. Improvement of surfactant flooding performance by application of nanoparticles in sandstone reservoirs. *Journal of the Japan Petroleum Institute*, 58(2):97–102, 2015.

[35] Adeline Dupas, Isabelle Henaut, David Rousseau, Philippe Poulain, Rene Tabary, Jean-Francois Argillier, and Thierry Aubry. Impact of polymer mechanical degradation on shear and extensional viscosities: Toward better injectivity forecasts in polymer flooding operations. In *SPE International Symposium on Oilfield Chemistry*. Society of Petroleum Engineers, 2013.

[36] J. Lecourtier, L. T. Lee, and G. Chauveteau. Adsorption of polyacrylamides on siliceous minerals. *Colloids and Surfaces*, 47:219–231, 1990.

[37] Pefferkorn. Polyacrylamide at solid/liquid interfaces. *Journal of Colloid and Interface Science*, 216(2):197–220, 1999.

[38] I. Guetni, I. Bihannic, F. Thomas, J. Duval, Y. Waldvogel, M. Pelletier, C. Marliere, D. Rousseau, F. Villieras. Clay-polymer interaction in enhanced oil recovery: impacts of clay type, ionic strength and hardness, Euroclay 2019.

[39] L. T. Lee, R. Rahbari, J. Lecourtier, and G. Chauveteau. Adsorption of polyacrylamides on the different faces of kaolinites. *Journal of Colloid and Interface Science*, 147(2):351–357, 1991.

[40] Jun Long, Zhenghe Xu, and Jacob H. Masliyah. Role of illite–illite interactions in oil sands processing. *Colloids and Surfaces A: Physicochemical and Engineering Aspects*, 281(1-3):202–214, 2006.

[41] Philippe. Coussot. *Rhéophysique: La matière dans tous ses états*. EDP Sciences, Les Ulis, 2013.

[42] Iwao Teraoka. *Polymer Solutions*. John Wiley & Sons, Inc, New York, USA, 2002.

[43] Bruno H. Zimm. Dynamics of polymer molecules in dilute solution: Viscoelasticity, flow birefringence and dielectric loss. *The Journal of Chemical Physics*, 24(2):269–278, 1956.

[44] John G. Kirkwood and Peter L. Auer. The visco–elastic properties of solutions of rod–like macromolecules. *The Journal of Chemical Physics*, 19(3):281–283, 1951.

[45] Albert Einstein. Investigations on the theory of the brownian movement by albert einstein, ph.d. *SERBIULA (sistema Librum 2.0)*, 1956.

[46] Patrick PERRIN and Dominique HOURDET. Polymères en solution. *Techniques de l'ingénieur Plastochimie et analyse physico-chimique*, base documentaire : TIB139DUO(ref. article : a3050), 1997.

[47] Gert. Strobl. *The Physics of Polymers: Concepts for Understanding Their Structures and Behavior*. Springer Berlin Heidelberg, Berlin, Heidelberg, third revised and expanded edition edition, 2007.

[48] Maurice L. Huggins. Theory of solutions of high polymers 1. *Journal of the American Chemical Society*, 64(7):1712–1719, 1942.

[49] R. C. Rivenq, Alain Donche, and Christine Nolk. Improved scleroglucan for polymer flooding under harsh reservoir conditions. *SPE Reservoir Engineering*, 7(01):15–20, 1992.

[50] Paul J. Flory. *Principles of polymer chemistry*. The George Fisher Baker non-resident lectureship in chemistry at Cornell university. Cornell University Press, Ithaca and New York, 1953.

[51] William B. Russel, D. A. Saville, and William Raymond Schowalter. *Colloidal dispersions*. Cambridge monographs on mechanics. Cambridge University Press, Cambridge, 1989.

[52] A. J.F. Siegert. *On the fluctuations in signals returned by many independently moving scatterers*. Radiation Laboratory, Massachusetts Institute of Technology, 1943.

[53] Robert Pecora. *Dynamic Light Scattering*. Springer US, Boston, MA, 1985.

[54] Stephen Brunauer, P. H. Emmett, and Edward Teller. Adsorption of gases in multimolecular layers. *Journal of the American Chemical Society*, 60(2):309–319, 1938.

[55] Pacelli Zitha. *Ecoulement non-stationnaire de polymeres hydrosolubles dans les milieux poreux*. PhD thesis.

[56] C. William Keighin and K. Sampath. Evaluation of pore geometry of some low-permeability sandstones-uinta basin. *Journal of Petroleum Technology*, 34(01):65–70, 1982.

[57] F.A.L Dullien and G.K Dhawan. Bivariate pore-size distributions of some sandstones. *Journal of Colloid and Interface Science*, 52(1):129–135, 1975.

[58] C. D. Barton. Clay minerals. In *Encyclopedia of Soil Science*. Ward Chesworth, 2008.

[59] Cornelis Klein, Cornelius S. Hurlbut, and James Dwight Dana. *Manual of mineralogy: (after James D. Dana)*. J. Wiley, New York, 21st ed., rev edition, 1999.

[60] Linus Pauling. The structure of the micas and related minerals. *Proceedings of the National Academy of Sciences of the United States of America*, 16(2):123–129, 1930.

[61] R. E. Grim. Clay mineralogy. page 384, 1953.

[62] Linus Pauling. The structure of the chlorites. *Proceedings of the National Academy of Sciences of the United States of America*, 16(9):578–582, 1930.

[63] John W. Gruner. The crystal structure of kaolinite. *Zeitschrift für Kristallographie - Crystalline Materials*, 83(1-6), 1932.

[64] G. W. BRINDLEY and KEITH ROBINSON. Structure of kaolinite. *Nature*, 156(3970):661–662, 1945.

[65] *Encyclopedia of Soil Science*. Ward Chesworth, 2008.

[66] A. N. Winchell. Studies in the mica group; part ii. *American Journal of Science*, s5-9(53):415–430, 1925.

[67] STERLING B. HENDRICKS. Polymorphism of the micas and diffuse x-ray scattering of layer silicate lattices. *Nature*, 143(3628):800, 1939.

[68] I. E. Odom. Smectite clay minerals: Properties and uses. *Philosophical Transactions of the Royal Society A: Mathematical, Physical and Engineering Sciences*, 311(1517):391–409, 1984.

[69] Markus Olin, Eini Puhakka, Jarmo Lehikoinen, Esa Puukko, Martti Hakanen, and Antero Lindberg. Characterisation of kaolinite and adsorption of europium on kaolinite. 2007.

[70] R.Sh Mikhail, Stephen Brunauer, and E.E Bodor. Investigations of a complete pore structure analysis. *Journal of Colloid and Interface Science*, 26(1):45–53, 1968.

[71] Rapier Dawson and Ronald B. Lantz. Inaccessible pore volume in polymer flooding. *Society of Petroleum Engineers Journal*, 12(05):448–452, 1972.

Transport de solutions de polymère dans des milieux poreux contrôlés de différentes minéralogies

La récupération assistée du pétrole est considérée comme une option intéressante pour les réservoirs à faible perméabilité. Cependant, son application peut s'avérer difficile pour des perméabilités inférieures à $100mD$, en raison des problèmes d'injectivité et de rétention élevée des additifs chimiques fréquemment observés dans ces cas. Ce travail de thèse vise à étudier l'impact des paramètres physico-chimiques et minéralogiques sur le transport des solutions de polymère dans des milieux poreux modèles de faibles perméabilités. Pour cela, des expériences d'injection de polymère ont été menées en utilisant des solutions d'HPAM de différentes forces ioniques et duretés et quatre milieux granulaires à base de quartz et trois types d'argiles: kaolinite, illite et smectite. Les résultats confirment le rôle majeur joué par la composition de l'eau d'injection (salinité et dureté) sur la conformation des polymères et sur les interactions polymères-minéraux. De fortes interactions entre le polymère et l'argile sont mises en évidence avec des différences significatives selon le type d'argile : bonne propagation et rétention élevée du polymère dans une argile non chargée et non gonflante (kaolinite) et faible propagation avec une rétention plus faible que prévu dans les argiles chargées ou gonflantes (illite, smectite). Ces résultats constituent de nouveaux éléments pour la compréhension du transport des solutions de polymères dans les réservoirs de grès à faible perméabilité.

Mots clés : Polymère, transport en milieu poreux, injectivité, faible perméabilité, récupération assistée du pétrole.

Transport of polymer solutions in controlled low permeability porous media of various mineralogies

Chemical Enhanced Oil Recovery (EOR) is considered as an attractive option for low permeability reservoirs, in particular where lack of gas supply does not allow gas injection processes. However, its application can be challenging for permeabilities below $100mD$, as poor injectivity and high chemical retention are frequently observed in these cases. This work aimed at investigating the impact of both chemical and mineralogical parameters on the transport of polymer solutions in well-controlled low permeability porous media. For that, polymer injection tests were carried out using HPAM solutions of different ionic strengths and hardnesses and four granular sand-clay packs using quartz and three types of clays: kaolinite, illite and smectite. Results confirm the major role played by the injection water composition (salinity and hardness) on polymer conformation and on polymer-minerals interactions. Strong interactions between polymer and clay are evidenced with significant differences according to the clay type: good propagation and high polymer retention in an uncharged and non-swelling clay (kaolinite) and poor propagation with lower retention than expected in charged or swelling clays (illite, smectite). These outcomes stand as new elements for understanding the transport of polymer solutions in low permeability sandstone reservoirs.

Keywords : Polymer, transport in porous media, injectivity, low permeability, enhanced oil recovery.